Zelfhelend beton - ingekapselde prepolymeren als helende agentia voor bewegende scheuren

Self-Healing concrete - encapsulated polymer precursors as healing agents for active cracks

João Feiteira

Promotor: prof. N. De Belie / dr. Ir. Elke Gruyaert
Proefschrift ingediend tot het behalen van de graad van
Doctor in de Ingenieurswetenschappen: Bouwkunde

Vakgroep Bouwkundige Constructies
Voorzitter: prof. dr. ir. L. Taerwe
Faculteit Ingenieurswetenschappen en Architectuur
Academiejaar 2017 – 2018

UNIVERSITEIT
GENT

ISBN xxx-xx-xxxx-xxx-x
NUR yyy
Wettelijk depot: z/2017/zz.zzz/zz

HOST INSTITUTION

Magnel Laboratory for Concrete Research
Faculty of Engineering and Architecture
Ghent University

EXAMINATION COMMITTEE

Prof. Hendrik Van Landeghem (chair)
Ghent University
Faculty of Engineering and Architecture

Prof. Stijn Matthys (secretary)
Ghent University
Faculty of Engineering and Architecture

Prof. Christian Grosse
Technical University of Munich
Faculty of Civil, Geo and Environmental Engineering

Prof. Danny Van Hemelrijck
Vrije Universiteit Brussel
Faculty of Engineering

Prof. Erik Schlangen
Delft University of Technology
Faculty of Civil Engineering & Geosciences

Prof. Francisco Antonio Gilabert Villegas
Ghent University
Faculty of Engineering and Architecture

Dr. Sandra Van Vlierberghe
Ghent University
Faculty of Sciences

FUNDING

healCON
concrete which repairs itself

The research leading to these results has received funding from the European Union Seventh Framework Programme (FP7/2007-2013) under grant agreement n° 309451 (HEALCON).

Fora da matemática que não tem que ver senão com números mortos e fórmulas vazias, e por isso pode ser perfeitamente lógica, a ciência não é senão um jogo de crianças no crepúsculo, um querer apanhar sombras de aves e parar sombras de ervas ao vento.

Other than mathematics which has nothing to do but with dead numbers and empty formulas, and because of that can be perfectly logical, science is nothing but a children's game at dusk, wanting to catch shadows of birds and to stop shadows of grass under the wind.

Bernardo Soares

(heteronym of Fernando Pessoa)

SAMENVATTING

Een mechanisme van autonome zelfheling kan worden voorzien in beton voor herstel van scheuren met een wijdte van enkele honderden micrometer. Op deze manier kan de levensduur van gewapende betonstructuren verlengd worden en de waterdichtheid gegarandeerd worden voor langere periodes. De zelfhelende technologieën die tot nu toe bestudeerd werden, stimuleren autogene zelfheling of zijn gebaseerd op de toevoeging van ingekapselde helende agentia.

Bij zelfhelend beton met ingekapselde prepolymeren, breken de capsules bij scheurvorming en vloeien de prepolymeren in de scheur en vullen deze. Vervolgens hardt het prepolymeer uit en vormt een samenhangend polymeer dat de tegenovergestelde zijden van de scheur verbindt. Het voordeel van het gebruik van polymeren is dat uit een ruim gamma producten met een breed bereik aan mechanische eigenschappen kan gekozen worden. Dit in tegenstelling tot andere zelfhelende technologieën waar mineralen met een hoge stijfheid en brosheid de scheur opvullen. Bij dergelijke materialen zal bij een stijging van de last of bij cyclische belasting de scheur opnieuw openen of zal een nieuwe scheur gevormd worden.

In het voorliggend werk werd nagegaan of bepaalde commerciële prepolymeren geschikt zijn voor het zelfherstel van bewegende scheuren. Daarnaast werd de opschaling van de technologie bestudeerd. Hiervoor moest op zoek gegaan worden naar capsules die het mengproces van beton overleven. Zoals met andere opkomende technologieën was er ook behoefte aan degelijke testmethodes die toelaten de zelfhelende efficiëntie te kwantificeren en praktijkomstandigheden te simuleren.

In een eerste fase van de studie werden verscheidene prepolymeren die verharden onder invloed van vocht gescreend. De screening gebeurde op basis van de viscositeit (een lage viscositeit is vereist voor goede verspreiding binnen in de scheur), de verlenging (een hoge verlenging is vereist om scheurbeweging te kunnen volgen) en hechting aan beton (een goede hechting is vereist voor het helen van bewegende scheuren). Met de gekozen prepolymeren werden acht

testreeksen samengesteld die varieerden qua viscositeit, schuimend vermogen en mechanische eigenschappen na verharding. De testen werden uitgevoerd op gescheurde mortelprisma's met glascapsules met een wanddikte van 0,18 mm. De reeks SLV (polyurethaan met super lage viscositeit) kwam als beste uit de proeven omwille van de goede verspreiding van het helend agens in de scheur en de beperkte wateropname via de geheelde scheur. Een wateropname vergelijkbaar met de wateropname in ongescheurd beton werd behaald. Het polymeer was eveneens in staat een rek van minstens 50% te weerstaan, waarna het los kwam van de scheurwanden. Deze rekcapaciteit kan echter voor bepaalde toepassingen, waar grote scheurbewegingen verwacht worden, nog onvoldoende zijn.

Methodes die toelaten de scheuroverbruggende eigenschappen continu op te volgen en falen te detecteren en bovendien het gedrag van stijve polymeren in bewegende scheuren te onderzoeken, werden op hun geschiktheid beoordeeld. Met behulp van akoestische emissie-analyse, gekoppeld aan digitale beeldanalyse was het mogelijk brosse breuk van een star schuimend polymeer te detecteren (rek = 9%). Met elektronenmicroscopie werd de contactzone tussen het polymeer en de matrix gevisualiseerd. Via in situ trekproeven in de elektronenmicroscoop werd beginnend falen van het starre schuim vastgesteld bij 5% verlenging. Dit was te wijten aan scheurvorming in de polymeermatrix en onthechting tussen het polymeer en de cementmatrix. Volledige onthechting trad op bij een verlenging van 16%. Voor een flexibele, continue polymeerfilm werd onthechting waargenomen voor het bereiken van 50% rek. In de veronderstelling dat de hechting voldoende is, wordt er voorgesteld gebruik te maken van polymeren met een hoge elongatiecapaciteit (> 100%) en elasticiteitsmodulus lager dan 10 MPa als helend agens voor realistische bewegende scheuren.

De weerstand van geheelde mortelprisma's tegen hoge hydrostatische waterdruk werd eveneens getest. De resultaten toonden aan dat de geheelde scheuren bij hoge waterdruk (getest tot 2 bar = 20 m waterkolom) afgedicht bleven. Daarnaast werden ook vermoeiingstesten uitgevoerd waarbij de scheur een cyclische beweging onderging. Simultaan werden ultrasoongolven door het proefstuk gestuurd. Er werd vastgesteld dat de rekcapaciteit van het SLV polymeer bij éénmalige heropening van de scheur ~ 50% bedroeg terwijl na honderden buigcycli de rekcapaciteit gereduceerd werd tot < 20% (relatief t.o.v. de originele scheuropening).

In aanvulling op de kleinschalige testen op mortelprisma's werden ook grootschalige testen uitgevoerd op betonproefstukken. In eerste instantie werden de capsules manueel op hun plaats gebracht. Met ultrasone transmissie-analyse was het mogelijk heling te detecteren en op te volgen: de amplitude van de ontvangen ultrasoonpuls steeg voornamelijk gedurende de eerste 10 uren na scheurvorming en stabiliseerde na 48 uren. De betonproefstukken met één enkele scheur werden in buiging herbelast. Omwille van het feit dat een groot gedeelte van het scheuroppervlak geheeld was, werd een behoorlijk sterkte-herstel van 47 of 74% vastgesteld, afhankelijk van de dimensies van het proefstuk. Het herstel in stijfheid bedroeg 19% of 75%. Ook andere niet-destructieve technieken werden ingezet. Vibratie-analyse was gemakkelijk te implementeren en kon de daling en stijging van de elasticiteitsmodulus van het beton detecteren respectievelijk na scheurvorming en heling. Het feit dat akoestische events konden gelokaliseerd worden, maakt akoestische emissie-analyse extreem nuttig. Op deze manier kan men immers garanderen dat specifieke emissies te wijten zijn aan schade die optreedt in de geheelde sectie.

Verschillende configuraties van capsules werden getest en hun potentieel voor opschaling werd beoordeeld. Terwijl sferische, polymerische microcapsules niet braken bij scheurvorming, waren cylindrische, polymerische capsules niet in staat het prepolymeer, dat uithardt onder invloed van vocht, stabiel te bewaren. Voor vochtgevoelige helende agentia bleken cylindrische, glazen capsules het meest geschikt. Deze capsules breken bij het ontstaan van zeer fijne scheuren in beton (~ 25 μm) en overleven het mengproces indien hun wanddikte tenminste 0,5 mm bedraagt. Een mechanisme om de capsules onder druk te plaatsen werd ontwikkeld, wat leidde tot een aanzienlijke verbetering van de vrijlating van het prepolymeer.

De finale opgeschaalde techniek werd getest. Hierbij werden glazen capsules (lengte = 30 mm; wanddikte = 0,5 mm) ingemengd in beton. Doseringen van 13 en 36 capsules per liter beton werden gehanteerd. In de betonproefstukken werden meerdere scheuren gecreëerd, maar slechts 2 van 6 scheuren vertoonden een goede dichting bij het aanbrengen van een hoge waterdruk. Naar schatting zouden ~ 50 capsules per liter beton vereist zijn om een degelijke afdichting te bekomen. In laatste instantie werd een kostenanalyse uitgevoerd waarbij de vermelde techniek vergeleken werd met alternatieve oplossingen. In vergelijking met een traditioneel betonherstel, zou het toevoegen van capsules met

helend agens aan het volledige betonelement te duur uitvallen. Toepassing van zelfhelend beton in de buitenste laag van het betonelement (5 cm) reduceert de kost met 19% in vergelijking met conventioneel herstel. Het plaatsen van bijkomende wapening zodat de scheurwijdte lager gehouden wordt dan 0,05 mm is echter het goedkoopste alternatief om scheurdichting te verkrijgen.

SUMMARY

Self-healing concrete aims at the autonomous healing of small cracks, with widths in the order of a few hundred micrometers. This way, the service life of reinforced concrete structures can be extended and their watertightness guaranteed for longer periods. Self-healing technologies studied so far are based either on promoting the autogenous self-healing that occurs naturally in concrete or on the addition of encapsulated healing agents.

With self-healing concrete based on encapsulated polymer precursors, capsules rupture upon crack formation and the precursors flow to fill the crack and subsequently cure to form a cohesive polymer bonding the opposite sides of the crack. Most importantly, polymers cover a wide range of mechanical properties that may allow overcoming the high stiffness and brittleness of mineral materials filling the cracks when other self-healing technologies are employed. Such mechanical properties of the healing material are thought to result in the reopening of healed cracks or the formation of new ones if the loading on the concrete element is increased or has a cyclic nature.

The major motivations behind the research presented here were the assessment of the fitness of commercial precursors for self-healing of active cracks and the upscaling of the technology, whose bottleneck was the inability of the capsules to survive when mixed into concrete. As with other emerging technologies, self-healing concrete lacks straightforward test methods to assess its performance, especially those that simulate field conditions, so the development of test methods was also a major motivation.

Several moisture-curing precursors of polyurethane were selected for screening based on their low viscosity (required for good dispersion inside a crack) and high elongation and adhesion to concrete (required for healing of active cracks). The precursors tested resulted in 8 series, which covered a wide range of properties in terms of viscosity, foaming potential and mechanical properties after hardening. The screening tests were performed on mortar prisms with a single crack and containing glass capsules with thin walls of 0.18 mm. Series SLV

(polyurethane of super low viscosity) stood out as the best performing due to its better dispersion upon release from the capsules and a reduction of water uptake through the healed cracks, to the level of sound specimens. This polymer was able to withstand a strain level of at least 50%, after which it detached from the crack faces, which may be below the crack movement magnitude found in some field structures.

A study was performed to assess the fitness of continuous monitoring methods to detect failure due to excessive strain on polymers bridging active cracks and to highlight the consequences of using stiff polymers for this application. Detection of failure through acoustic emission analysis coupled with DIC was possible only in case of failure due to brittle fracture of a rigid foam after 9% strain, which generated high-energy acoustic events. Direct observation of interfaces with SEM in-situ loading allowed determination of failure of a rigid foam due to cracking of the polymer matrix and detachment at the interface with the cementitious matrix, with an onset at 5% strain and complete detachment at 16% strain. For a flexible, continuous film of polymer based on a non-foaming precursor, detachment occurred before 50% strain. Assuming adequate adhesion, polymers with high elongation (>100%) and modulus of elasticity much lower than 10 MPa are suggested if cracks subjected to a realistic amplitude of movement are targeted.

Healed mortar prisms were also tested for their resistance against high hydrostatic pressure and fatigue due to cyclic crack movement, with the latter involving parallel monitoring with transmitted ultrasound pulses. The healed cracks remained sealed under all pressures tested, up to 2 bar (or 20 m of water column). Strain limits were overall reduced to below 20% of the original crack size due to fatigue under hundreds of bending cycles, while under a single cycle the strain limit of the SLV polymer had been determined to be around 50%.

Performance assessment proceeded at a large scale with concrete specimens healed with the best performing SLV precursor, but still using pre-placed glass capsules. With ultrasound transmission analysis it was possible to detect and monitor healing, as an increase of maximum amplitude of ultrasonic pulses occurred mostly during the first 10 hours after cracking and stabilized after 48 hours. The concrete specimens containing a single healed crack were loaded under bending and a considerable 47% or 74% regain of strength, depending

on the dimensions of the specimens, was achieved due to healing of a large part of the cracked plane, while stiffness increased by either 19% or 75%. Trials were performed with additional non-destructive techniques. Vibration analysis was easy to implement and able to detect both a decrease and an increase of elastic modulus of the concrete specimens respectively after cracking and after healing. Localization of acoustic events made acoustic emission analysis particularly useful, as it allowed guaranteeing that specific emissions were due to damage occurring at the healed section.

Several configurations of capsules were tested in order to assess their potential for upscaling of self-healing concrete. While spherical polymeric microcapsules did not rupture when crossed by a crack, cylindrical polymeric capsules were not able to keep a moisture-curing polyurethane stable. Cylindrical glass capsules were then determined to be the best encapsulating technique when moisture-sensitive healing agents are used. They also ruptured when crossed by very small cracks in concrete of ~25 μm and survived concrete mixing if their wall was at least 0.5 mm thick. A mechanism for pressurizing the capsules was also developed, leading to a considerable improvement of the release of precursor.

To test a final upscaling solution, glass capsules 30 mm long and with a wall thickness of 0.5 mm were mixed into concrete at a dosage of 13 and 36 capsules per litre and moulded into specimens, on which multiple cracks were created. Partial success was obtained, as 2 out of 6 cracked planes were well sealed when tested for water flow under high pressure. A higher dosage of capsules, estimated to be about 50 capsules per litre would be required to achieve a consistent sealing effect. Finally, a cost assessment of this solution was performed and compared to alternative options. Addition of capsules to a whole concrete slab would be too expensive compared to a typical repair action. If self-healing concrete is applied only to the outer 5 cm layer of the concrete element, the cost of this solution becomes 19% cheaper than conventional repair, but still more expensive than the cheapest alternative solution to achieve sealed cracks, which is using additional reinforcement to keep the crack size below 0.05 mm.

1. INTRODUCTION

1.1. Mechanisms of self-healing in concrete

Materials possessing self-healing properties are automatically repaired without external intervention, if the damage is not too severe. This phenomenon can be found in natural materials, such as bone, skin or wood, but during the last few decades sustained research has been performed on engineered self-healing properties within most groups of materials, including the metal, ceramic, polymer and bituminous groups, but also the cementitious group, which includes concrete.

Generally, self-healing can be achieved either through the intrinsic properties of a material (autogenous healing) or by embedding a healing agent in its matrix (autonomous healing). The almost utopian concept of automatic repair is aligned with the demand for sustainability of modern societies. If repair starts automatically upon the onset of damage, the material lasts longer and the product or structure made of such material has its service life extended, thus delaying the need for replacement or for external repair action. With a delayed need for replacement, less raw materials are consumed, which improves environmental sustainability, while the lack of need for repair actions improves economical sustainability, as long as the additional cost of implementing self-healing properties is considerably below the cost of repair actions, which usually require expensive labour.

Within the materials with potential self-healing properties, the case of concrete is unique, since damage in the form of small cracks is unavoidable and expected due to its brittle nature (virtually no ductile deformation) and low strength under tensile stress. Thus, in reinforced concrete structures, cracks of up to 300 μm wide are generally allowed by design codes (e.g. ACI 2001, CEN 2004a). Even larger cracks can be allowed in case they are aesthetically tolerated, as the larger the crack, the easier it is to detect it. Another unique aspect of concrete is its intrinsic self-healing properties, i.e. autogenous healing, which can happen due to different mechanisms. Especially inside cracks developed during the

early ages of concrete, cement particles that remain unhydrated can hydrate and fill the crack with hydration products. Another possible mechanism of autogenous healing is the carbonation of $Ca(OH)_2$ leached from the cementitious matrix, with accumulation inside the crack of the resulting $CaCO_3$. Particles carried by flowing water can also settle and seal the crack. It is thus clear that the presence of water is required for autogenous healing to occur, but also required is a certain degree of crack size restriction, although the reported maximum crack size that can be healed through autogenous healing varies considerably, e.g. values in the range 10-300 μm have been reported by different authors (Van Tittelboom and De Belie 2013). Based on this, and because the reported healing products formed are equally diversified (Huang et al. 2016), it can be concluded that autogenous healing is a highly inconsistent and unpredictable method of self-healing.

Some of the mechanisms of engineered self-healing (i.e. autonomous healing) aim at stimulating the naturally occurring autogenous healing. An example of these methods is the partial replacement of cement by conventional supplementary cementing materials such as fly ash and blast furnace slag, which remain unreacted for longer periods, thus increasing both the amount of particles available for hydration at the moment of cracking and the volume of hydration products filling the crack. Addition of superabsorbent polymers (SAPs) to the concrete matrix can also stimulate autogenous healing by increasing the availability of moisture during dry periods. This is due to the fact that particles of SAPs can absorb several times their weight in water and slowly release it to the surrounding environment. An additional mechanism occurring with the addition of SAPs is the immediate sealing of cracks upon water ingress into the cracks. As the SAP particles located at the crack's faces swell, they partially or completely seal the crack. The seal is lost during dry periods, as the SAP particles shrink and release the contained water, but it is regained as soon as water flows into the crack again. Current challenges regarding this research topic involve the control of the swelling kinetics of SAP particles, so that swelling in the early, fresh state of concrete is avoided, as this would result in large voids in the concrete matrix and reduced mechanical properties. This can be achieved by coating the SAP particles with a degrading layer that temporarily isolates them from the surrounding water and that should last until the concrete hardens (Pelto et al. 2016). SAPs with pH-responsiveness that have considerably

reduced swelling capacity in cement filtrate, which simulates the exposure to water in fresh concrete, have also been achieved by Mignon et al. (2015).

A comprehensive overview of these self-healing mechanisms and the remaining ones mentioned throughout this section has been compiled in multiple, recent publications (De Rooij et al. 2013, Van Tittelboom and De Belie 2013, Huang 2016) that can be consulted for additional details and thorough lists of research papers on each mechanism.

A particularly ingenious mechanism of self-healing is the addition to concrete of bacteria that precipitate $CaCO_3$. Dormant bacterial spores are added to concrete along with the required nutrients, which they metabolize as soon as abundant water and/or oxygen are available, which occurs once a crack develops in the concrete matrix. The metabolism can differ depending on the type of bacteria, but it results nonetheless in the precipitation of $CaCO_3$ inside the crack. However, the alkaline environment of the concrete matrix can damage the bacteria, which require protection through encapsulation or by embedding them in a protective material. An important advantage of bacterial healing is the large volume of healing material that can be generated by bacteria, with the precipitated $CaCO_3$ crystals occupying many times their volume inside a crack, as shown in Figure 1.

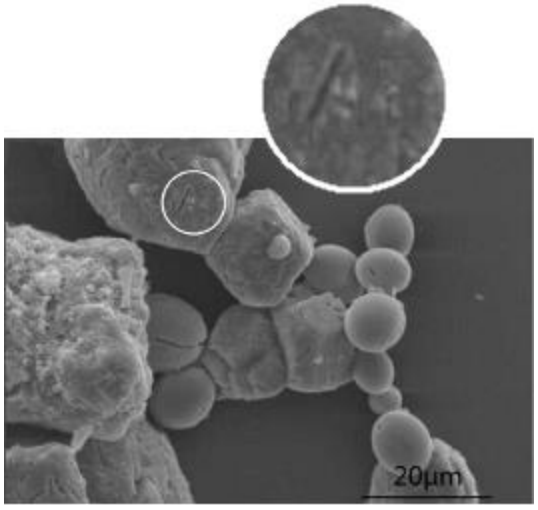

Figure 1: contrast between the large volume of $CaCO_3$ crystals and the size of precipitating bacteria as shown by their highlighted imprints (Xu et al. 2015).

This is probably the autonomous self-healing mechanism that is the easiest and potentially the cheapest to implement at a large scale. Field projects led by Delft University have already implemented it in a large liquid containing structure in The Netherlands and in an irrigation canal in Ecuador (Sierra-Beltran et al. 2015).

Another major mechanism of self-healing concrete is achieved by adding encapsulated polymer precursors to a concrete matrix. This was the approach used in the research described in this book. With this technique, capsules rupture upon crack formation and polymer precursors are released, which flow to fill the crack and subsequently cure (harden) to form a cohesive polymer bonding the opposing faces of the crack. A substantial difference to the other self-healing mechanisms described is the time necessary for healing. Upon cracking, there is an immediate release of a large amount of polymer precursor, which hardens within hours, depending on the type of polymer, thus completing the healing process. This contrasts with the several weeks usually needed to fully heal cracks in the size range of 200-300 μm by the other mechanisms mentioned. This is shown in Figure 2, where the evolution in time of the healing process inside a crack is displayed for both a mineral admixture and a polymeric healing agent.

Other mechanisms of self-healing include the addition of mineral and chemical admixtures that react with the elements in the cementitious matrix and expand or swell when in contact with water. These compounds can also be encapsulated to guarantee that they are active only upon cracking of the concrete matrix. A particularly interesting aspect of this mechanism is the possibility of achieving amorphous, gel-like healing materials, as reported by Litina (2015).

Finally, vascular systems have also been used to improve the self-healing properties of concrete. These mimic the function of veins in supplying to the damaged areas the compounds that are involved in the healing process. Continuous tubes are installed inside the moulds of the concrete element before placement of concrete. When the hardened concrete element cracks, the tubes rupture at the cracked sections and release the healing agent that had been previously loaded into the tubes. The latest developments include field trials of concrete panels with an embedded vascular system combined with tendons of shape memory polymers, which can shrink to partially close cracks (Pilegis et al. 2016).

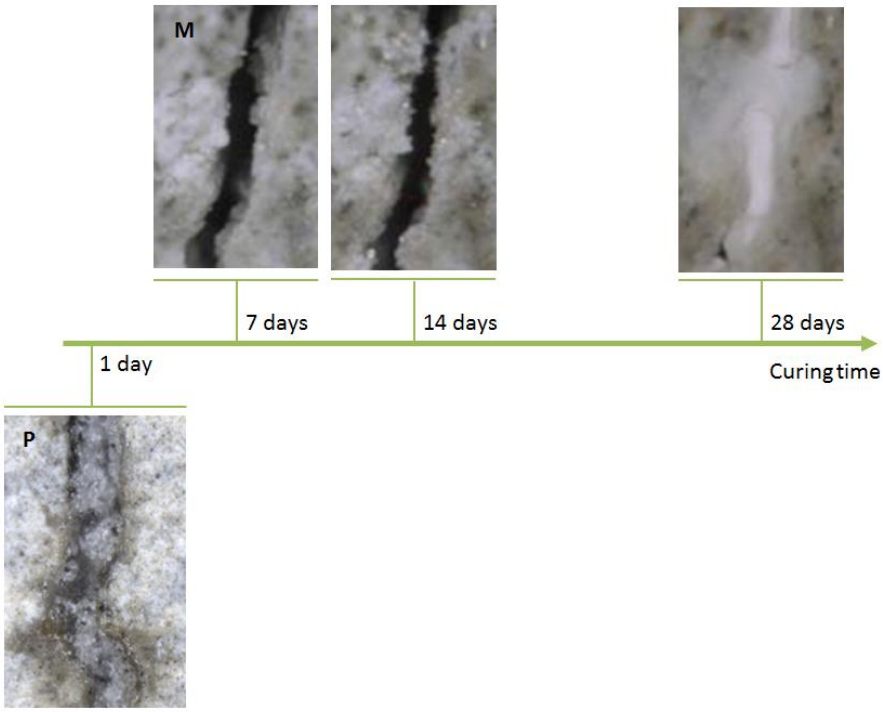

Figure 2: slow evolution of healing based on (M) mineral admixtures (Ahn and Kishi 2010) compared to (P) encapsulated polymer precursors (Feiteira et al. 2016).

1.2. Field of application

A first important differentiation in terms of field of application is related to the type of cracks that need healing: either early age cracks formed in plastic concrete or cracks developing in hardened concrete. ACI (2007) provides a thorough and detailed description of the multiple causes of the two types of cracking.

Early age cracks can occur due to plastic shrinkage of concrete, caused by uncontrolled evaporation of moisture from surface concrete or self-desiccation of the cement paste (autogenous shrinkage). They can also occur due to excessive thermal gradients in large concrete elements or due to settlement, which is potentiated when voids are present between the poured concrete and restraining elements such as rebars or formwork. For this type of cracks, bacterial self-healing or self-healing mechanisms that promote autogenous healing would

usually be best suited, as long as they are not encapsulated. The reason for this is that most encapsulated healing agents are released after a mechanical trigger, i.e. after the stresses responsible for crack development also rupture the capsule. During the plastic phase of concrete, its load bearing properties are not fully developed, but it's also unlikely that the bond between capsules and cementitious matrix is fully developed, thus rupturing of capsules is equally unlikely. SAPs are particularly well suited for minimizing autogenous shrinkage, as they can release the absorbed water which is then available for the internal curing of concrete.

In hardened reinforced concrete, cracks can develop unexpectedly due to a number of reasons, including poor practices and overloads during construction, which can be more severe than those experienced in service (ACI 2007). However, as mentioned in the previous section, reinforced concrete is designed to crack even under the expected service loads.

While these cracks allow permeation of water and gases involved in different deleterious phenomena of concrete, even design codes (ACI 2001) remark that their role regarding the overall durability of concrete structures is controversial. Raupach (1996) showed that while an increasing crack size (within the range 100-500 μm) reduces the time for onset of corrosion, the long term steel mass loss after 2 years was almost independent of crack size. Concrete composition and thickness of the concrete cover had a much higher effect on corrosion-related durability. This seems to be the reasoning behind the European design code (CEN 2004a), which limits crack size to a fairly large 400 μm and specifies instead different levels of thickness for the concrete cover to guarantee durability under a certain environmental exposure scenario.

However, even if the size of cracks is not clearly correlated with corrosion and durability, cracked concrete is still considerably more susceptible to corrosion than sound concrete. Van den Heede et al. (2016) estimated that 0.3 mm cracks reduce the time for depassivation of steel and onset of corrosion from 104 years (sound concrete) to 8 years. One of the potential applications of self-healing is thus guaranteeing the durability of concrete structures that require an extra-long service life or are exposed to aggressive environments. Examples of these structures are shown in Figure 3. Self-healing must, of course, have a favourable cost when compared to alternative repair actions, which require labour

and thus are usually expensive. The same study by Van den Heede concluded this to be true for encapsulated polymer precursors if the cost of encapsulation is kept low. However, in specific cases, repair actions can be difficult to perform due to limited accessibility and in this situation concrete with self-healing properties will have an advantage, regardless of its cost.

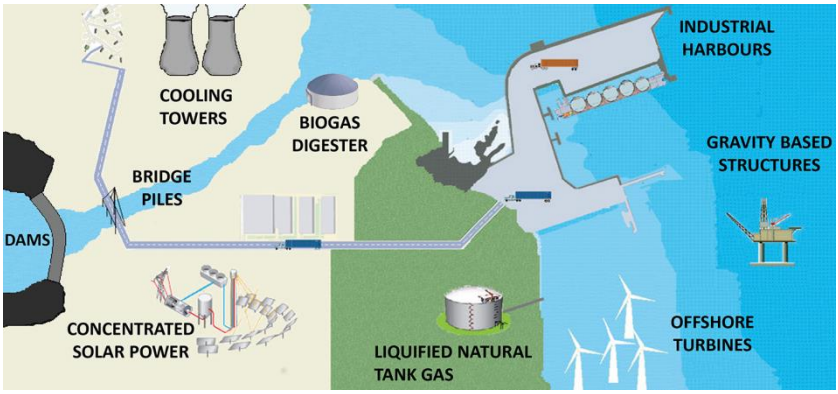

Figure 3: examples of reinforced concrete structures that might benefit from self-healing properties (Simon 2016).

Other than structures that are particularly demanding in terms of durability, self-healing might also find an application in liquid containing structures for which leaking is unacceptable. Examples of these structures are also shown in Figure 3. Crack size seems to be a more critical factor in the permeability of cracked concrete than in the corrosion of reinforcing steel. The permeability of cracked concrete is more than 6 orders of magnitude higher than sound concrete and it increases exponentially in function of the crack width (Akhavan et al. 2012). The non-linear increase of permeability in function of the crack size is widely reported and it is particularly severe in the range 0.05-0.2 mm (Wang et al. 1997). For crack sizes lower than 0.05 mm it is expected for a water flow to stop within a few weeks due to self-healing, even if under hydrostatic pressure (Edvardsen 1999 and Reinhardt and Jooss 2003). For ACI (2001) the allowed crack size for water retaining structures is 0.1 mm, while Eurocode 2 (CEN) specifies a size between 0.05 mm and 0.2 mm, depending on the ratio between hydrostatic pressure and the thickness of the element and for situations where leakage has to be limited. For situations where only minimal leakage is allowed or no leakage is permitted, liners or prestressing steel have to be used. Self-

healing concrete can be a valid alternative to these measures or to the massive usage of reinforcing steel required to achieve crack sizes as low as 0.05 mm, especially since a dense mesh of steel can increase the difficulty of placing and compacting concrete. Van den Heede et al. (2014) reported that in a slab element the amount of steel necessary to reduce the maximum crack size from approximately 0.2 mm to 0.05 mm more than doubled.

2. MOTIVATION

2.1. Self-healing of active cracks

The techniques that promote autogenous self-healing, such as the addition of superabsorbent polymers or the use of supplementary cementing materials, rely on cement hydration products and precipitated $CaCO_3$ to fill the cracks. The same can be said of bacterial autonomous self-healing, which also relies on $CaCO_3$ as healing material. Compared to these techniques, an advantage of encapsulated polymer precursors is the fact that polymers can be found in a wide range of mechanical properties and have good adhesion to most substrates. Most importantly, polymers allow overcoming the high stiffness and brittleness of mineral materials filling the cracks when the other self-healing techniques are employed. Such mechanical properties of the healing material are thought to result in the reopening of healed cracks or the formation of new ones if the loading on the concrete element is increased or has a cyclic nature. This has been confirmed by Dry et al. (2003), who studied polymers with distinct stiffness. Dry et al. found that the use of polymers with high stiffness such as cyanoacrylate resulted in new cracks formed during loading of healed specimens, while an undisclosed foaming agent and a silicone-based polymer with lower stiffness resulted in reopening of the original crack.

Motivated by the scarce data available on this topic, one of the main original contributions of the research presented in this book is the assessment of the strain capacity of polymers while bridging healed cracks, i.e. the magnitude of crack movement the polymers can resist before failure in this application. The strain capacity is a performance parameter that, while not yet found in the relevant literature published to date, is of extreme importance for the implementation of self-healing technologies in real structures, considering that active cracks are very often present due to temperature gradients or traffic loads.

The lack of available data is also true for long term monitoring data of cracks in field concrete structures and thus there is no clear indication of what should be

the target strain capacity for polymers bridging active cracks. However, a 100% elongation seems to be a reasonable performance requirement, considering that cracks are expected to double their width in the long term due to fatigue caused by cyclic loading (ACI 2001). On the other hand, a 10% elongation has been set elsewhere as a requirement for injection products used for the repair of active cracks (CEN 2004b). It is, however, a requirement for daily crack movements, which realistically should be expected to increase in the long term.

A single cycle of crack movement in a field structure can also often exceed 10% of the original crack size. Cruz and Raupach (2016) reported that crack movements of approximately 30% were found in a waterway structure. Criel et al. (2014) also reported crack movements much larger than 10% on real scale T-beams designed according to Eurocode 2. Testing of these beams under laboratory conditions included multiple events exceeding the quasi-permanent load, simulating construction loads at an early age of the concrete element. During these events, the average crack size in the beams increased from 0.14 mm to 0.30 mm, a crack size increase of 114%. The magnitude of crack movements found in field structures is however seldom reported in the literature, but anecdotal reports have also mentioned the existence of crack movements in excess 100% by many times due to high loads from traffic on bridges.

2.2. Encapsulation and upscaling

At the start of the research program described in this book, the most obvious bottleneck for upscaling of self-healing concrete based on encapsulated polymer precursors was the encapsulation itself. The challenging part of encapsulation seemed to be finding capsules that could be added to fresh concrete during mixing. Used in this way, as an addition for concrete, capsules would need to withstand the mechanically aggressive mixing process, while at the same time being able to rupture when crossed by cracks of a typical size in concrete.

Most of the existing studies had been however performed on proof-of-concept, small scale specimens, using pre-placed glass capsules and careful moulding of specimens. Thus, only a few publications addressed the actual implementation of this technology at a large scale, but even those relied on manual pre-placement of the capsules.

Dry (2000) used glass tubes manually placed in large concrete decks to assess healing of shrinkage and shear cracks, but the dimensions of the tubes and their resistance to mechanical stresses during placing were not disclosed. Van Tittelboom et al. (2015) used short glass and ceramic tubes covered in a layer of cement paste and placed at the bottom of moulds for large concrete beams. The cement paste surrounding the glass tubes protected them from the mechanical stresses experienced during casting and the flow of concrete during moulding slightly displaced the capsules into the interior of the concrete element. It is debatable if manual pre-placement of capsules at specific locations is practical at a large scale in field sites. In that sense, capsules that could be used as a typical concrete addition and added during mixing of concrete would be preferable, as they would be compatible with current industrial production of concrete and field practice. Van Tittelboom et al. (2015) also tried protecting the tubes by embedding them in thicker cement paste bars, but still they did not resist mechanical mixing.

Spherical microcapsules containing polymer precursors have already been shown to withstand the mechanically aggressive mixing of concrete (Yang et al. 2011). However, the use of microcapsules in the context of concrete mimics their pioneering use for self-healing of a polymer matrix (White et al. 2001), which targets only the healing of very narrow cracks, in the order of a few micrometres. It is important to consider that an application in self-healing concrete poses very different challenges to the use of microcapsules, as healing of cracks in the range 0.1-0.3 mm is expected. Another important difference is that microcapsules are mixed into a liquid phase when used for self-healing of a polymer matrix, while in concrete they have to be mixed into a much more aggressive phase that includes solid particles.

The liquid polymer precursors are typically released from the capsules after mechanical triggers i.e., once a certain damage level in concrete is achieved, after which a crack crosses the capsule and eventually causes its rupture. However, more complex chemical triggers have also been suggested, by taking advantage of the ingress of chloride ions in maritime environment (Xiong et al. 2015) or the decrease of pH (Dong et al. 2015) in concrete once cracks are formed. These events can act as chemical triggers that induce a progressive degradation of the capsule, thus releasing the healing agent. However, these triggering degradation mechanisms are inherently more complex than mechani-

cal triggers and no evidence is shown that the release can be easily timed under real conditions.

A second major motivation behind the research presented in this book was thus the design and testing of capsules with material properties and geometry that would allow them to be added to fresh concrete during mixing and to rupture under a mechanical trigger once embedded in hardened concrete. Research reported here is limited to the use of glass and polymeric capsules, but alternative materials exist that have been developed by other authors. Van Tittelboom et al. (2011) assessed the fitness of ceramic capsules as carriers for self-healing agents in concrete, Formia et al. (2015) tested cementitious capsules and Minnebo et al. (2016) developed inorganic phosphate cement and clay capsules.

2.3. Collaboration within the healCON project

One final major motivation was the testing of self-healing solutions developed within the European project healCON, but also the development of test methods capable of quantifying self-healing properties whenever the existing methods revealed unfit.

The healCON project was carried within the theme 'Self-healing materials for prolonged lifetime' (NMP.2012.2.1-3) of the Seventh Framework Programme. The project, which started in January 2013, aimed at further developing self-healing concrete to create durable and sustainable concrete structures and was funded by EU-FP7. The coordinator of the project was Prof. Nele De Belie (Ghent University) and the consortium partners included universities, research institutes and industry partners from several different European countries: Acciona (Spain), Avecom (Belgium), Ceinnmat (Spain), COWI (Denmark), Danish Technological Institute (Denmark), Delft University of Technology (The Netherlands), Devan (Portugal), Fescon (Finland), Technical University of Munich (Germany) and VTT Technical Research Centre (Finland).

3. SCREENING OF POLYMER PRECURSORS

This chapter was adapted from the article Self-healing of moving cracks in concrete by means of encapsulated polymer precursors (Feiteira et al. 2016).

While also assessing the healing and sealing efficiency achieved with several polymer precursors, the main original contribution of this chapter is the assessment of their strain limit when bridging healed, active cracks, as stated in this study's motivation. Several commercial precursors with a rheology already optimized for usage in concrete were tested in order to have a wide range of properties available and their compatibility with expected requirements of field structures was assessed.

3.1. Polymer precursors tested

All the precursors used are commercially available as crack injection products for concrete structures. To assure compatibility with the self-healing of active cracks, minimum requirements were set during the selection process, namely a maximum viscosity of approximately 500 mPa·s to allow the agent to flow inside the crack due to capillary forces and, after curing, an elongation of at least 100% and good adhesion to concrete. A low viscosity also allows the liquid precursor to penetrate the capillary pores of the cementitious matrix, thus forming an additional, mechanical bond after hardening. The reaction time is also an important parameter, as even precursors with a viscosity lower than 500 mPa·s will fail to fill a crack if significant curing occurs within seconds. These properties of the selected precursors are listed in Table 1, as sourced from their technical sheets, along with the designations adopted for this study.

All of the chosen precursors are single component polyurethane-based products that cure upon contact with moisture. Although these are commercial products and thus their specific composition is unknown, they can be generally described as the result of a reaction between a polyisocyanate with two or more isocyanate (NCO) groups and a polyol with two or more hydroxyl (OH) groups, thus resulting in a polyurethane precursor, as summarized in Figure 4. Final

curing occurs after contact with moisture in a two-step reaction, from which CO_2 is released, as shown in Figure 5. The release of CO_2 during curing is responsible for the foaming properties of these products.

Table 1: designation and relevant properties of the polymer precursors tested.

Commercial name	Designation	Viscosity	Elongation
HA Flex LV AF	LV	550 mPa·s	100%
HA Flex SLV AF	SLV	200 mPa·s	100%
HA Safefoam NF	FOAM	290 mPa·s	160%

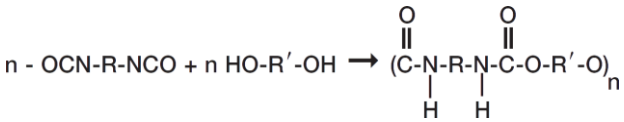

Figure 4: chemical reaction between a polyisocyanate and a polyol to form a polyurethane.

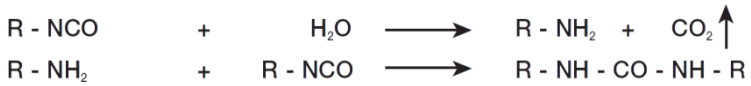

Figure 5: moisture-curing of a polyurethane and resulting release of CO_2.

LV and SLV stand for low viscosity and super low viscosity respectively and can be combined with an accelerator (HA Cut Cat AF), which reduces the time for reaction and induces a foaming effect, which can aid the completely fill the cracks. FOAM shows a strong and immediate foaming action and expansive behaviour upon reaction with moisture with no need for mixing with additional components. The precursors were combined with accelerator or water in order to achieve eight series with distinct properties in terms of viscosity, foaming effect and moisture availability. These series were used throughout the tests described in this chapter and are listed and described in Table 2.

Table 2: designation and description of series tested.

Series	Accelerator	Additional moisture
LV	-	-
LV.W	-	1:1
LV.A	5 wt%	-
SLV	-	-
SLV.W	-	1:1
SLV.A	5 wt%	-
FOAM	-	-
FOAM.W	-	1:1

3.2. Regain of mechanical properties

Although not one of the main motivations of the research work presented in this book, regain of mechanical properties was also determined. Its assessment was performed on healed, realistic cracks created by bending. Non-realistic cracks were also used in the form of mortar specimens separated by spacers and bonded with the polymers studied.

3.2.1. Tensile testing of bonded mortar specimens

Tensile tests were performed on bonded mortar specimens to observe the mechanical response of the polymers under tensile strain, while also providing additional data on the failure mode.

The mortar mix design consisted of cement CEM I 42.5 N, 0/4 mm sand, a cement-to-sand ratio of 1:3 and a water-to-cement ratio of 0.45. Mixing and moulding were carried out according to the procedure described in EN 196-1 and the specimens were cured in high moisture conditions (>90% RH) at 20 °C for at least 28 days.

The tensile tests were performed on Ø50 mm mortar cylinders separated by 0.3 mm spacers and bonded with each series of precursors. A total of 3 specimens was tested for each series.

The bonded mortar cylinders were loaded in displacement-controlled tests at 1 mm per minute, considering the displacement output by the test machine. The strain on the polymers was calculated based on the mean displacement moni-

tored via three LVDTs installed over the bonded section and equally spaced around the cylinder. Given the much lower stiffness of polymers compared to mortar, the displacement measured is then the elongation imposed on the layer of polymer bonding the two halves of the specimen. The specimens were loaded until failure.

The results from this test give a preliminary indication of the fitness of the different polymers studied to the intended application, in particular their capacity to withstand an elongation of at least 100%. For all polymers, an elastic behaviour (i.e. a linear stress-strain curve) was observed but only for very small strains (less than 5%), as shown in Figure 6. This figure shows only the curves for a representative specimen of each series tested. The stiffness calculated at a strain of 2% is shown in Table 3 along with other important parameters.

As expected, the stiffness of non-foaming polymers (LV, LV.W, SLV and SLV.W) was much higher. For these polymers, after the initial linear part of the curves there is a sharp decrease of stiffness and the load drops progressively. For the foaming precursors (LV.A, SLV.A and FOAM.W), the stiffness decreases progressively while the load increases. This can be qualitatively assessed in the curves shown in Figure 6, even though the strain values may lack accuracy due to bending between the two halves of the specimens once the stiffness starts decreasing.

The foaming effect induced by the accelerator is very clear on the stress-strain curves of LV.A and SLV.A (compared to LV and SLV respectively), as the mechanical response changes drastically and approaches that of the FOAM polymer. The addition of water (LV.W and SLV.W), however, had little effect on the mechanical response, suggesting that the limited moisture present in a cement matrix may be enough to guarantee full curing of the precursor.

More importantly, it was shown that the bonding did not fail completely before 100% strain for any of the polymers under study, thus showing potential for withstanding large crack movements. The stiffness decrease observed can be thought of as due to a combination of plastic deformation of the polymers and partial rupture or detachment from the crack walls and thus cannot be directly related to a loss of water tightness, which is assessed in section 3.3. It can already be speculated at this point that the polymers selected have a limited ca-

pacity to create strength regain in healed concrete, due to their low stiffness and strength when compared to the properties of concrete itself.

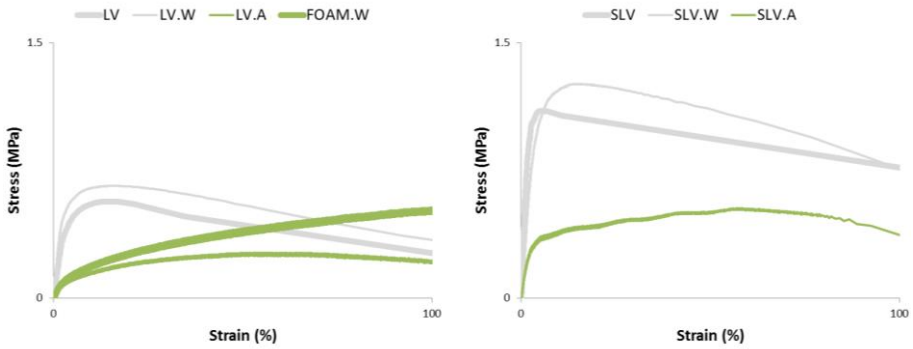

Figure 6: stress-strain curves resulting from tensile loading of cylindrical mortar specimens bonded by polymers.

Table 3: parameters of stress-strain curves shown in Figure 6.

Series	Stiffness (MPa)	Maximum stress (MPa)	Failure mode
LV	9.43 ± 1.97	0.54 ± 0.07	debonding
LV.W	13.68 ± 3.75	0.78 ± 0.16	debonding
LV.A	1.25 ± 0.65	0.25 ± 0.02	debonding + polymer rupture
SLV	29.93 ± 6.67	1.56 ± 0.33	debonding
SLV.W	22.00 ± 4.19	1.21 ± 0.15	debonding
SLV.A	4.63 ± 2.46	0.36 ± 0.17	debonding + polymer rupture
FOAM.W	2.11 ± 0.80	0.47 ± 0.03	partial debonding

3.2.2. Bending of healed mortar specimens

The mechanical performance of polymers was also assessed in mortar prisms containing encapsulated polymer precursors and cracked under a bending load. This way, a realistic crack was created and self-healed once the precursors flowed out of the ruptured capsules.

The polymer precursors were encapsulated in glass tubes with an external diameter of 3.35 mm and a wall thickness of 0.18 mm, cut to a length of 50 mm and sealed with Poly(methyl methacrylate) glue. The same encapsulation meth-

od and materials have been initially used by Van Tittelboom et al. (2011), who investigated which type of material, shape and dimensions of capsules result in efficient release of healing agent. Earlier, Li et al. (1998) had already established the suitability of glass capillaries as carriers through in-situ observation of breakage and release of healing agent. Glass capsules with such a thin wall cannot be mixed with concrete as they are too fragile. However, they are appropriate carriers for testing healing agents at a laboratory scale, where they can be preplaced in moulds.

Realistic cracks were created under bending on 40x40x160 mm^3 mortar prisms reinforced with two Ø3 mm threaded steel bars. The steel bars were fixed in the moulds and a pair of glass capsules was glued to each steel bar with cyanoacrylate glue, at their centre, where a crack is expected during 3-point bending. The final configuration of the specimens is shown in Figure 7.

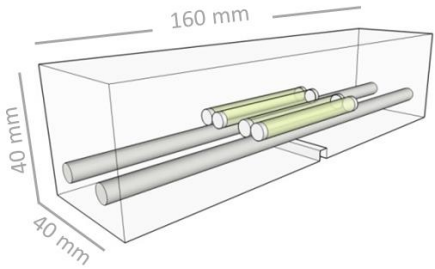

Figure 7: mortar prism used for creating realistic cracks under 3-point bending; capsules were glued to Ø3 mm threaded steel reinforcement bars placed 1 cm from the side and bottom faces.

For each pair of capsules, one capsule was filled with healing agent, while the other one was left empty, or filled with water for the series where it was intended to assess the effect of increased moisture availability. During trial tests, the distance of approximately 2 cm separating both capsules filled with polymer precursors had resulted in most of the crack being covered by the precursors after capsule breakage. For the series including accelerator, this component was mixed with the precursor prior to capsule filling. This mix has been shown to remain stable for several months and reacts only upon contact with moisture. As glass capsules have been shown to act as additional reinforcement (Tsangouri et al. 2013), the specimens contained a square notch of 5 mm (Figure 7) to guarantee that the crack would appear at the middle section.

The reinforced mortar prisms were loaded in displacement-controlled 3-point bending tests at 0.18 mm per minute in such a way that the capsules broke and a crack approximately 0.3 mm wide remained after unloading. This crack opening is mentioned in design codes as the maximum allowed for reinforced concrete structures in most exposure conditions. The displacement measured is the output of an LVDT installed at the middle of the bottom face of the specimen over a span of 20 mm, where the crack is expected. After a period of 3 days at 20 °C and 60% RH, to allow the healing agent to flow and fully cure, mortar specimens with a single healed crack were ready for testing.

During bending of healed mortar prisms, evidence of healing can already be seen. If at least partial healing occurred, a stiffness increase is observed during the reloading of healed specimens, compared to the reloading of non-healed ones. This can be easily seen in Figure 8, which shows the initial part of the curves during reloading, for all the precursors tested.

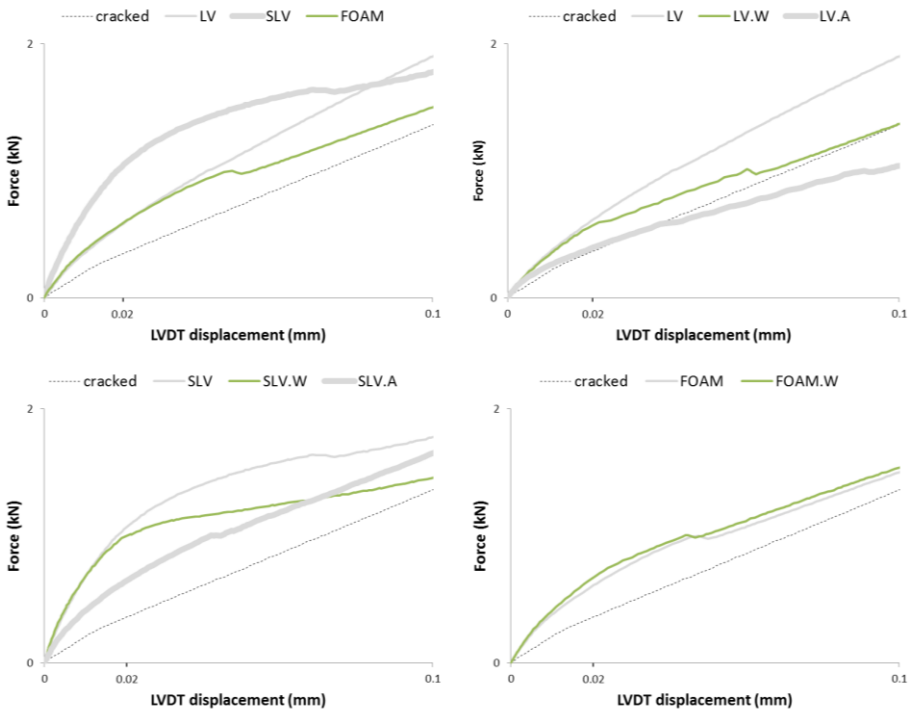

Figure 8: differences in stiffness during bending of healed specimens.

It is clear, by comparing the slope of the force-displacement curve of a healed specimen from the SLV series with the slope of a cracked, non-healed specimen, that there is an obvious stiffness increase due to healing. It is also clear that for specimens healed with the SLV precursor, the stiffness decreases sharply after only a very small crack widening corresponding to an LVDT displacement of approximately 0.02 mm. Both this feature and the overall effect of polymers on the bending stiffness of healed specimens agree with the mechanical behaviour of the polymers determined in the previous section and shown in Figure 6. The stiffness regain achieved with healing in the initial 0.02 mm displacement range is listed in Table 4 for the different precursors. For larger displacements, the stiffness is comparable to that of a cracked, non-healed specimen, as the polymer contributes only with a plastic deformation at this stage, as suggested by the results shown in Figure 6. This type of regain of mechanical properties was calculated according to the formula below.

$$Stiffness\ regain = \frac{S_{healed} - S_{cracked}}{S_{sound} - S_{cracked}} \times 100\%$$

The parameters involved in the calculation are S_{sound} or stiffness of a sound specimen, $S_{cracked}$ or stiffness of a cracked, non-healed specimen and S_{healed} or stiffness of a healed specimen. Stiffness regain varies then between 0% for specimens with no regain and 100% for specimens whose stiffness increased to the level of a sound specimen.

Table 4: average stiffness regain calculated at 0.02 mm displacement during reloading of healed specimens.

Series	Stiffness regain (%)
LV	16 ± 2
LV.W	11 ± 3
LV.A	1 ± 1
SLV	35 ± 2
SLV.W	35 ± 5
SLV.A	20 ± 4
FOAM	16 ± 2
FOAM.W	14 ± 3

The results for the different series agreed qualitatively with the stiffness of the respective polymers, as calculated from the tensile tests and listed in Table 3 and thus the higher stiffness increase compared to cracked, non-healed specimens was observed for the SLV series. However, the area of the crack faces covered by the polymer is also expected to have an effect on the regain. Overall and as expected, the stiffness regain values were low due to the low stiffness of the polymers used.

3.3. Water uptake through healed cracks

To assess the healing efficiency in terms of regain of water tightness achieved with the different series of polymer precursors, the capillary water uptake through healed cracks was determined.

The test procedure was based on the method described in the European standard EN 13057 and consisted of bringing the cracked face of the samples into contact with water and monitoring the mass of water uptake due to capillary absorption. The test was performed on the same specimens described in section 3.2.2., which had a single crack at midspan with a 0.3 mm crack mouth size. Before performing the test, the specimens were partially waterproofed with adhesive aluminium foil, to maximize the effect of the crack on the total amount of water uptake, as shown in Figure 9.

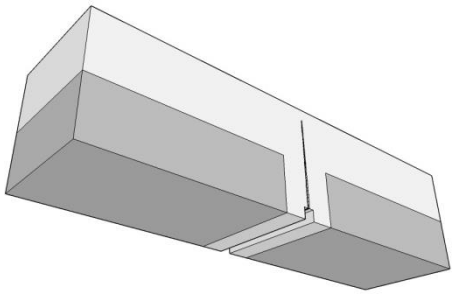

Figure 9: a waterproofing coating of aluminium foil covers the side and bottom faces of the mortar specimen, except for a section of 10 mm to each side of the crack.

The water level in the container did not exceed by more than 2 mm the top of the notch. After the start of the water absorption test, the specimens were weighed frequently for a period of 8 hours (at 15 min, 30 min, 1 h, 2 h, 4 h, 6 h,

8 h), following the removal of the excess of water on their faces with absorbing paper. As the specimens had to be retested following crack widening, after each absorption test, the specimens were dried in an oven at 50 °C so that the total amount of water absorbed during the test was lost, considering a maximum acceptable difference of ±10%. Complete drying to constant mass was not performed to avoid any potential damage to the polymers due to prolonged exposure to high temperatures. Additionally, complete drying was not considered strictly necessary, as small differences in the moisture content of the mortar matrix have a small effect on the results, compared to the water uptake through the crack.

In this test, the water uptake of a specimen containing a fully healed crack would be comparable to that of a sound specimen, while being much lower than the uptake of a specimen containing an open crack. This is shown in Figure 10, where the absorption curve of a specimen healed with the SLV precursor is plotted. Testing of specimens containing partially healed cracks would result in a water uptake between that of sound specimens and specimens with an open crack.

Through linearization of absorption curves, by expressing water uptake as a function of the square root of time, a sorption coefficient (sorption rate) was obtained and used as a single parameter to compare the performance of the different series. The results are shown in Figure 11.

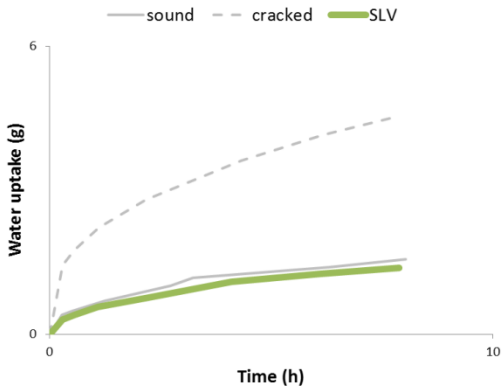

Figure 10: water uptake due to capillary sorption in sound specimens and specimens containing open (cracked) and fully healed (SLV) cracks.

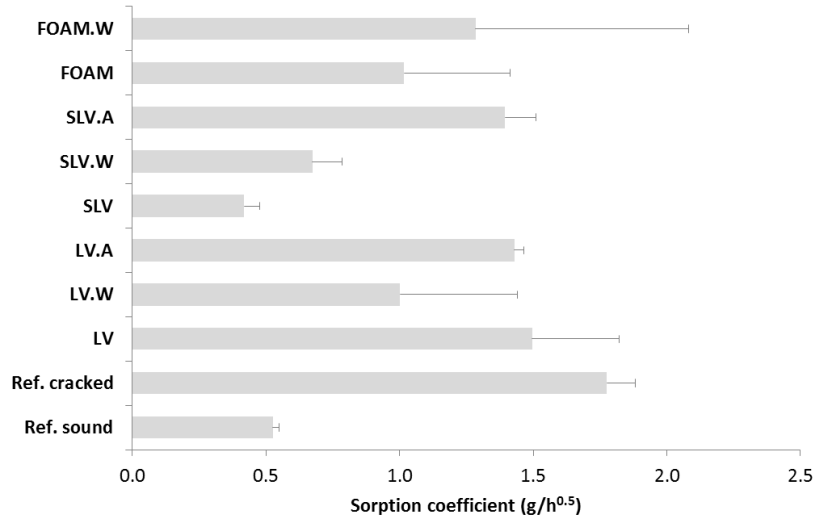

Figure 11: sealing performance of precursors assessed through capillary water uptake through healed cracks; error bars show standard deviation of each series.

Only the use of the SLV precursor led to a significant decrease in water absorption, compared to that of specimens containing open cracks. The sorption coefficient for the series SLV and SLV.W is comparable to that of sound samples, thus proving the full crack sealing achieved with the SLV precursor.

For the LV and FOAM precursors, sealing was only partial, which is shown by the high sorption coefficient approaching that of specimens containing open cracks. Supplying of additional water at the moment of cracking (series LV.W and SLV.W) had little effect on the sealing capacity, while the use of a foaming-inducing accelerator (series LV.A and SLV.A) had a detrimental effect.

During testing, the performance differences between the series were clearly visible, as the water fronts for the SLV and SLV.W series were the only which did not advance along the crack's profile, even after several hours.

The sorption coefficients obtained from linearization of absorption curves were also used to quantify self-healing according to the formula below.

$$Healing\ efficiency = 1 - \frac{SC_{healed} - SC_{sound}}{SC_{cracked} - SC_{sound}} \times 100\%$$

The parameters involved in the calculation are SC_{sound} or average sorption coefficient of a sound specimen, $SC_{cracked}$ or average sorption coefficient of a cracked, non-healed specimen and SC_{healed} or sorption coefficient of an individual healed specimen. The resulting healing efficiency varies then between 0% for specimens with no improvement of water tightness relative to cracked, non-healed specimens and 100% for specimens whose water tightness increased to the level of a sound specimen. The results are shown in Table 5.

Table 5: healing efficiency based on the reduced water uptake through healed cracks.

Series	Healing efficiency (%)
LV	22 ± 26
LV.W	62 ± 35
LV.A	28 ± 3
SLV	109 ± 5
SLV.W	88 ± 9
SLV.A	30 ± 9
FOAM	61 ± 32
FOAM.W	39 ± 64

Results in terms of healing efficiency obviously follow the trend of the water absorption results shown in Figure 11, with the SLV and SLV.W series showing a very high healing efficiency. An efficiency above 100%, as determined for the SLV series means that on average the specimens healed with the SLV polymer precursor absorbed less water than sound, uncracked specimens. This can be either due to a small variability of the mortar matrix in terms of absorption properties or due to the low viscosity SLV precursor impregnating the mortar matrix inside the crack.

3.4. Strain limit

By comparing the capillary water uptake results presented in section 3.3 to those obtained after widening of the healed cracks, the strain limit of the polymers in a self-healing application was determined. Widening of healed cracks was achieved in a stepwise manner, so that the polymer bridging the crack faces

was elongated by 50% and 100% of the initial crack width. Although the loading cycles take place at different times, as capillary absorption tests have to be performed between each cycle, Figure 12 shows all the successive cycles for a specimen healed with the SLV precursor.

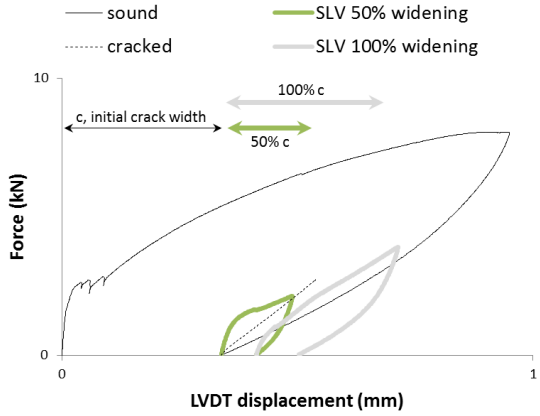

Figure 12: force-displacement curves of cracking and crack widening cycles for healed and non-healed mortar specimens.

Only well healed specimens should be subjected to this procedure and an increase in water uptake is expected if the polymer fails to follow the crack movement, thus making it possible to detect the strain level (or crack opening) at which failure occurred. However, for specimens with cracks that are only partially healed, water uptake can even decrease with an increasing crack opening, as the capillary forces would decrease in the sections of the crack that are not healed.

For this reason, the procedure was only applied to the SLV and SLV.W series that showed high healing efficiency and the results are shown in Figure 13. For both series, the sealing effect remained even after the healed cracks were widened by 50% of the initial crack width. However, after widening of 100%, the sorption coefficient increased significantly, suggesting that the strain limit for the polymer in this application occurs at a strain level between 50% and 100%. Although this guarantees compatibility with the requirements set by CEN (2004b) at a minimum of 10% elongation for polymers used as injection products, it would not be fit for many field structures which are subjected to crack movements above 100%, as discussed in section 2.1.

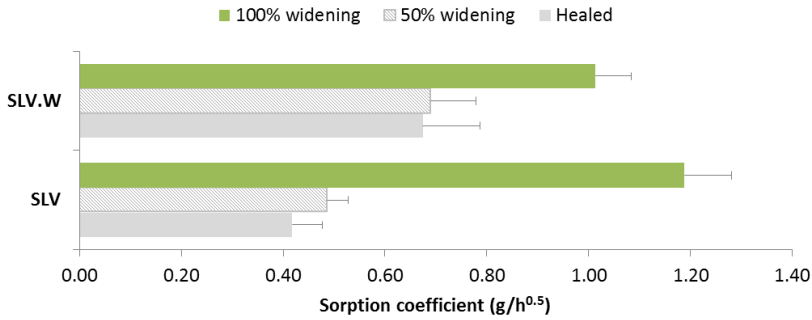

Figure 13: sealing performance of precursors after widening of healed cracks; error bars show standard deviation of each series.

After healing and between each reloading cycle, healed cracks were also observed on a microscope. Images were acquired at the sections of the cracks where polymer could be seen at the face of the specimens. This way, it was possible to assess qualitatively if any local failure had occurred after crack widening and which failure modes occurred. Examples of these sequences of images are shown in Figures 14 and 15.

For the non-foaming products LV and SLV, Figure 14 shows that failure occurred due to detachment from the crack walls between 50% and 100% strain. For the foaming products LV.A, SLV.A and FOAM, failure occurred mostly due to continuous rupture of the closed foam cells, as shown in Figure 15. It was also shown that no new cracks developed alongside the original one after the cracks were widened.

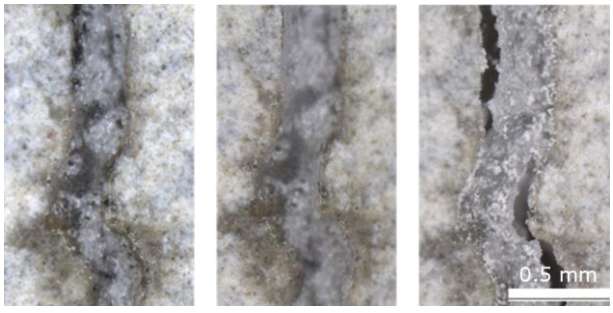

Figure 14: detachment of polymer due to widening of a crack healed with the non-foaming SLV precursor; from left to right: after healing, after widening by 50% and after widening by 100%..

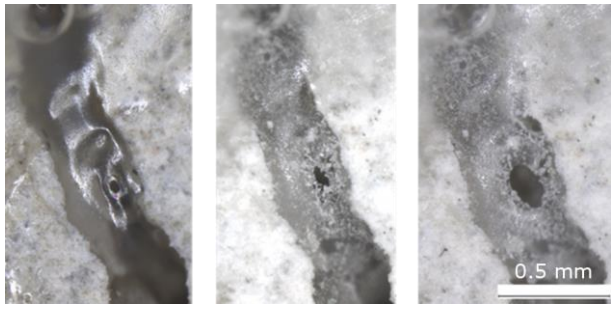

Figure 15: rupture of foam cells due to widening of a crack healed with the foaming FOAM precursor; from left to right: after healing, after widening by 50% and after widening by 100%.

3.5. Healed crack area

A separate set of specimens was moulded with smooth metal bars as reinforcement and later cracked and healed using the same procedure described in section 3.2.2. The smooth metal bars allowed easier splitting of the specimens after the cracks had been healed. This way, the area where the polymer precursor had dispersed to after being released from the capsules could be assessed. Figure 16 shows, highlighted, the area where hardened polymer was found on either of the crack faces. For this figure, the most representative specimen of the overall results of each series was used.

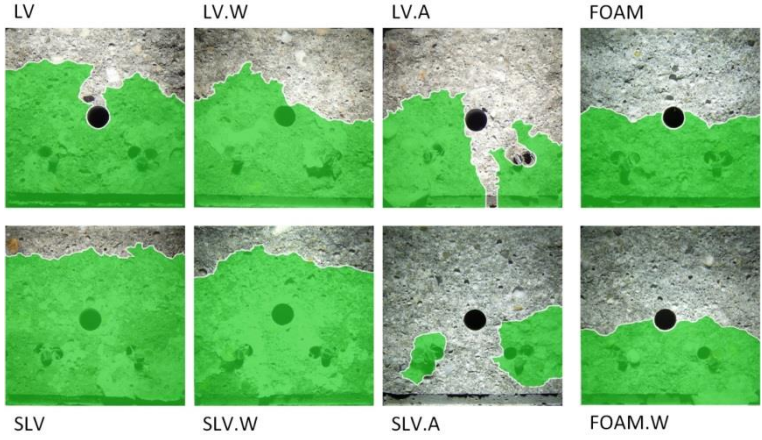

Figure 16: crack faces after complete splitting of the healed specimens; the area highlighted shows the surface that was found covered with polymer.

It is shown that the SLV precursor had the widest dispersion due to its lower viscosity. A supply of additional water in separate capsules slightly reduced the dispersion of the polymer precursor, agreeing with the findings of Gardner et al. (2014), who showed that moisture can limit its capillary rise. The use of an accelerator (series LV.A and SLV.A) considerably reduced the bridged crack area most probably due to the resulting shorter reaction time, as the accelerator had no noticeable effect on viscosity. The potential benefit of an expansive, foaming reaction was not noticed, as the bridged crack area was lower for the FOAM series compared to the LV and SLV series where dispersion occurred mostly due to capillary forces.

More importantly, considering the sealing efficiency of the different precursors, as assessed in the previous section, the results shown in Figure 16 confirm the extreme relevance of the viscosity of polymeric healing agents when a sealing effect is desired. Even though an apparent barrier against water ingress could be found for several of the series according to Figure 16, the results shown in Figure 11 indicate that this barrier is only consistently continuous for the series SLV and possibly for the series SLV.W. It is possible that the cell network of the FOAM polymer is not completely closed, thus still allowing water to be absorbed by capillarity.

3.6. Chapter overview

Eight series based on three different polymer precursors were tested for their healing performance. Series based on the SLV precursor stood out as the best performing and this precursor was thus used for most of the remaining tests described in this book.

The following conclusions were drawn:

- ► stiffness regain was limited and was at best 35% for the SLV series, even when cracks were fully healed; this was a consequence of using flexible polymers and was not seen as a disadvantage, as stiffer polymers would increase the stress at the interface between polymer and concrete matrix, thus increasing likeliness of failure;
- ► only two series, both based on the SLV precursor, showed good healing efficiency (88% and 109%) regarding the blockage of water uptake through healed cracks;

► healed cracks from series with good healing efficiency were widened by either 50% or 100% of their initial crack width and subjected again to water uptake tests; failure of the polymer to keep the cracks sealed occurred at a strain level above 50%, which may not be compatible with all field structures;

► failure of foaming polymers within active cracks occurred due to rupturing of the foam cells, while polymers forming a continuous film failed due to detachment from the crack walls;

► split cracked planes revealed that good healing efficiency resulted from superior dispersion inside the crack, which was promoted by the usage of precursors with lower viscosities; foaming properties had the opposite effect and resulted in a reduced dispersion of the precursor.

4. STIFF VS. FLEXIBLE POLYMERS IN ACTIVE CRACKS

This chapter was adapted from the article Monitoring crack movement in polymer-bas\ed self-healing concrete through digital image correlation, acoustic emission analysis and SEM in-situ loading (Feiteira et al. 2017).

Continuous monitoring techniques were used to monitor the performance of polymers when bridging active cracks, as an alternative to stepwise methods such as the one described in section 3.4. Both flexible and stiff polymers were used and the fitness of the monitoring techniques to detect a potential failure of such distinct polymers to withstand crack movement was also assessed. This part of the study also sets basic requirements for polymers used as healing materials of active cracks. A schematic overview of the research described in this chapter is shown in Figure 17.

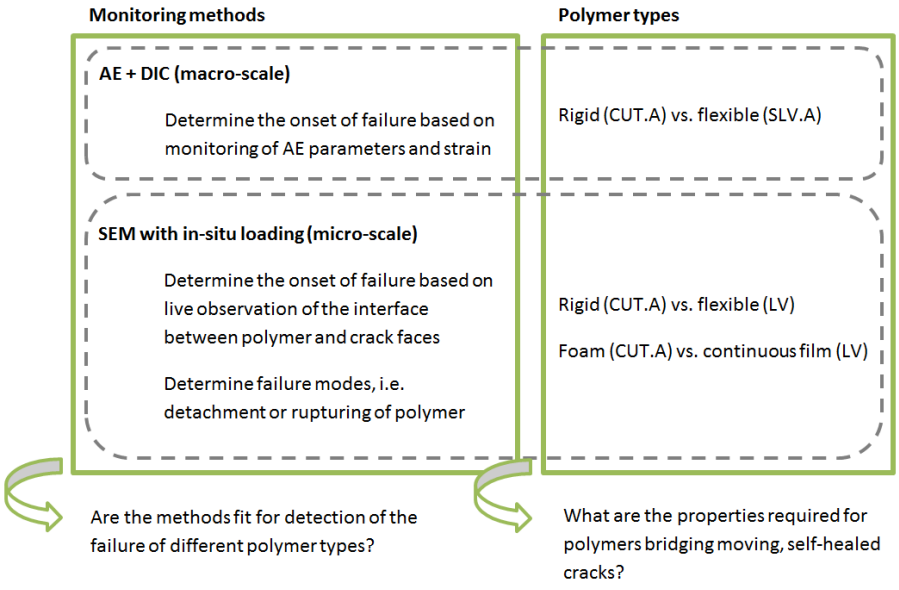

Figure 17: schematic of the research study; see tables 6 and 7 for the description of polymer series LV, SLV.A and CUT.A.

Materials. The precursors designated LV and SLV.A described in the previous chapter were used for this test. These are products curing into flexible polymers, with SLV.A curing into a foam and LV curing into a continuous film. For comparison purposes, the precursor CUT.A was also used and it can be classified also as a foaming product but with a stiffer mechanical response. The viscosity of the products, their potential for foaming and the tests performed on each one are listed in Table 6. To achieve a considerable foaming effect upon contact with moisture, the precursors in series SLV.A and CUT.A were mixed with 2 wt% of a second component (part of the commercial product) which also had an accelerating effect on curing, to avoid collapsing of the foam.

Thin polymer films were prepared by curing the precursors between glass sheets separated by 1 mm thick silicon spacers and exposed to ambient moisture for at least 3 days. The mechanical properties achieved after curing are listed in Table 7, being the average of 5 tensile tests performed at a rate of 1 mm/s (10 mm/s for the high elongation series LV) on 70x10x1 mm^3 specimens cut from the thin polymer films. The test curves are shown in Figure 18 for a representative specimen of each series.

Table 6: basic properties and tests performed on each series of polymer precursors.

Series	Viscosity	Foaming	Testing methods
LV	550 mPa·s	no	SEM with in-situ loading
SLV.A	200 mPa·s	yes	AE + DIC
CUT.A	350 mPa·s	yes	SEM with in-situ loading / AE + DIC

Table 7: mechanical properties of the cured polymer precursors determined by testing thin films.

Series	Tensile strength	Elongation at maximum stress	Elastic modulus	Failure
LV	2.92 ± 0.21 MPa	81 ± 9%	10 ± 1 MPa	ductile
SLV.A	0.20 ± 0.05 MPa	10 ± 2%	5 ± 1 MPa	ductile
CUT.A	0.50 ± 0.26 MPa	4 ± 1%	22 ± 4 MPa	brittle

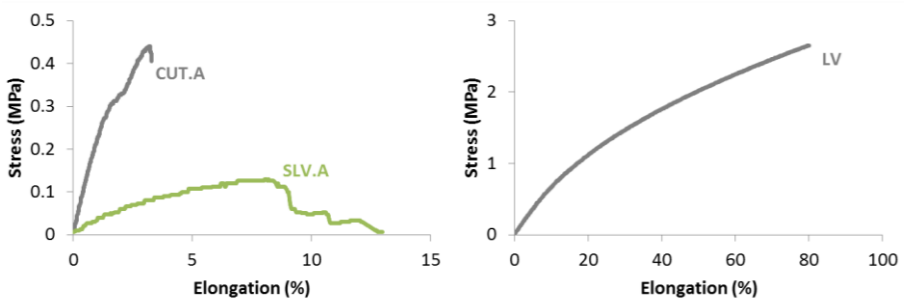

Figure 18: tensile tests performed on thin films of the polymers selected for the study; one representative curve is shown for each polymer series.

4.1. Acoustic emission and DIC analysis of healed mortar specimens

Since the decade of 1970, acoustic emission (AE) methods have been used to capture the full waveforms or parameters of acoustic events occurring in concrete, eventually being developed into a non-destructive technique to monitor and predict damage in concrete structures (Grosse 2008). More recently, it has been used by researchers to investigate the efficiency of novel self-healing techniques applied to concrete, although essentially those based on the naturally occurring autogenous healing (Granger et al. 2007) and on the encapsulation of rigid, brittle polymers, as reported by Malm and Große (2014), Tsangouri et al. (2013) and Van Tittelboom et al. (2012, 2015). In this study, both brittle and flexible polymers are used to assess the fitness of AE analysis to detect their failure by continuous monitoring. This would be of particular interest in the case of flexible polymers, as in the previous chapter no features clearly ascribed to failure could be found in the loading curves of specimens healed with such polymers.

Experiment. Mortar specimens with dimensions 40x40x160 mm^3 were moulded with 2 embedded glass capsules containing either the precursor SLV.A or CUT.A. The tubular capsules had an external diameter of 3.35 mm, a wall thickness of 0.18 mm, a length of 50 mm and were positioned at the midspan of the specimen, where a single crack occurs during 3-point bending. The mortar consisted of cement CEM I 42.5 N, 0/4 mm sand, a cement-to-sand ratio of 1:3 and a water-to-cement ratio of 0.45. Mixing and moulding were performed according to the methods prescribed in EN 196-1 and the specimens were cured in sealed conditions at 20 °C until they were cracked at 47 days of age.

The specimens were also reinforced with a 10 mm wide FRP strip along their length. The FRP was not used as a conventional reinforcement but as a way to stop the crack from reaching the very top of the specimen and avoid complete splitting. Thus, it was positioned in the compressive zone during bending. Figure 19 shows the final specimen configuration, which also contains a notch to guarantee that a crack forms exactly at midspan.

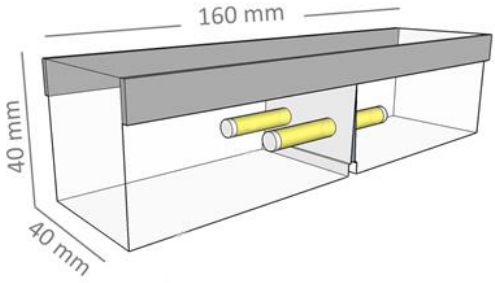

Figure 19: schematic representation of cracked mortar prisms used for AE and DIC analysis; a pair of capsules was placed at the mid-section, 10 mm away from the sides and from the 5 mm deep notch.

A layer of white spray paint was applied on the surface of the mortar specimens and a black speckle pattern was sprayed with an air brush on the surfaces used for the digital image correlation (DIC) measurements. After cracking the specimens in 3-point bending tests, a single crack of ~0.25 mm was obtained and the polymer precursor was left to disperse and cure inside the crack for 3 days at room ambient conditions. The large size of the crack, the dry curing conditions and the short period between cracking and testing guarantee that any existing healing is not due to the naturally occurring autogenous healing.

After curing, one AE sensor Physical Acoustics R15 with a resonant frequency of 150 kHz was attached to the side of the specimens, close to the bending crack, and the specimens were reloaded at a speed of 0.04 mm/min (displacement of the bending machine's piston). As the acoustic events related to damage in a cementitious matrix have low energy, it is necessary that resonant sensors are used, as these amplify the acoustic impulse and transform it into a usable electrical impulse with enough amplitude. The choice of resonant frequency should reflect the type of damage being studied, as acoustic events with a frequency much higher or much lower than the resonant frequency of the sensor

are detected with a reduced amplitude or are not detected at all. Additionally, events occurring increasingly further away from the sensors are also detected with a progressively decreasing amplitude and thus multiple sensors would be preferred. For these reasons, the AE analysis described in this section is seen as a simple, preliminary study and a much larger study would be needed to optimize the setup for the damage being studied, which can include damage in the cementitious matrix, detachment of the polymer from the crack walls or rupturing of the polymer. The acoustic events on each specimen were monitored and recorded until the healed crack was visibly reopened, i.e. a crack width of ~1 mm was achieved.

At the same time, the displacements and strains on one of the side faces of each specimen were also monitored with a pair of DIC cameras capturing high resolution images in a periodical mode, each 2 s. General recommendations for DIC measurements mentioned by Sutton et al. (2009) were followed. This included aligning the cameras on a fixed axis positioned on top of a tripod parallel to the specimen, projecting diffuse light on the area to be tested and performing a calibration analysis with the DIC software package VIC-3D, so that an acceptably low projection error was achieved.

Results. Acoustic emission analysis was performed on two specimens healed with a rigid foam (CUT.A 1 and 2) and two specimens with a flexible foam (SLV.A 1 and 2), to assess its potential for detection of failure of these types of polymers in the context of self-healing concrete. Simple parameter analysis was performed, including the counting of hits, the normalized energy contained in an acoustic emission and the rise angle (RA) of its wave. The RA is considered to be the ratio of rise time to amplitude of the acoustic wave, as suggested by Ohtsu (2010). As the resonant sensors used are only sensitive to a narrow band of frequencies, an accurate analysis of the frequency of acoustic events was not performed.

The mechanical loading of the specimens in itself results in acoustic emissions that are recorded over the thresholds set for the test, even long before any failure stage is achieved. This creates a background noise, above which any acoustic events useful for the detection of failure have to stand. The background noise can be seen in Figure 20, which shows the acoustic hits acquired during loading of a sound specimen until failure, while creating the crack to be healed.

In this plot it is clear that the majority of events is limited to energy levels below 100 and rise angles below 1 μs/dB, with a dense cloud of data shown in these intervals. For this reason, the test results displayed in Figure 21 show the plots of energy and RA truncated below these levels, as any events with an energy level occurring due to failure of polymers within the truncated range would be difficult to distinguish from the background noise.

During loading of the healed specimens, the different series showed similar peak loads and bending stiffness (Figure 21), despite the remarkable differences between the polymers used (see Table 7). This is due to the fact that the loading response is a function not only of the mechanical properties of the polymer filling the crack, but also of the area effectively bridged by the polymer inside the crack due to healing, which inevitably shows variability between specimens. The bending load curves in Figure 21 show differences in the failure mode, which is brittle in case of the rigid CUT.A series (sudden considerable load drop), while a progressive load reduction is observed in the case of the flexible SLV.A polymer. The progressive load drop of the specimens healed with a flexible polymer is in line with the experience described in chapter 3 and the lack of clear features pointing to failure was a major motivation to assess the potential of AE analysis to detect it.

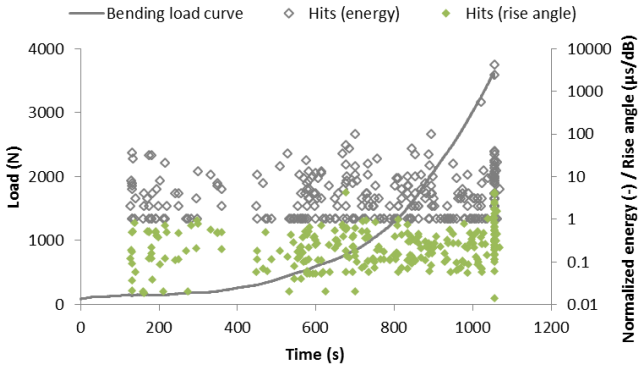

Figure 20: bending load, acoustic hits and relevant acoustic emission parameters until failure of a sound specimen; the cloud of data points acquired before failure establishes the background noise of the tests.

Regarding the data acquired by AE analysis during loading of healed specimens (Figure 21), although no correlation was observed between the total number of

acoustic events and the type of polymer, vertical discontinuities can be seen in the cumulative hits curves for the CUT.A precursor (time window 200-300 s), which occur during the brittle failure. The vertical discontinuities are related to a sudden burst of acoustic events occurring due to the catastrophic failure occurring for the series healed with the brittle polymer.

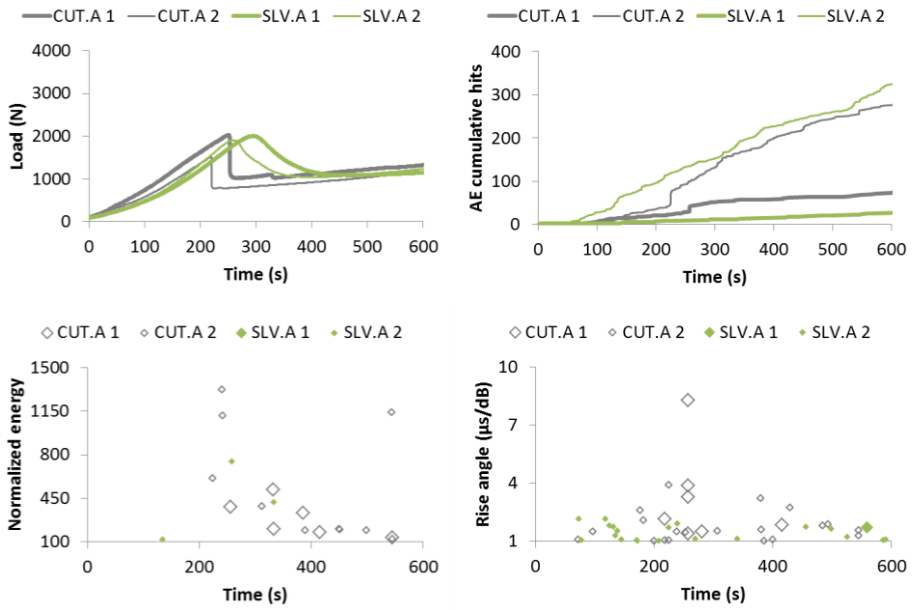

Figure 21: bending load curves, acoustic hits and relevant acoustic emission parameters during widening of healed cracks.

For the specimens healed with the rigid CUT.A polymer, there were high energy hits (energy >100), coinciding with the peak load and sudden load drop, which can thus be attributed to brittle failure. Several other high energy hits were detected during subsequent crack widening, in a total of 16 hits for both specimens together. These high energy hits have energy levels at least one order of magnitude above most acoustic events taken as background noise, which makes them particularly fit for monitoring of failure. In the case of the flexible polymer SLV.A, there were two hits above the noise level for the SLV.A 2 specimen, with one coinciding with the peak bending load, but none for the SLV.A 1 specimen. The lack of high energy hits in the case of the flexible SLV.A polymer can be explained by the fact that the acoustic emission compo-

nent (as opposed to plastic deformation or surface energy) of the energy expended during fracture is generally higher in the case of brittle materials (Pollock 2011), while the mechanical response of the polymer SLV.A shows plastic deformation (Figure 18).

The AE data acquired thus suggests that monitoring of the acoustic wave energy allows clear detection of the onset of failure of concrete healed with brittle polymers, but not with flexible ones. The detection of failure of specimens healed with a flexible polymer may be more clearly assessed through methods that determine the permeability of healed cracks, such as the approach used in section 3.4.

The plot of the rise angle shows that there are hits with high RA (>1 μs/dB) during the peak bending load for the CUT.A specimens, but also before failure occurred. For the specimens healed with the flexible SLV.A polymer, there are also hits with high RA, but they are similarly spread around the peak load. Additionally, all hits with high RA were at best one order of magnitude above the background noise shown in Figure 20. Thus, despite the fact that several hits could be attributed to the brittle failure of the rigid CUT.A polymer, single monitoring of the rise angle does not seem to be fit for accurate identification and monitoring of any potential failure of self-healed concrete, as random acoustic events occur above the noise level.

After unloading the specimens, it was noticed that additional crack branches appeared around the crack mouth of the specimens healed with the CUT.A polymer. Impregnation with fluorescent epoxy resin and visual assessment under optical microscope allowed clear highlighting of all the voids, including parts of the crack mouth that were not filled with polymer and the new crack branches, as shown in Figure 22. The additional cracks probably formed due to the fact that the rigid CUT.A polymer effectively transfers stress across the crack faces, to areas around the original crack that already exhibited a certain degree of damage. It is thus possible that high energy and high RA hits ascribed to the failure of the brittle, rigid polymer also occur due to the development of new crack branches. As both types of event occurred after peak load and most probably at the same moment, the detection of either of them is still a good indication of failure of the specimen at the healed crack due to excessive strain on the polymer.

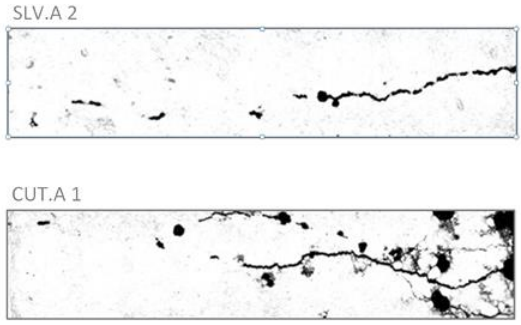

Figure 22: analysis of the voids (in dark) around the crack mouth revealed new crack branches after failure of the specimens healed with the rigid CUT.A polymer.

Parallel DIC analysis conducted for one specimen of each series showed additional evidence of the distinct failure modes of specimens healed with rigid or flexible polymers. Figure 23 shows that at the peak load occurring at approximately 250 s (see Figure 21 for load curves), there was a considerable crack mouth widening for the specimen healed with the CUT.A rigid polymer, while a progressive widening was observed in the case of the flexible SLV.A polymer. This can also be clearly seen both in the monitoring of the cracks' contours along their height (Figure 24) and in the magnitude of the strain developed around them (Figure 25). Given an original crack mouth size of 0.25 mm and considering the displacement shown in Figure 24 for the peak load (the crack mouth is at a height of 0%), the maximum strain on the CUT.A polymer before failure occurred was 9%.

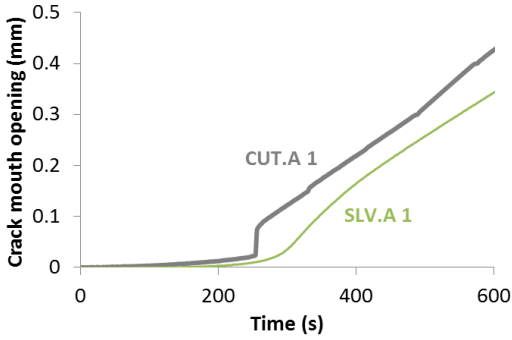

Figure 23: crack mouth opening monitored by DIC analysis during widening of healed cracks.

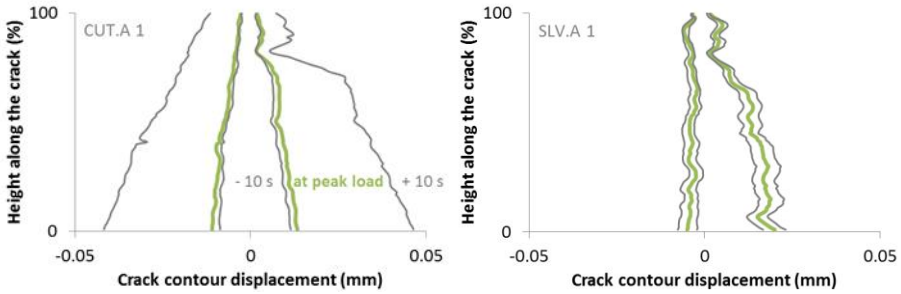

Figure 24: DIC monitoring of the crack opening along the full height of the crack; the crack's left and right contours are shown at peak load and at snapshots taken 10 s before and after.

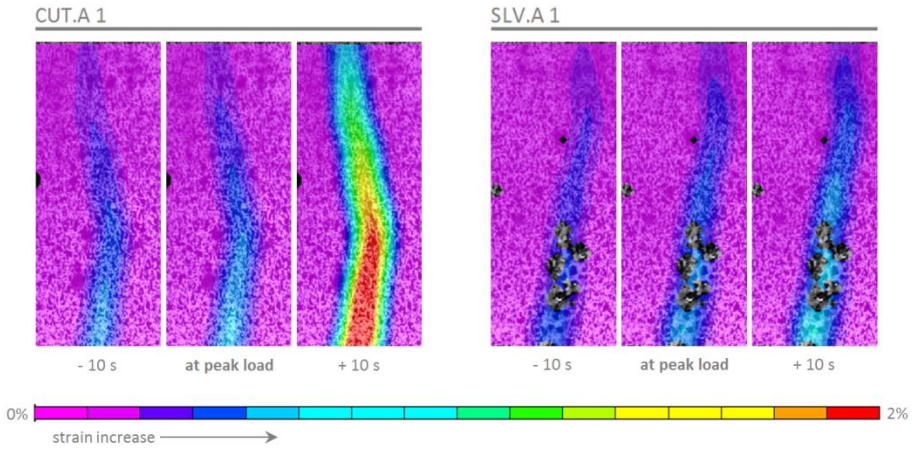

Figure 25: DIC monitoring of strain along the crack height at peak load and at snapshots taken 10 s before and after.

4.2. SEM with in-situ loading of bonded dog-bone specimens

Experiment. Small, 30 mm long dog-bone specimens were moulded out of cement paste with a water-to-cement ratio of 0.35 and cement CEM I 52.5 R. After hardening, the specimens were manually cracked approximately at their mid-section and the two halves separated by a ~0.3 mm gap, as shown in Figure 26. This gap was then filled with polymer and allowed to cure for a minimum of 3 days before testing. To perform the test, the surfaces to be observed were carbon coated and the specimens were clamped to the special SEM stage with in-situ tensile loading. Once the stage was inside the SEM chamber, tensile

loading was applied to the specimens at a loading rate of 1 μm/s, while high magnification images and a video were recorded.

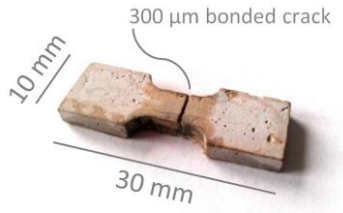

Figure 26: dog-bone specimen used for the tensile tests performed inside an SEM chamber; the crack at midspan has an area of 5x5 mm².

Results. This technique was successful at allowing a deeper understanding of the relationship between the tensile loading curves of specimens exhibiting cracks bridged with polymers and their failure due to excessive strain.

This relationship is shown in Figures 27 and 28 for one of the small cement paste dog-bone specimens cracked and bonded with the rigid CUT.A polymer foam. At the surface of the dog-bone specimen a progressive detachment of the polymer from the crack faces was observed and the sequence of high magnification images in Figure 28 shows the precise moments of the onset and the full detachment, as well as a highlight of the occurrence of micro-cracking in the polymer itself. Detachment is clearly identified by the bright areas at the crack edges, resulting from the loss of continuity of the electrical conductive coating required by SEM. These events are also localized in the loading curve shown in Figure 27. The onset of detachment can thus be linked to the considerable stiffness reduction in the loading curve, while the full detachment occurs nearly at peak load. The results show a strain capacity of approximately 16%, considering the full detachment at peak load the failure point, while onset of detachment occurs for a strain of 5%.

The performance of a flexible, non-foaming polymer was also studied and Figure 29 shows also detachment of the polymer from the crack faces at the surface of the dog-bone specimen. In this case, exact determination of the moments of onset and full detachment was not possible, but it is shown that detachment occurs before a strain of 50% is achieved, corresponding to the displacement shown in Figure 29. However, even after full detachment, it is clear at the middle of the crack section that the polymer is considerably stretched

with no visible damage to its matrix. Additionally, this flexible polymer was able to hold residual load much longer after peak load, compared to the rigid polymer.

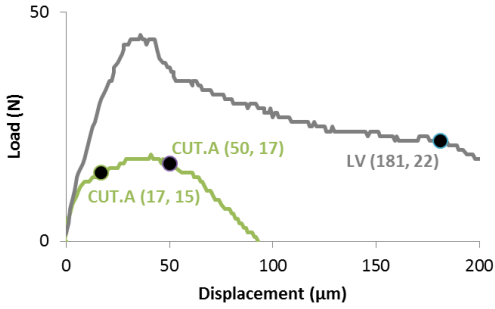

Figure 27: load-displacement curves of SEM in-situ tensile tests on small dog-bone specimens; the data points corresponding to the SEM images shown in Figures 28 and 29 are highlighted.

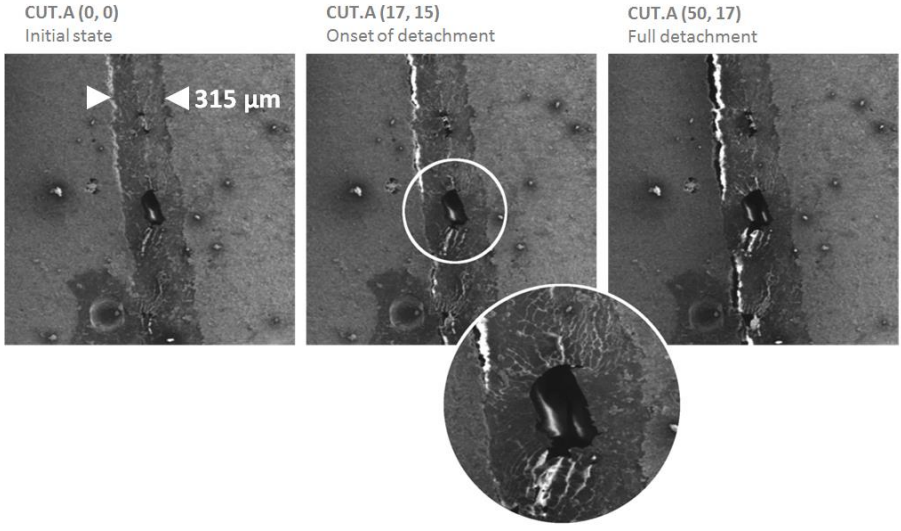

Figure 28: progressive failure due to detachment of the rigid, foaming CUT.A polymer from the cementitious matrix at the crack's mouth; micro-cracking in the polymer matrix also occurred (circular highlight); the sequence of SEM images corresponds to the data points in Figure 27.

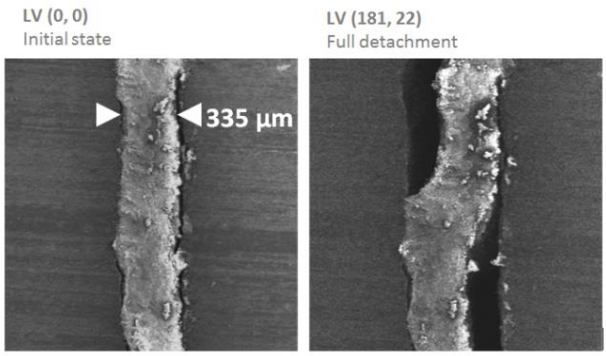

Figure 29: failure due to detachment of the flexible, non-foaming LV polymer from the cementitious matrix at the crack's mouth; the sequence of SEM images corresponds to the data points in Figure 27.

After completion of the tests, the two halves of the specimens were split and the opposite crack faces were observed under SEM. The foams cells of the CUT.A polymer were very obvious on the crack faces, as shown in Figure 30. It was observed that the overall failure mechanism was a mix of rupture of the walls of the foam cells and detachment of the polymer from the crack faces in areas where a larger amount of polymer had accumulated between cells or at areas close to the outside surface of the specimen, as shown previously in Figure 28. Another relevant feature shown in Figure 30 is the fact that the foam cells may have an irregular shape and varying dimensions, thus not necessarily guaranteeing a continuous barrier against ingress of water or other potentially aggressive agents for concrete.

For specimens bonded with the non-foaming LV polymer (Figure 31), where a large area of the crack was bridged by polymer, detachment was the only failure mechanism observed. The detached polymer was found covered with a thin layer of cement paste, as evidenced in Figure 31 by the areas with a rough texture on both crack faces.

Despite the clear usefulness of the test method in providing very accurate data on the failure mechanisms, the very small scale at which the test is performed and the fragility of the test specimens make it unfit for larger, more significant studies, as several attempts are usually needed before a successful test is achieved.

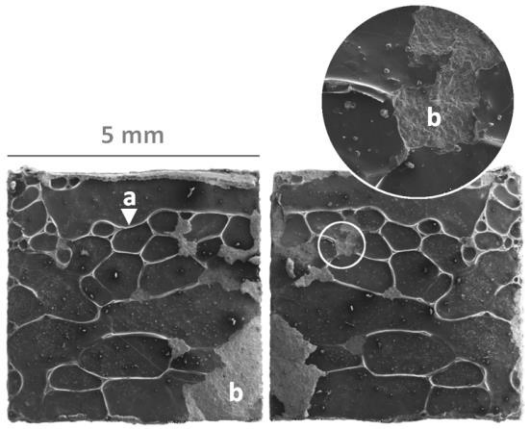

Figure 30: opposite faces of a crack bridged with the rigid, foaming CUT.A polymer after failure; both rupture of the foam's cell walls (a) and detachment of larger areas of polymer (b) occurred.

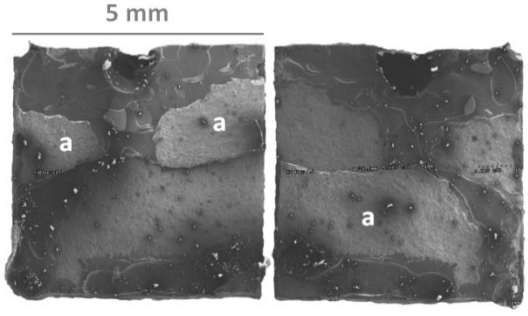

Figure 31: opposite faces of a crack bridged with the non-foaming, flexible LV polymer after failure, which occurred essentially due to detachment of polymer from the crack faces; different areas of the polymer remained attached to one of both sides of the crack (a).

4.3. Requirements for polymers bridging active, self-healed cracks

The occurrence of additional cracks during bending of mortar prisms healed with the rigid CUT.A polymer shows that polymers with an elastic modulus much lower than 22 MPa should be used if crack movement is expected after healing. By lowering the elastic modulus to 5 MPa (SLV.A series), the occurrence of new cracks was avoided, with the original crack reopening instead after a certain amplitude of crack movement.

In the case of small dog-bone cement paste specimens under tensile load, no new cracks were created, but the rigid CUT.A polymer failed partly due to detachment observed at the outside surface of the specimen, with the onset of failure happening at 5% strain and full detachment taking place at 16% strain. The flexible polymer LV, with a lower elastic modulus of 10 MPa, still failed due to detachment, for a strain of less than 50%. The maximum strain values for the polymers studied here may still not be enough to withstand crack movements found in a lot of field structures.

Regarding the requirements for maximum strain, a parallel can be made with injection products for concrete. The only obvious difference after hardening of the polymer inside the crack is the fact that the crack faces are not contaminated by debris in the case of self-healed cracks, as healing occurs immediately after crack formation, and thus the bond between polymer and the cementitious matrix is potentially better. While the polymer series LV would probably fulfil the requirements of the EN 1504-5 standard for injection of cracked concrete (CEN 2004b), which specifies a minimum 10% elongation for polymers to be injected into active cracks, it is debatable whether this value is realistic. It is reported by ACI (2001) that, due to fatigue alone, in the long term the original crack opening can double in size, implying that any polymer bridging such crack would have to withstand a strain of 100% while remaining attached to the crack walls. A single cycle of crack movement in a field structure can also often exceed 10% of the original crack size. Cruz and Raupach (2016) reported that crack movements of approximately 30% were found in a waterway structure. The magnitude of crack movements found in field structures is however seldom reported in the literature, but anecdotal reports have also mentioned the existence of crack movements in excess of 100% due to high loads from traffic on bridges.

The results discussed above suggest that precursors used as encapsulated healing agents in self-healing concrete should cure into polymers with elastic modulus much lower than 10 MPa, so that the stress at the interface with the cementitious matrix is minimized and the polymer can withstand the strain without detaching from the crack walls. An elongation of at least 100% should also be a requirement, along with adequate adhesion to a cementitious matrix, assumed as 2 N/mm^2 by CEN (2004b) for force transmitting filling of cracks. Polymer precursors that cure into a continuous film also seem preferable. Even

though foams reduce the stress at the interface and allow the failure to occur in the polymer itself, i.e. at the walls of the foam cells, localized failure due to detachment still occurs in areas where polymer has accumulated, often at the intersection between cells, thus breaking the continuity of the cell structure and hindering the barrier properties of the polymer.

4.4. Chapter overview

Continuous monitoring techniques were used to detect failure of polymers to follow crack movement, as an alternative to stepwise methods described in section 3.4. With non-destructive techniques consisting of acoustic emission analysis and digital image correlation, failure was easier to detect when stiff polymers were used. On the other hand, SEM with in-situ loading allowed very accurate detection of different stages of failure for different polymer types. Equally important was the possibility to determine mechanical requirements for polymers used as healing materials for active cracks.

More detailed conclusions are listed below:

► the analysis of acoustic emissions successfully detected failure under bending load of specimens self-healed with a rigid polymer foam (elastic modulus of 22 MPa); brittle failure occurring due to excessive strain on the polymer bridging the healed crack originated acoustic emissions with an energy level of at least one order of magnitude higher than the background noise and a high rate of occurrence of acoustic events; other parameters such as rise angle and frequency of the acoustic waves were not useful in detecting failure;

► digital image correlation tests performed in parallel detected a high rate of increase in the crack opening during failure of this rigid polymer foam, which occurred for a strain of 9%;

► none of the above mentioned features could be observed however during loading of specimens healed with a flexible polymer foam (elastic modulus of 5 MPa) and thus failure of such type of polymer is best assessed through tests that determine the permeability of the healed cracks;

► tensile tests performed inside an SEM chamber made it possible to distinguish both the onset and the complete failure due to detachment of the rigid polymer foam, occurring for strain levels of respectively 5% and 16%;

a flexible polymer forming a continuous film (elastic modulus of 10 MPa) inside the crack failed most probably under higher strains, but still for a crack movement lower than 50% of the original crack opening.

► to withstand crack movements found in field structures, flexible polymers with an elastic modulus much lower than 10 MPa should be used in the context of self-healing concrete; the lower elastic modulus will reduce the stress at the interface between the polymer and the cementitious matrix at the crack faces, reducing the chance of detachment before the strain limit of the polymer matrix is achieved;

► polymer precursors to be used as encapsulated healing agents for self-healing concrete should also cure into polymers with adequate adhesion to a cementitious matrix (>2 N/mm^2) and high elongation (>100%) if active cracks are targeted;

► a lower elastic modulus also reduced the stress transferred across the crack faces during bending and avoided the opening of new cracks next to the original crack, which occurred for specimens healed with the rigid polymer.

5. TESTING OF MORTAR SPECIMENS UNDER REALISTIC CONDITIONS

This chapter is dedicated to performance testing of healed specimens still at a small, mortar scale, but under more realistic conditions often found in field structures. The sealing efficiency of encapsulated polymer precursors was already determined in section 3.3 through capillary water uptake tests, but this self-healing mechanism will only be fit for water containing structures if the polymer sealing the cracks withstands high hydrostatic pressure. It can also be argued that the limit determined in section 3.4 is only valid if the healed crack is subjected to only one cycle of crack movement, while active cracks in field structures can be subjected to thousands of cycles over their service life. These topics will then be further developed in the following sections.

5.1. Permeability under hydrostatic pressure

Water containing structures were identified as a type of structure that could clearly benefit from self-healing properties and it was already shown in section 3.3 that encapsulated polymer precursors can effectively seal cracks. However, the water uptake results described in section 3.3 do not mimic the field conditions of such structures, as they are usually subjected to substantial hydrostatic pressure.

To achieve a more realistic assessment of the barrier properties of healed cracks, a test method was developed at TUDelft by Tziviloglou et al. (2014) under the scope of the healCON project. The specimens are 40x40x160 mm^3 mortar prisms with the same configuration and cracking protocol described in section 3.2.2 (Figure 7), but also containing a cylindrical Ø5 mm hole across the whole length, through which water flows. This hole is created by crossing the moulds with a steel rod positioned at the centre of the specimen's cross-section and removing it after 1 day of curing. This detail can be seen in Figure 32, which represents the whole setup. A picture of the actual setup used for the tests can be seen in section 8.1, Figure 80, where it was used for testing larger concrete specimens. The specimens were cured in sealed conditions at 20 °C for at least 14 days before being cracked and tested.

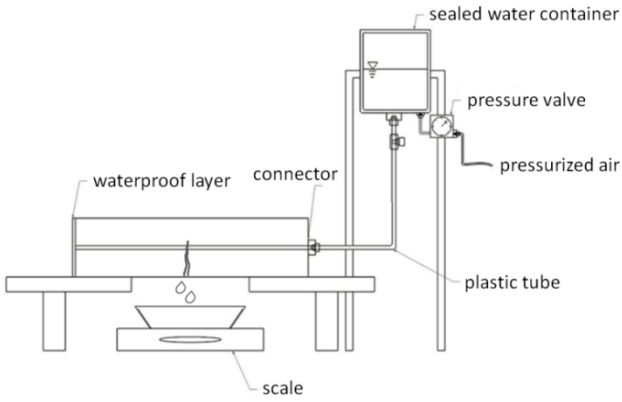

Figure 32: test setup for assessment of water flow through healed cracks; adapted from Tziviloglou et al. (2014).

A short sample preparation procedure should be followed prior to testing. One of the two top faces of the sample is covered with an insulating layer (preferably a fast-hardening glue), to avoid water flowing from that end of the hole. On the other top face, a connector is fixed, and a plastic tube is connected to it. The plastic tube attached to the sample is connected to a water reservoir under pressure on the other end. Water passes through the plastic tube and the Ø5 mm hole and leaks out of the crack. The water falls in a container placed on an electronic scale which is connected to a computer that records the experimental data, i.e. water weight and time.

The water flow observed with this test is typically linear, unless the flowing water contains any residues that may clog the small opening of the cracked section surrounding the hole that crosses the specimen, in which case a progressive reduction of flow would be observed. The specimens were not saturated prior to testing, as it was observed that the flow was linear over long periods of time even if the starting conditions were unsaturated. Examples of the linear flow for different degrees of crack healing are shown in Figure 33.

As a constant flow rate can be determined, the sealing efficiency of an individual specimen can be calculated by applying the formula below, where $WF_{cracked}$ is the average water flow (g/min) of non-healed specimens with open cracks and WF_{healed} is the water flow of a healed specimen.

$$Healing\ efficiency = \frac{WF_{cracked} - WF_{healed}}{WF_{cracked}} \times 100\%$$

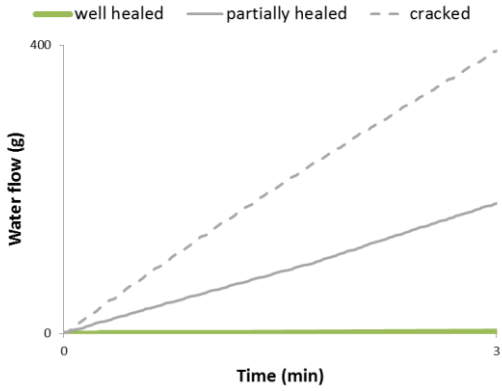

Figure 33: typical linear water flow through cracks with different degrees of healing.

In this test there is no constant crack width, as the specimens are cracked under a bending load and thus cracks have a triangular profile, so it is not possible to measure the water flow through a constant crack size and obtain the respective permeability coefficient. This is however a practical, quick performance test, by which it is possible to conclude whether the healing agent works sufficiently well at sealing cracks when under a considerable hydrostatic pressure.

Specimens with a crack mouth of approximately 0.3 mm were used for this test and the capsules had different dimensions than the ones used in section 3.2.2, with an external diameter of 5 mm and a wall thickness of 0.8 mm. Only two capsules were used, one attached to each of the reinforcing steel bars. Trial tests revealed that the presence of the hole at the centre of the cracked section had an effect on the way the liquid precursor dispersed once released from the capsules, which made it additionally difficult to achieve well healed specimens. For this reason, the solution described in section 7.3.3 for improving the release of precursor was used. The precursor SLV was mixed with 5 wt% of benzoyl peroxide (BPO) and 5 wt% of accelerator (see section 3.1), equivalent to series SLV.A+BPO mentioned throughout this book. This way, pressurized capsules were obtained and for the majority of the specimens the precursor was able to flow and fill the cracked sections completely around the hole that supplies water during the test.

Four series of three specimens were moulded and from the total of 12 specimens, 8 were perfectly healed, with no observed flow when a pressure of 0.05

bar was used. This contrasts with the ratio of specimens perfectly healed during initial trials when only the SLV precursor was used (5 out of 21) or when it was mixed only with BPO, without accelerator (2 out of 12). Figure 34 shows the water flow at 0.05 bar for the four specimens that were only partially healed. Such a low pressure, equivalent to approximately 0.5 m of water head, should be used for calculation of healing efficiencies, as it is unlikely to damage the healing material. The tests ran for 5 minutes and the flow was perfectly constant for all specimens tested. While one of the specimens had a very little flow, the remaining ones had a flow rate at the same level of reference specimens with open cracks. The average healing efficiency determined at a pressure of 0.05 bar for the total 12 specimens was 82% ± 32%.

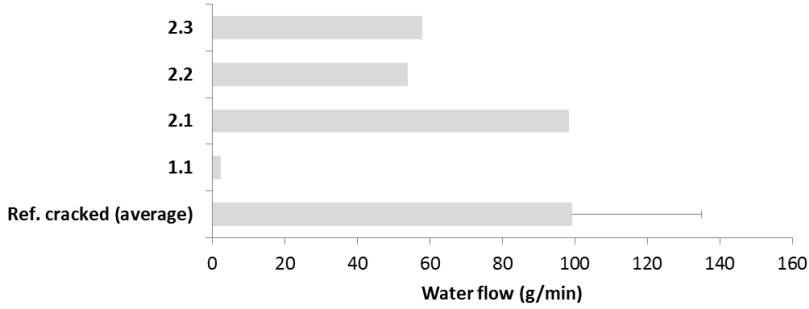

Figure 34: water flow at 0.05 bar of specimens only partially healed and average flow for reference specimens with open cracks (ref. cracked); error bar shows standard deviation.

Other than the overall healing efficiency for a particular self-healing solution, this test can also be used to assess the resistance of the healing material to high hydrostatic pressures. The 8 perfectly healed specimens were tested at increasingly higher levels of hydrostatic pressure at 0.05 bar, 0.5 bar, 1 bar and 2 bar and no water flow was observed for any of them. This shows that water pressure should not be a concern when polymers with similar properties to the ones tested here are used as healing materials.

The perfectly healed specimens were divided in three series of at least two specimens whose cracks were widened to different levels. The strain levels were purposely chosen around the strain limit calculated in section 3.4 for the SLV series (only SLV precursor). The SLV and SLV.A+BPO series would normally not be directly comparable, as the addition of accelerator to the SLV precursor

induces considerable foaming. However, due to an interaction of the accelerator with BPO, the foaming effect is considerably hindered, probably due to partial consumption of amines in the accelerator for the decomposition of BPO, as amines are one of the listed reducing agents of the BPO used. The results of combined widening of the cracks and different levels of hydrostatic pressure are shown in Figure 35.

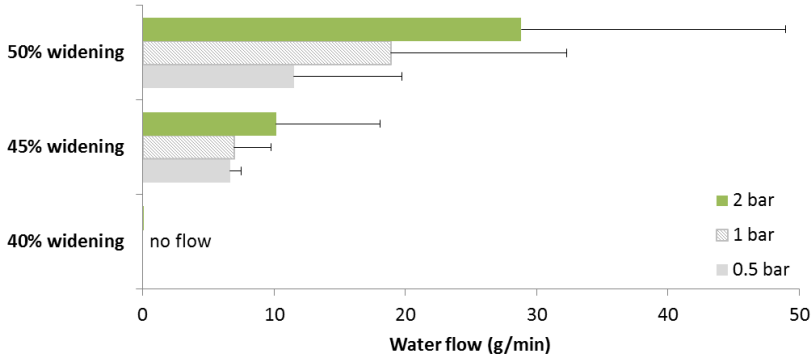

Figure 35: average water flow of well healed specimens after widening of the cracks and under different levels of pressure; error bars show standard deviation.

Water flow was still not observed when the cracks were widened by 40% of their original size, even for pressures as high as 2 bar (or approximately 20 m of water head). However, a small increase to 45% widening resulted in clear water flow, although still much lower than the average water flow observed for specimens with open cracks shown in Figure 34. At 50% widening, the water flow sees an additional increase, which confirms that the polymer starts failing at a strain level of 45%, which is due to progressive detachment from the crack walls as shown in chapters 3 and 4. This way it was possible to both confirm and more accurately determine the strain limit of the SLV precursor (as used in SLV.A+BPO series). To achieve lower standard deviation values than the ones shown in Figure 35 and thus improve statistical significance, a larger number of specimens could be tested, with a suggested minimum of 5 specimens.

5.2. Analysis with ultrasonic pulse transmission

A trial test with cracked concrete specimens (Gruyaert et al. 2015) revealed that healing due to dispersion and hardening of polymer precursors inside a crack

results in a considerable amplitude increase of ultrasound shear wave pulses transmitted through the specimens. This simple parameter, the maximum amplitude of an ultrasonic pulse, can then be used to monitor the evolution of the healing process. This application is similar to the use of ultrasound pulse transmission to monitor hardening of early-age concrete, during which amplitude and velocity of the pulses increase considerably due to the transition from fluid to solid (Reinhardt and Große 2004). The maximum amplitude was also used to monitor a potential and progressive failure of the polymers to bridge the opposite faces of an active crack, as detachment from the crack faces or rupturing of the polymer would result in an open crack again and thus in a decrease of the amplitude gained with healing. Again, a parallel can be made with the use of this technique in the field of structural health monitoring, as cracks developing in concrete result in a decrease of the amplitude of transmitted ultrasound pulses (Karaiskos et al. 2015). The use of amplitude as the monitoring parameter instead of the more common pulse velocity, for which precise onset determination is needed, allows easier processing. This is however only possible because for the application proposed here the sensors stay in a single position during the whole measurement, while for structural health monitoring usually several positions are inspected and the amplitude will vary considerably between positions due to coupling alone. More complex parameters have been used in the context of self-healing concrete, such as diffusivity and arrival time of the ultrasound pulses (In et al. 2013), although only for autogenously healed concrete.

The mortar specimens used had the same configuration as the ones described in section 4.1 and shown in Figure 19. The only minor modifications were a narrower FRP strip 7 mm wide, so that slightly larger cracks of approximately 0.3 mm were obtained, and a shorter specimen length of 150 mm to allow enough clearance between a specimen with sensors attached and the mechanical loading setup. Capsules also had different dimensions than the ones used in section 4.1, with an external diameter of 5 mm and a wall thickness of 0.8 mm.

The type of specimen used, with FRP strips in the compression zone instead of steel bars in the tensile zone, reduces the efficiency of release of the precursor from the capsules. This happens due to a wide crack opening suddenly during the cracking procedure, compared to the slow crack opening observed when specimens contain embedded steel bars as reinforcement (Figure 7).

Due to this, it was initially difficult to obtain well healed specimens that could be tested, if only the best performing SLV precursor was used. This precursor was then mixed with accelerator (see section 3.1), which also induces a foaming effect that could improve its release from the capsules. Further improvements were obtained by mixing the precursor with benzoyl peroxide (BPO), whose mechanism and effect on release is described in section 7.3.3. The series of precursors tested are listed and described in Table 8. Of all the series tested, it was considerably easier to achieve well healed specimens with the SLV.A+BPO combination.

Olympus V150-RB shear wave sensors were coupled to the specimens with silicone gel and a FreshCon system from Smartmote was used to generate, trigger and acquire pulses of 800 V and a pulse width of 5 μs. The emitting and receiving shear wave sensors were positioned at opposite sides of the specimens, on the smaller, moulded 40x40 mm² faces, so that the ultrasound pulses were forced to travel across the cracked section. The sensors were kept in place with an elastic band around the specimens.

For specimens whose healing was monitored, the faces where the sensors were coupled were first covered with a layer of spray paint to avoid absorption of the coupling silicone gel by the mortar matrix during the long periods of monitoring. In all cases, it was of extreme importance for the faces of the specimen to be as flat and smooth as possible, to guarantee good and stable coupling.

Table 8: designation and description of series tested.

Series	Accelerator	BPO
SLV.A	5 wt%	-
SLV+BPO	-	5 wt%
SLV.A+BPO	5 wt%	5 wt%

5.2.1. In-situ hardening of polymer precursors

As mentioned, an increase of the maximum amplitude is expected for ultrasonic pulses transmitted across a crack during the healing process. This is shown in Figure 36, along with the evolution of the shape of the ultrasound wave during

healing. Similar changes in wave shape were reported by In et al. (2013) for autogenous healing.

It is not possible to individually assign either dispersion or hardening of the polymer precursor to the different phases of amplitude increase, although, given that shear waves were used, hardening probably accounts for most of the amplitude increase. Liquid phases, such as the polymer precursor immediately after being released from the ruptured capsules, offer high resistance to the transmission of shear waves. Thus, simple filling of an open crack with a liquid polymer precursor is not expected to result in considerable increase of wave amplitude when compared to hardening of the precursor.

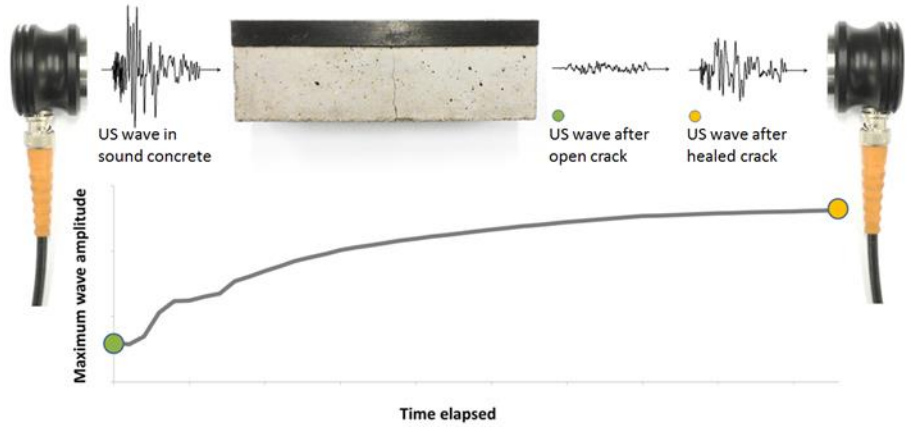

Figure 36: increase of wave amplitude during healing when ultrasound pulses are transmitted across a single crack.

The healing process was monitored with ultrasound pulses for two specimens from each series listed in Table 8. The expected increase in amplitude for the SLV.A specimens is shown in Figure 37. The absolute maximum amplitude at the start of the measurement varies between specimens due to the heterogeneous nature of the mortar matrix and the effectiveness of coupling between the sensors and the specimen, which depends on how flat and free of voids the surface of the specimen is. Due to this, any potential differences between series are best observed if the evolution of maximum amplitude is plotted using a normalized axis, as shown in Figure 38. Normalization was achieved by shifting the curves to start at a zero amplitude and expressing amplitude as a fraction of the maximum value measured during the testing period.

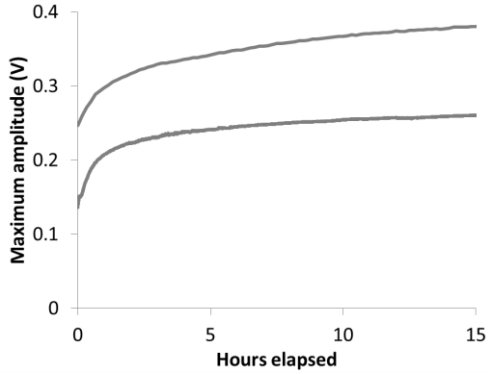

Figure 37: monitoring of ultrasonic shear waves transmitted across a cracked section during healing in mortar specimens from the SLV.A series.

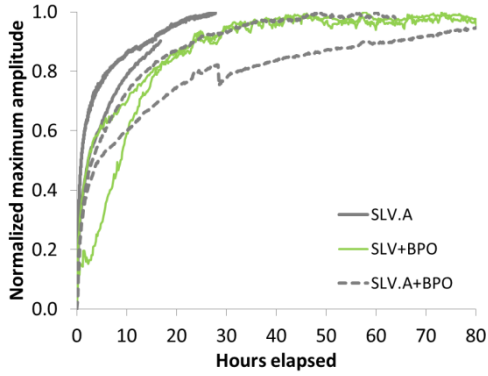

Figure 38: normalized maximum amplitude of ultrasonic shear waves transmitted across a cracked section during healing in mortar specimens.

Even though the specimens from the SLV.A series were monitored for a shorter period, it is clear that the evolution of the maximum amplitude of shear waves was similar for all series, with most of the increase happening during the first 10 hours after cracking of the specimens and a stabilization of the measurements after 48 hours. It can then be concluded that at least 2 days are required for proper curing of these precursors inside a real crack and that the moisture available in an cementitious matrix is enough to achieve it. A faster increase of amplitude could be expected for the series with added accelerator, as it was empirically noticed that in those cases the polymer hardened faster. It is thus probable that the high rates of increase for all series during the first

hours of the test are due to the dispersion of the liquid polymer inside the crack as opposed to hardening.

In the case of open cracks in specimens with no self-healing properties, a similar test would result in stable amplitude of the shear waves (documented only in section 6.1 for larger concrete specimens). Only minimal and progressive increase or decrease of amplitude would be observed, compared to the magnitude of changes shown in Figure 38. The slight changes observed over several hours for specimens with open cracks can be explained by a progressive improvement or worsening of coupling. In this case, where silicone gel was used as coupling agent, further dispersion of an excess of gel under the pressure of the elastic band keeping the sensors in place can occur or a thin layer of gel can be partially absorbed by the mortar matrix.

5.2.2. Fatigue resistance of polymers in active cracks

Transmission of ultrasound pulses can also be used to monitor changes in continuity between the faces of a healed crack. The continuity can be progressively lost due to rupturing of the polymeric matrix or due to detachment of the polymer from the crack faces, which would result in a loss of amplitude of the ultrasound waves transmitted across the crack. This is of particular interest as a continuous monitoring technique to detect failure during multiple cycles of crack movement, which can be applied to determine a potential failure due to fatigue. In this context, a healed mortar specimen is said to be susceptible to fatigue-induced failure if the polymer used as healing material progressively detaches or ruptures when subjected to multiple cycles of crack movement at their limit strain level (determined in section 3.4) or at lower strain levels.

A protocol was developed to achieve multiple loading and unloading cycles applied to a mortar specimen at the same time that ultrasound sensors were attached to it and ultrasound pulses were transmitted continuously. The physical layout of the setup is shown in Figure 39, where the elements of the FreshCon system can be seen. In the same figure a specimen is highlighted, ready to be tested. Besides the elastic band guaranteeing proper coupling, metal plates were glued to the bottom of the specimen to avoid vertical slipping of the sensors. An LVDT was also positioned at the bottom of the specimen, across the single crack at midspan to control the loading cycles.

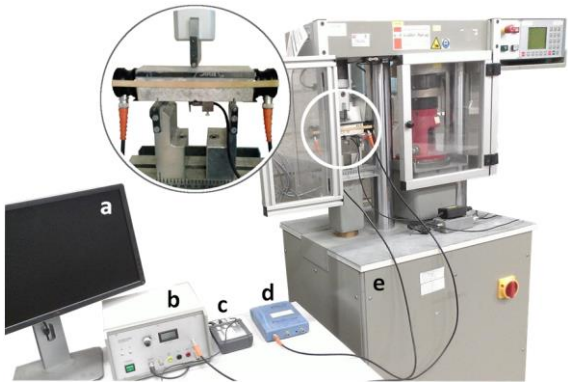

Figure 39: setup for fatigue assessment with combined ultrasound transmission via a FreshCon system consisting of a computer loaded with the FreshCon software (a), amplifier (b), trigger (c) and oscilloscope (d); the highlight shows a specimen with coupled sensors positioned in the loading machine (e).

Cyclic loading occurred under 3-point bending, with each cycle defined as a crack width increase from a starting LVDT displacement of 0.05 mm to the desired maximum displacement, corresponding to a certain strain on the polymer filling the crack, followed by unloading back to the base displacement of 0.05 mm. The base displacement is required to counteract the progressive difficulty in returning the crack to its original size, due to unrecoverable deformation after hundreds of cycles. Additionally, even if the polymer had detached, it would still be able to make contact with the crack faces if the crack returned to its original size and thus it would be difficult to detect failure. A visual representation of the cycles is shown in Figure 40. After each cycle, a holding period of 5 s was introduced at the displacement of 0.05 mm, so that the monitoring equipment could acquire data in stable and well defined conditions.

It was the amplitude of the ultrasound waves acquired in these stable conditions that was used to monitor changes in continuity across the crack. Ultrasound pulses were emitted every 2 s during cyclic loading, so that at least two amplitude data points are available during the 5 s holding time under a stable 0.05 mm displacement. A loading speed of 0.013 mm/s was used, resulting in a frequency of approximately 0.07 Hz (number of loading cycles per second), which varies slightly depending on the maximum displacement level set for the test.

Figure 40 also shows that the data points with higher maximum amplitude occur naturally during the holding period, when the crack size is smaller. This allowed using the upper envelope of the maximum amplitude data to represent the evolution of the maximum amplitude under stable conditions, which was achieved by processing the data in the software Matlab. It is thus expected that the envelope stays stable over time if the polymer does not fail to follow the crack movement, while a progressive decrease would suggest detachment of the polymer from the crack faces or rupturing of the polymer matrix, which reduces the continuity across the crack.

The tests were performed for a period up to three hours, equivalent to approximately 700 cycles. Longer periods would not be possible, as eventually the unrecoverable deformation of the specimen is higher than the base displacement of 0.05 mm.

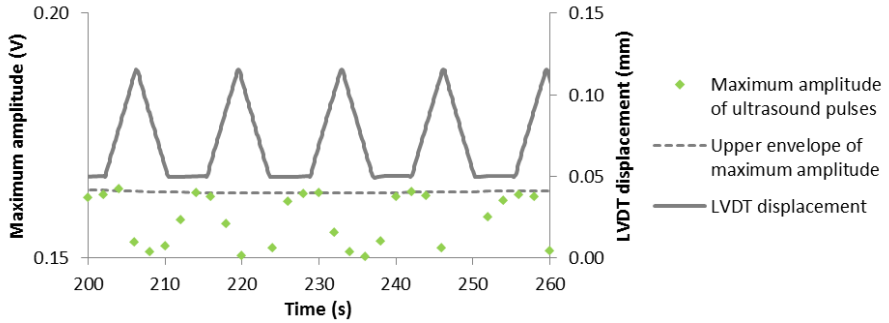

Figure 40: protocol for assessing resistance to fatigue, combining multiple loading cycles and transmission of ultrasound pulses across a mortar specimen with a single healed crack.

During trial tests it was found that the loading machine, fitted with a mechanical jack, was introducing a lower frequency noise component in the acquired ultrasound waves. Such noise had not been found in previous trials on larger concrete specimens loaded in a machine fitted with a hydraulic jack (section 6.4). Before further analysis and processing of the results, the ultrasound data had thus to be filtered to remove the noise, which was also accomplished in Matlab using a fourth order Butterworth highpass filter with a cutoff frequency of 3 kHz. The effect of this filter on the original waveform is shown in Figure 41.

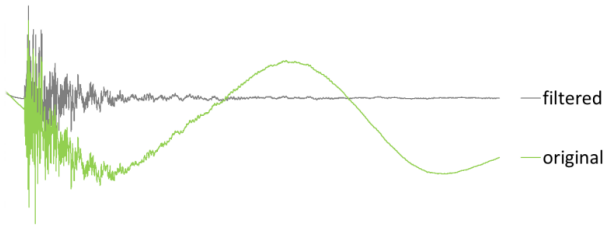

Figure 41: filtering of lower frequency noise induced by the loading machine.

Specimens from each series were tested at strain levels lower than the strain limit determined for the SLV polymer in section 3.4 (higher than 50%), as multiple cycles of crack movement are expected to reduce the strain at which the polymer detaches from the crack faces.

Testing of reference (REF) specimens with open, non-healed cracks results in a stable envelope of maximum amplitude, with just a slight and progressive increase (Figure 42), which can be due to slow improvement of coupling of the sensors throughout the test or the displacement of small particles inside crack.

When the fatigue resistance of SLV.A specimens was assessed at a strain level of 20%, the evolution of the envelope of maximum amplitude is identical to that of REF specimens with non-healed, open cracks, as shown in Figure 42. The bottom curve of SLV.A series shows however a decrease after about 500 cycles that suggests at least a partial loss of continuity across the crack faces. This was confirmed with microscopic analysis of sections from the crack mouth. Images were taken from these sections both before and after the test, so that they could be compared and a potential detachment or rupturing of the polymer matrix could be detected. Figure 43 shows that specimens from the SLV.A series tested at a strain level of 20% contained healed crack sections where no failure occurred even after several hundred cycles (Figure 43, left), while other sections showed detachment of the polymer from the crack faces (Figure 43, right).

It should be noted that the immediate decrease of the envelope at the beginning of the measurements (overlapped with the vertical axis) is due to the initial widening of the crack up to the base displacement of 0.05 mm.

At a strain level of 35%, variations of the envelope are more drastic and unexpected, as the envelope increases, which suggests an improvement of the conti-

nuity across the crack faces. This improvement is due to the release of remaining liquid precursor from inside the ruptured capsules, whose dispersion and progressive hardening results in an amplitude increase of the shear waves. As most of the polymer initially bridging the crack detached from the crack faces after several loading cycles at a strain level of 35%, it exposed the openings of the ruptured capsules. As the precursor used for this series had foaming properties, which were potentiated by exposure to moisture after rupturing of the capsules, new precursor could be clearly seen leaching out of the crack during the test.

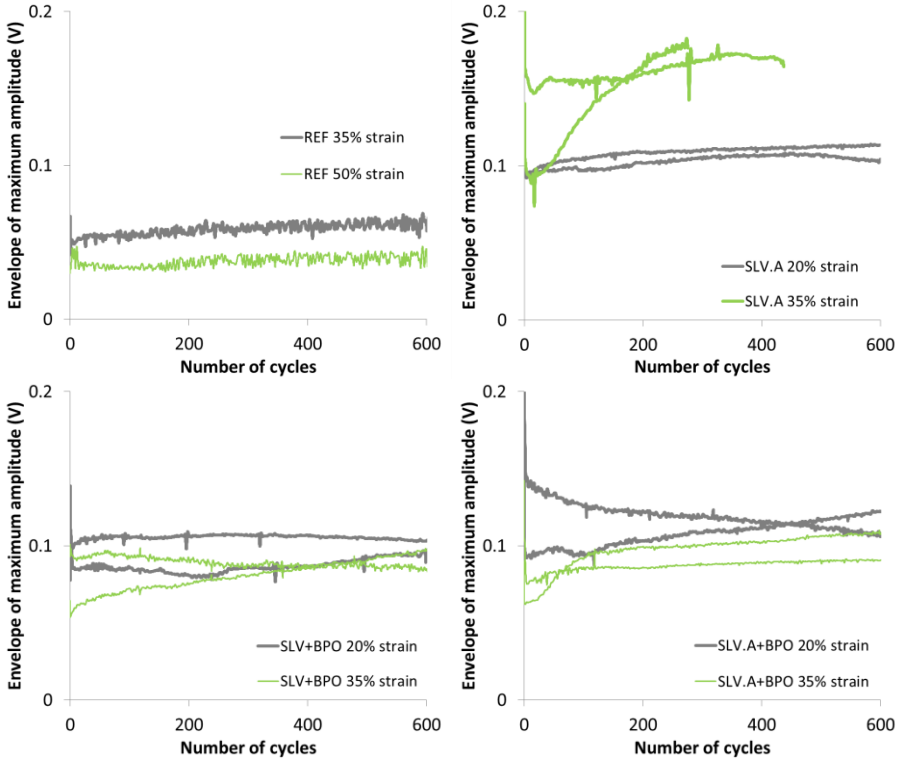

Figure 42: evolution of the envelope of maximum amplitude of ultrasound pulses transmitted across healed mortar specimens during multiple cycles of crack movement.

It could then be concluded that for the foaming precursor SLV.A, even a low strain of 20% results in partial failure due to fatigue if multiple cycles of crack movement are applied. At higher strains, failure seems to occur faster, after less

than 200 cycles. The results suggest that this polymer would not be compatible with the conditions found in many field structures, where crack openings can increase in size by more than 100%, as discussed in section 2.1. This reinforces the idea discussed in the previous chapter that polymers with good adhesion to concrete but with a much lower modulus of elasticity would be preferable, in order to minimize the stress at the interface between polymer and cementitious matrix. A precursor curing into a gel-like material would be ideal.

The two types of evidence of failure were also observed for the remaining series, as shown in Figure 42, i.e. a progressive decrease of the envelope of maximum amplitude due to detachment of the polymer or a more substantial increase of the envelope due to the release of new precursor, which was also often noticed at the surface of the specimens during the tests. This occurred even for the lower strain level of 20%.

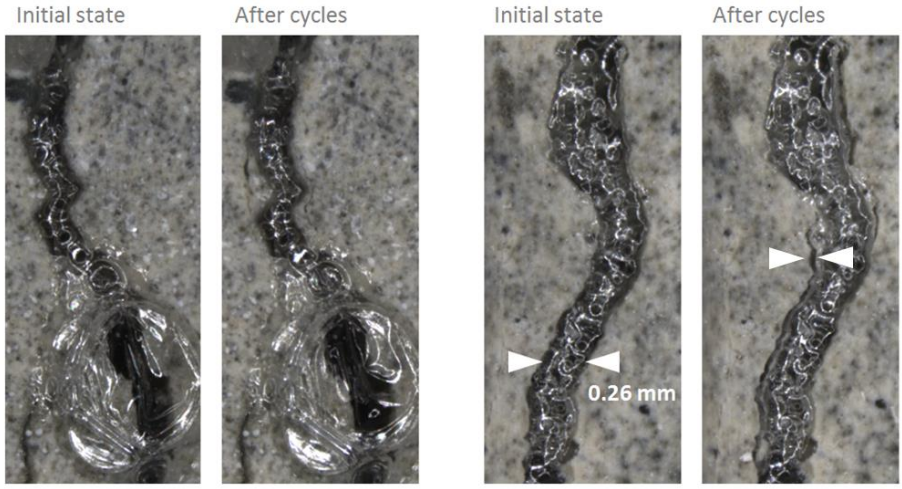

Figure 43: healed crack sections from the SLV.A series before and after a fatigue test performed at a strain level of 20%; detachment of the polymer from the crack walls is seen in the section at the right, after cycles (between arrows).

For the SLV+BPO series, increases of the envelope observed were not as dramatic as for the remaining series, as no accelerator was added to the precursor and thus its foaming potential was lower and any release of new precursor would be slower. This series can be directly compared to the SLV series for which a strain limit of at least 50% was determined in section 3.4, with the only

difference being the addition of BPO to improve its release (discussed in section 7.3.3). It was thus concluded that multiple cycles of crack movement reduced considerably the strain limit of this polymer, after which detachment occurs, to a value below 20%. Additionally, detachment of the polymer from the crack faces, which seems to be progressive based on the continuously decreasing slope of some of the curves in Figure 42, occurs within 600 cycles and a much larger amount of cycles is expected for an active crack over the service life of a field structure.

The load carried by the specimens was also recorded during the fatigue tests, to check whether it would also reflect any changes due to the detachment of the polymer from the crack faces. However, regardless of any failure due to detachment, it was observed that the only considerable changes in the load curves was a progressive decrease during the first 20 cycles, as shown in Figure 44. This progressive decrease was most probably due to additional damage occurring in the mortar matrix at the upper section of the specimens that was still connected after they were cracked.

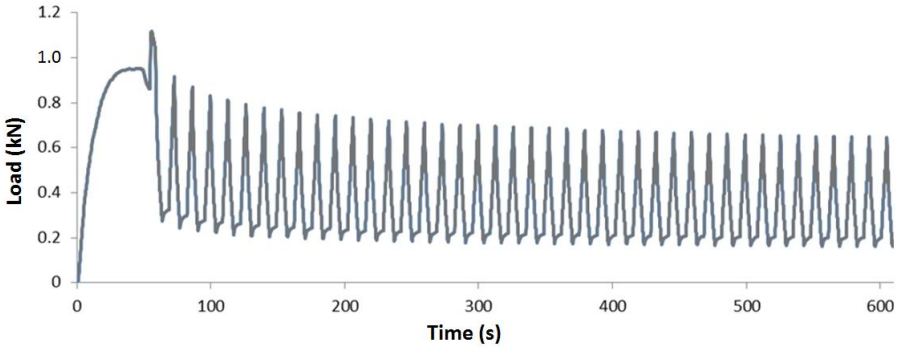

Figure 44: evolution of the load carried by the specimens during the first 40 cycles of a fatigue test.

5.3. Chapter overview

Self-healing was tested under more realistic conditions, but still on a small scale. Mortar prisms healed with the best performing SLV precursor were subjected to high hydrostatic pressures and multiple cycles of crack movement to assess their susceptibility to failure due to fatigue, as both conditions are often found in field structures. While hydrostatic pressures did not cause failure of the pol-

ymer bridging healed cracks, the maximum strain withstood by the polymer before failure was considerably reduced due to fatigue induced by multiple cycles of crack movement.

More detailed conclusions are listed below:

► testing of 12 specimens under hydrostatic pressure resulted in an average healing efficiency of 82% ± 32%;

► for 8 of the specimens, no leaking was observed even for the maximum pressure tested of 2 bar, or approximately 20 m of water head;

► the resistance to high hydrostatic pressure remained even if a crack was widened by 40% of its initial size, but a progressive increase of water flow was observed for higher strain levels;

► monitoring of healing with ultrasound transmission consistently revealed a considerable increase of maximum amplitude of the ultrasound pulses during the first 10 hours due to the dispersion and hardening of the precursor inside a crack; after approximately 48 hours the amplitude stabilized, which should then be the minimum time needed for curing of the precursor under in-situ conditions, inside a crack;

► during multiple cycles of loading and unloading of the specimens, monitoring of the upper envelope of maximum amplitude of ultrasound pulses allowed detecting failure; considerable decreases or increases of the envelope were related respectively to a detachment of the polymer or a release of remaining polymer from the capsules after failure of the hardened polymer bridging the crack;

► failure was detected at strain levels of 20%, which is much lower than the strain limit of the SLV polymer determined in section 3.4 for a single cycle of crack movement, by which it was concluded that the strain limit of the polymer is considerably reduced due to fatigue.

6. CONCRETE SPECIMENS WITH PRE-PLACED GLASS CAPSULES

An important motivation for the research performed was the upscaling of self-healing concrete based on encapsulated polymer precursors. To achieve it, this self-healing technique had to be tested at the concrete scale, which differs from the mortar scale (Chapter 5) essentially in the fact that larger aggregates are present in the cementitious matrix. Once capsules rupture and the polymer precursor flows into the crack, it will have to occasionally bridge large surfaces of gravel particles split during cracking of concrete. Moreover, compared to a crack in mortar, a crack in concrete exhibits a higher tortuosity. In this chapter, the tests described were still performed on specimens with pre-placed glass capsules with thin walls, which is not an appropriate technique for upscaling. The development of capsules that can be added to concrete during mixing took place at a later stage and is described in Chapter 7.

Larger concrete specimens also allowed testing non-destructive techniques that can potentially be used for assessing the performance of self-healing concrete based on a wide range of self-healing mechanisms or for assessing the potential of these techniques for monitoring self-healing field structures. The non-destructive tests were carried out with support from healCON partner TUM and the research campaign was divided between two periods, at UGent and at TUM. The specimens tested had dimensions of 55x15x15 cm^3 for the campaign carried out at UGent and 55x15x10 cm^3 for the specimens at TUM. Four pairs of glass capsules 10 cm long, with a diameter of 3.3 mm and a wall thickness of 0.18 mm were pre-placed with nylon strings crossing the moulds before pouring of concrete. Capsules contained the precursor SLV and were sealed with PMMA glue. The specimens were also reinforced with two Ø6 mm ribbed steel bars that were used in the compressive zone during loading, which allowed better control of the crack size during loading. The final configuration of the specimens is shown in Figure 45. The concrete composition used is shown in Table 9.

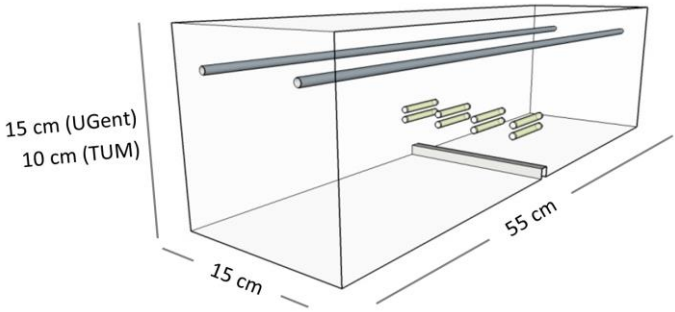

Figure 45: concrete specimen reinforced with Ø6 mm ribbed steel bars placed 3 cm away from sides and top; four pairs of glass capsules were pre-placed 4 cm apart over a guiding notch, at 1/3 of the specimen's height.

Table 9: concrete mix composition.

Material	Dosage (kg/m^3)
Sand 0/4 mm	686
Gravel 4/8 mm	502
Gravel 8/16 mm	809
CEM I 42.5 N	300
Water	150

Demoulding occurred at 24 hours, followed by a storage period of 28 days under water, after which the specimens were moved to a climate room at 20 °C and 60% RH. Before the cracking stage, a notch with a depth of 5 mm was sawn in the middle of the specimens, as illustrated in Figure 45, to guide and standardize the geometry of the cracks. An LVDT was placed across the notch to monitor crack size during loading. The specimens were cracked in a 3-point bending setup with crack width controlled loading (speed of 0.6 mm/min) and the bending load was applied until a crack width of at least 1 mm was achieved, which resulted in a crack mouth size in the range of 0.3-0.35 mm after unloading.

6.1. In-situ hardening of polymer precursors

The same technique based on ultrasound transmission described in section 5.2.1 was also used on larger concrete specimens to assess the evolution of the

curing process occurring inside a crack when the polyurethane precursor is released and gets in contact with the moisture present in the concrete matrix.

The ultrasound sensors were coupled to the centre of each of the 15x15 cm^2 (10x15 cm^2 for specimens tested at TUM) faces of the concrete specimen, with one of them generating the ultrasonic pulse and the other one, located on the opposite side of the specimen, acquiring the signal that travelled across the cracked section. Olympus V150-RB shear wave sensors were coupled to the specimens with hot glue and a FreshCon system from Smartmote was used to generate, trigger and acquire pulses of 800 V and a pulse width of 5 μs.

The maximum amplitude of the ultrasonic pulse was monitored over time for a few specimens in order to detect a possible increase of amplitude due to the dispersion and hardening of polyurethane precursor, which enables a better transmission across the crack. It can be seen in Figure 46 that self-healing takes place mostly during the first 24 hours, as after that the rate of increase in amplitude decreases substantially. By comparison, it can also be seen that a reference specimen with empty capsules exhibits no considerable increase in amplitude.

The initial amplitude of the ultrasonic waves and the magnitude of its increase is however distinct for different specimens. This can be due to the slight differences in crack profile and size, but also due to the effectiveness of the coupling between sensors and specimen and its stability over long periods of time. Given that this type of test can last for several days, good coupling is critical, as otherwise a slow decrease of amplitude can occur even in stable conditions due to decoupling of the sensors. As the above mentioned differences between specimens are difficult to avoid, results are best shown in normalized plots (see section 5.2.1), as shown in Figure 47. Presented this way, it becomes clear that the increase of maximum amplitude due to dispersion and hardening of the polyurethane precursor evolves in the same way regardless of the specimen. A fast increase of amplitude during the first 10 hours is followed by a progressive decrease in the rate of increase until the amplitude almost stabilizes after 48 hours. It is not clear however if any of these phases can be ascribed to either dispersion or hardening of the polymer precursor.

The results indicate that complete curing of the precursor in in-situ conditions (inside a concrete crack) takes at least 48 hours, after which any further evolution of its mechanical properties takes place slowly.

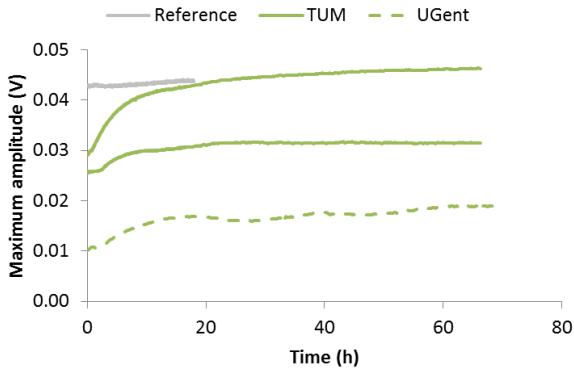

Figure 46: monitoring of ultrasonic shear waves transmitted across a cracked section in concrete specimens.

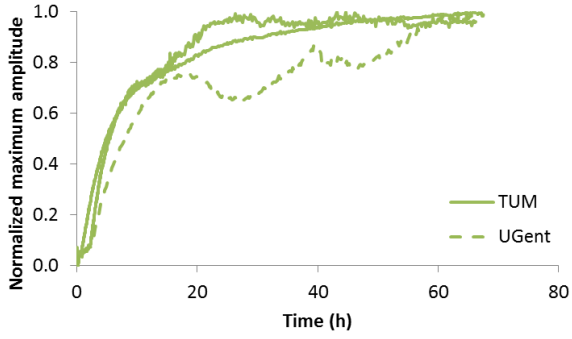

Figure 47: normalized amplitude of ultrasonic shear waves transmitted across a cracked section in self-healing concrete specimens.

6.2. Regain of mechanical properties

After a period of at least 3 days, to allow complete curing of the polymer, the specimens were reloaded in the same 3-point bending setup and the stiffness regain was determined according to the formula described in section 3.2.2, while the strength regain is simply the ratio between the peak load of a healed specimen and the peak load of the same specimen during the first loading, when no crack was present. Representative loading curves are shown in Figure 48 and the overall quantitative results are listed in Table 10.

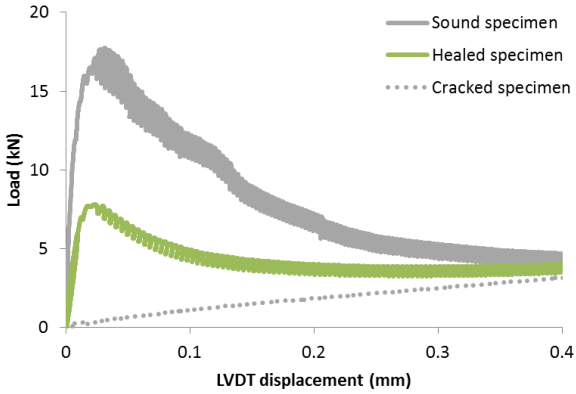

Figure 48: loading curves of representative sound and healed concrete specimens.

Table 10: regain of mechanical properties due to healing.

	Mean	Standard deviation
UGent (2 specimens)		
Strength regain (%)	47	3
Stiffness regain (%)	19	14
TUM (4 specimens)		
Strength regain (%)	74	18
Stiffness regain (%)	75	21

In Figure 48 it can be seen that healing resulted in partial regain of strength, with the curves of healed specimens exhibiting a peak load, which is absent in curves of cracked specimens whose load is carried only by the weak reinforcement placed at the top. A considerable strength regain of 47% (UGent) and 74% (TUM) was achieved, although this was not an objective of the research presented here. In a way, a high strength regain is even undesired, as it means that the polymer filling the crack is able to carry a substantial load, which increases the stress at the interface between polymer and concrete matrix. If the polymer detaches from the crack face, the sealing effect is lost and the durability of the concrete element is hindered, defeating the initial aim of self-healing as presented here. The calculated stiffness regain had a high deviation essentially due to the stiffness differences between specimens in their sound, uncracked state.

Absolute stiffness of individual healed specimens was very similar, indicating a similar healed area of the cracked plane, as shown in the next section. The higher regain of mechanical properties of TUM specimens was due to their lower height, which results in a lower bearing capacity in the sound state. Given the smaller dimensions but similar healed area, the regain of mechanical properties is necessarily higher.

6.3. Healed crack area

After reloading to assess the regain of mechanical properties, the specimens were completely split to determine the area of the crack covered by polymer and representative images of the crack faces are shown in Figure 49. The contours of the area where polymer was found were highlighted with a felt pen directly on the crack face and digital pictures were taken. The healed area was then quantified by counting its total amount of pixels and comparing it to the pixel count of the whole crack face.

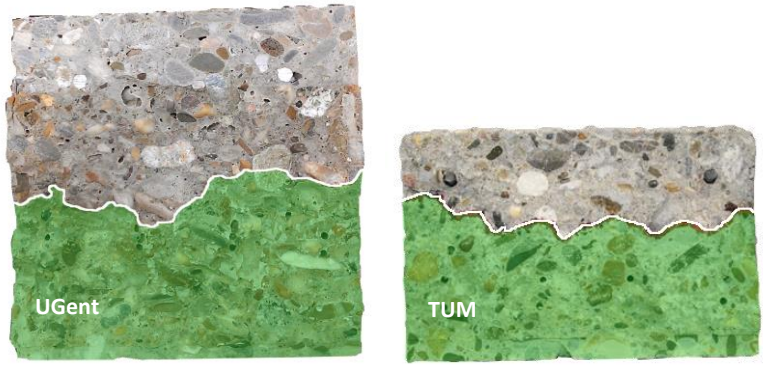

Figure 49: split cracked plane of a concrete specimen, where healed areas are highlighted in green.

Despite the differences in the height of the specimens, the healed are was consistent and similar for both configurations. The total healed area for the specimens tested at UGent was 117 ± 10 cm², while specimens tested at TUM had a healed area of 94 ± 6 cm². The slightly smaller healed area observed in the TUM specimens can be due to their excessively narrow or non-existent cracks in the upper parts of the specimen, as crack mouth size is similar but the total height of the specimen is smaller. The narrower crack profile near the top of

the TUM specimens could then have limited the dispersion of the polymer precursor due to its viscosity.

6.4. Trials with non-destructive techniques

Further tests were performed on the concrete specimens healed with the SLV polyurethane precursor and analysed by the TUM research team dedicated to non-destructive testing. Preliminary results compiled by Gruyaert et al. (2015) are presented below.

Vibration analysis had already been described in the literature as a way to characterize damage in concrete (Neild et al. 2003) and was here assessed as an alternative, non-destructive technique for quantification of healing. With this technique, an impulse hammer is dropped on one side of the crack from a fixed height and an accelerometer acquires the vibration signal on the opposite side. The data is then processed and correlated with the elastic modulus of the material through which the vibrations propagated. Typical results are shown in Figure 50.

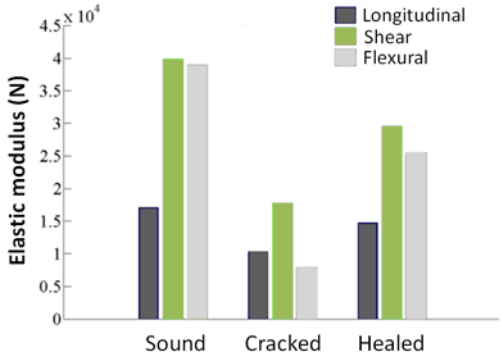

Figure 50: elastic modulus of concrete specimens assessed through vibration analysis; adapted from Gruyaert et al. (2015).

All the moduli of elasticity analysed decreased drastically once the concrete specimens were damaged by introducing a single crack with the 3-point bending setup described in the previous section. After the required curing period of 3 days to allow the polymer precursor to disperse and harden, the measurements were repeated and a considerable regain in all elastic moduli was observed, although without reaching the initial modulus of a sound specimen.

This technique can then be used to detect healing and possibly to qualitatively assess the area of the crack effectively healed. Given that this technique is relatively easy to implement and that these results were achieved without any damage to the specimen, it can be of particular relevance for field tests on larger elements.

Acoustic emission analysis can also be a useful technique in detecting the activation of self-healing or the failure of the polymer to follow crack movement. This was already discussed and tested at a smaller scale using mortar specimens in section 4.1. Larger concrete specimens allow however the use of multiple sensors, making possible the localization of the acoustic events. This way, any very high energy acoustic events or a burst of events can be more accurately associated to a specific physical event, such as rupturing of capsules or detachment of polymer from the crack faces when healed specimens are reloaded. Initial results published by Malm and Grosse (2014) were further expanded in Gruyaert et al. (2015). The distribution of the multiple sensors on a specimen is represented in Figure 51.

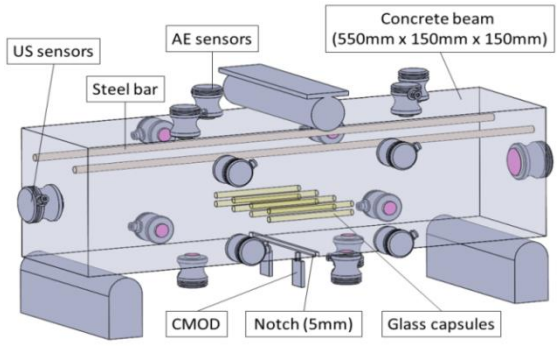

Figure 51: placement of multiple acoustic sensors for localization of acoustic events (Gruyaert et al. 2015).

An example of a test result is shown in Figure 52, which shows a burst of acoustic events occurring during reloading of a healed specimen. No such burst occurred however in reference specimens with an open crack (Gruyaert et al. 2015). This burst resulted in a slight discontinuity in the cumulative curve of events that is typical of localized, sudden damage and thus the respective signals were chosen for further localization analysis. A localization algorithm was applied to the data and the result is also displayed in Figure 52, which shows that

the acoustic events occurred at midspan, in the section containing the single healed crack.

Localization of acoustic events can thus provide additional evidence of failure of the healing material to follow crack movement, which is critical in the case of flexible healing materials, as is the present case. A flexible polymer will typically generate less acoustic hits than a rigid polymer during failure, as discussed in Chapter 4. This was also confirmed by Flohr et al. (2015), who used the same protocol described here and detected a higher amount of acoustic events when a rigid epoxy polymer was used as healing material, even if the healed area was smaller than the one shown in Figure 49. However, in a more realistic situation, where multiple cracks develop, localization accuracy decreases, as demonstrated and quantified by Tsangouri et al. (2016). This occurs because the existence of cracks between an acoustic emission and the transducers do not guarantee important principles of localization theory, such as the homogeneity of material properties and direct paths between acoustic event and the transducers.

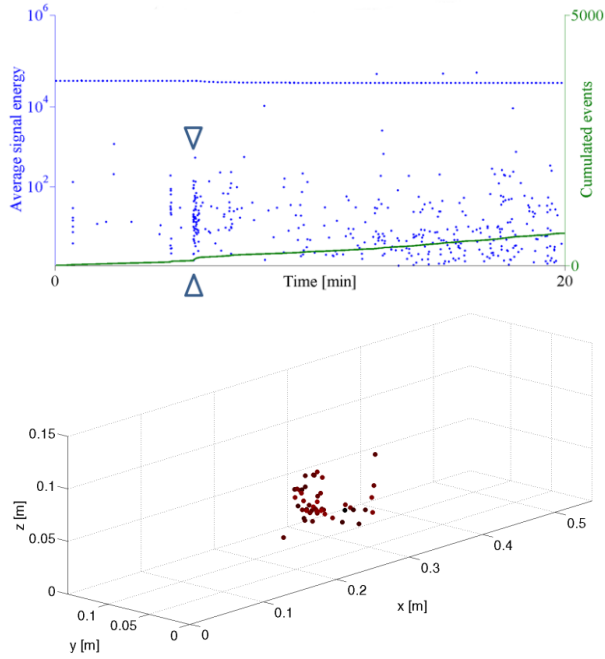

Figure 52: burst of acoustic events (between arrows) during reloading of a healed concrete specimen and respective localization within its matrix; adapted from Gruyaert et al. (2015).

The protocol also provided the localization of signals with very high energy occurring during cracking of the specimens, which corresponded very accurately to the position of the glass capsules (Gruyaert et al. 2015). Despite the accuracy, the localization algorithm is not as critical for this application, as it was already known (Tsangouri et al. 2013) that brittle rupturing of glass capsules generates acoustic signals with an energy much higher than the typical acoustic events occurring during loading of a concrete specimen and are thus easier to detect. This technique would however be difficult to implement in a field structure due to the lack of flexibility for positioning the sensors.

6.5. Chapter overview

On this chapter, self-healing based on encapsulated polymer precursors was tested at a larger scale, on concrete specimens, but still with pre-placed capsules that are not compatible with a field application. The larger specimen size allowed using multiple non-destructive techniques.

The following conclusions were drawn:

- ► with ultrasound transmission analysis it was possible to detect and monitor healing, as an increase of maximum amplitude of ultrasonic pulses occurred mostly during the first 10 hours after cracking and stabilized after 48 hours;
- ► a considerable 47% or 74% regain of strength, depending on the dimensions of the specimens, was achieved due to healing of a large part of the cracked plane; stiffness regain attained either 19% or 75%;
- ► several trials were performed with additional non-destructive techniques; vibration analysis was easy to implement and able to detect both a decrease and an increase of elastic modulus of the concrete specimens respectively after cracking and after healing; localization of acoustic events made acoustic emission analysis particularly useful, as it allowed guaranteeing that specific emissions were due to damage occurring at the healed section.

7.1. Spherical polymeric microcapsules

Spherical microcapsules were supplied by healCON partner Devan. These capsules were produced via interfacial polymerization between two phases consisting of droplets of healing agent (SLV precursor) in an immiscible phase (water) carrying a compound that stimulates curing of the healing agent. In this process, the healing agent used cannot be soluble in water and ideally cannot react with water, or at least it should react slowly by having some degree of hydrophobicity, as does the SLV precursor. The polymerization reaction occurring at the interface between the two immiscible phases is controlled by both reaction time and temperature, ideally resulting in a polymerized shell over the liquid healing agent. After interfacial polymerization is complete, the capsules are washed and dried and supplied in a powder form.

Several batches of microcapsules were tested, each one with slight modifications that aimed at improving their performance. The description and evolution of the batches is shown in Table 11. The changes introduced by batches 3 to 6 were done on top of the improvements introduced by batch 2.

Table 11: sequential description of the improvements made to the microcapsules

Batch	Description
1	Low core content
2	Improved core content
3	Addition of an alginate layer
4	Hydrophilic functionalization of the shell
5	Attempt of higher core content
6	Attempt of larger size

The capsules had mostly a spherical shape, with a small part of them having a droplet shape, as shown in Figure 53. All of the capsules resembled the ones shown in this figure, independently of the batch they belonged to, except for the capsules with an additional alginate layer. The capsules were initially observed under a stereo microscope which, due to its limited depth of field at high magnification, required EDF processing (extended depth of field) of the micrographs. EDF combines a stack of micrographs taken at different focal points resulting in an image completely in focus. This was achieved by using an EDF plugin within the image analysis program ImageJ. Observation under the microscope helped validating the particle size distribution of the capsules obtained from a laser diffraction equipment (Malvern Mastersizer) using wet dispersion in demineralized water and shown in Figure 54. Most of the capsules had sizes ranging from 50 μm to 100 μm. The size distribution was similar for all batches (except for double wall capsules), given that the manufacturing process was the same. Even a last attempt at achieving larger capsule sizes (batch 6) resulted in a similar size distribution.

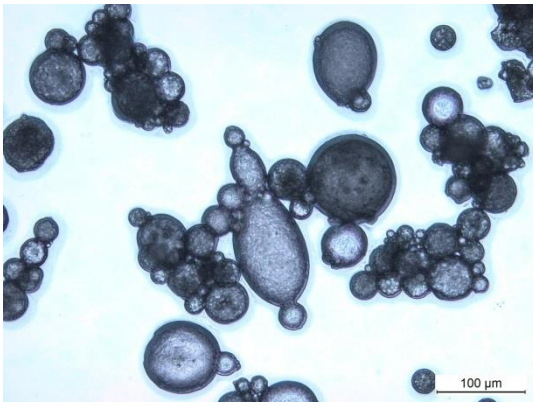

Figure 53: microcapsules dispersed in water (batch 1) and observed on a stereo microscope.

The capsules with a second wall of alginate (batch 3), which would increase the stability of the liquid core, were large spherical particles of approximately 1 mm. These were preliminary considered unfit as it was easily seen by naked eye that they were simply detaching from the cementitious matrix once embedded in cement paste specimens that were cracked. Additionally, the particles tested

were not single microcapsules with a second shell but instead multiple microcapsules inside a particle of alginate.

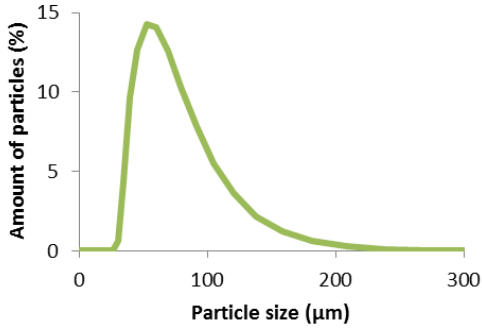

Figure 54: particle size distribution of microcapsules.

Throughout testing of the multiple batches it was noticed that the capsules were often forming clusters, as seen in Figure 53, but also that some of the batches caused a considerable delay of the setting of cement, which was thought to have been due to inconsistent washing during production, after synthesis.

7.1.1. Stability over time

The core content was determined by the manufacturer of the capsules via the soxhlet method, through which the wall of the capsules is dissolved and the content is extracted, weighed and compared to the total initial weight of the whole capsules. The first batch of capsules had no liquid core content after only a couple of weeks after synthesis, which meant that even if they ruptured, no healing agent would be available for healing. This was thought to be due to the fact that the amount of isocyanate, one of the functional groups of the polymer precursor used as healing agent, was too low. This would lead to a capsule shell too permeable to moisture, resulting in progressive curing of the core. The manufacturer of the healing agent agreed on increasing the amount of isocyanates and a new batch of capsules (batch 2) was synthesized. This batch had capsules with a core content close to 40 wt%. The core content decreased slightly over time, as shown in Figure 55, but the decrease was slow, which allowed further testing.

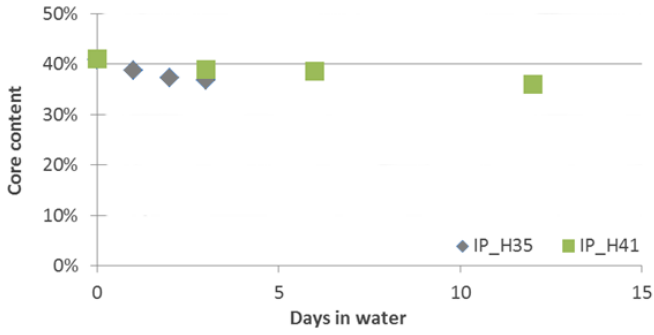

Figure 55: stability of the core content (wt%) of two production runs of capsules from batch 2.

7.1.2. Rupture and release of healing agent

Microcapsules were embedded in small cement paste specimens of 3x1x16 cm^3 to assess if they ruptured when embedded in a cementitious matrix. A specific dosage of microcapsules was not used, but instead an unrealistically high amount was used, so that it would be easy to detect them under SEM observation. The cement paste specimens were manually cracked after 14 days of curing inside plastic wrap and at a temperature of 20 °C. Small sections with cracked faces were carbon-coated and further prepared for SEM observation.

Figure 56 clearly shows that microcapsules from batch 2 were not rupturing, as they appear as whole capsules detached from the opposing crack face. Negatives from capsules that stayed attached to the opposing crack face can also be seen at the left side of the micrograph. A void can also be seen surrounding the capsules shown in Figure 56. This could have been the cause for detachment and it was the reason for synthesizing a new batch of capsules with a hydrophilic functionalization of the shell (batch 4). However, no improvement was observed and a void could still be seen between capsule and cementitious matrix, as shown in Figure 57.

Despite the void surrounding the capsules, throughout the SEM observations of different batches, it was noticed that a very limited amount of capsules were rupturing, but only the ones with sizes much larger than the average (>100 μm). This is the case for the capsule shown in Figure 57, which also shows that unexpectedly the capsules did not consist of a shell with a hollow core, but instead

they consisted of a dense particle with multiple small cores. This was thought to be an effect of uncontrolled foaming during the interfacial polymerization of the shell. It was obvious at this point that such dense particles would be much stronger than hollow shell particles and thus would have a much lower probability of rupturing.

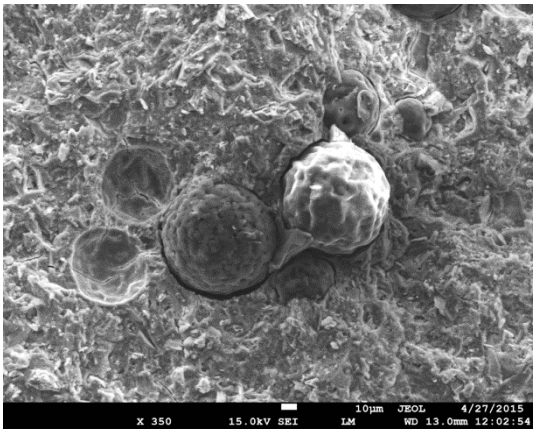

Figure 56: SEM micrograph showing detached microcapsules (batch 2) in a cementitious matrix after cracking.

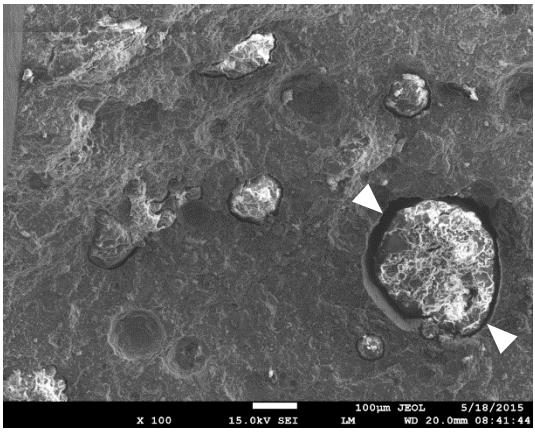

Figure 57: SEM micrograph showing a ruptured large microcapsule (batch 4; between arrows) embedded in a cementitious matrix after cracking.

To more clearly expose the multiple core structure of the capsules, they were embedded in an epoxy matrix that was manually cracked and washed in acetone

to remove any leaking polymer precursor. As the adhesion to the epoxy matrix is much higher than to a cementitious matrix, in this case even microcapsules with a size <100 μm were ruptured, exposing the multiple cores that can be seen in Figure 58. The existence of multiple cores would make it extremely difficult to release enough healing agent, particularly since the size of the microcapsules (50-100 μm) was already small compared to the targeted crack size in concrete (100-400 μm).

Last attempts at producing microcapsules with a larger core content (batch 5) or a larger size (batch 6) were not successful, resulting in microcapsules with properties similar to batch 2. At this point the development of microcapsules for encapsulation of a reactive polyurethane precursor with the available technology was considered unfeasible and was stopped.

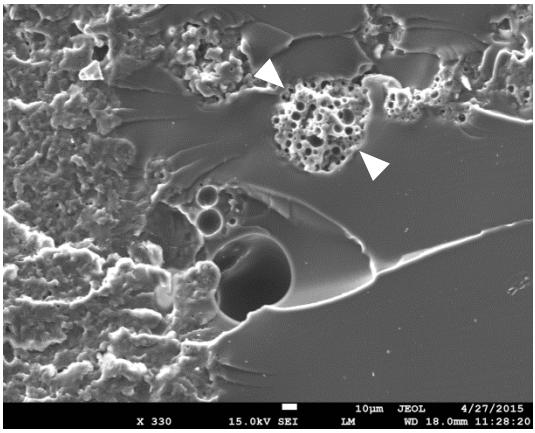

Figure 58: SEM micrograph showing the exposed multiple core structure of a ruptured microcapsule (batch 2; between arrows) embedded in an epoxy matrix after cracking.

7.1.3. Resistance to mixing

One single attempt at isolating the microcapsules from freshly mixed mortar was made for batch 1, before other bottlenecks in the development of microcapsules were revealed. The method is documented here for future reference.

Microcapsules were dispersed in the mixing water at a dosage of 3 wt% relative to the mass of cement used in the mortar mix. The mortar mix consisted of a sand-to-cement ratio of 3:1 and water-to-cement ratio of 0.5. The mixing pro-

cess was carried according to the specifications of EN 196-1. After mixing, a small portion of fresh mortar was diluted in isopropanol and sieved between aperture sizes 69 μm and 125 μm, which corresponded approximately to the size range of most capsules. The sieves were then put under flowing water to remove any remaining cement paste. The material retained between the sieves was dispersed in water and observed with a stereo microscope, which revealed that the material consisted essentially of whole microcapsules and few fine particles of sand (Figure 59). As the capsules were found intact, retaining their spherical shape, it could be concluded that they survived the aggressive mixing process. However, this fact was not surprising, as after further research it was found that the microcapsules consisted of dense particles with multiple cores and that batch 1 had no remaining liquid core content.

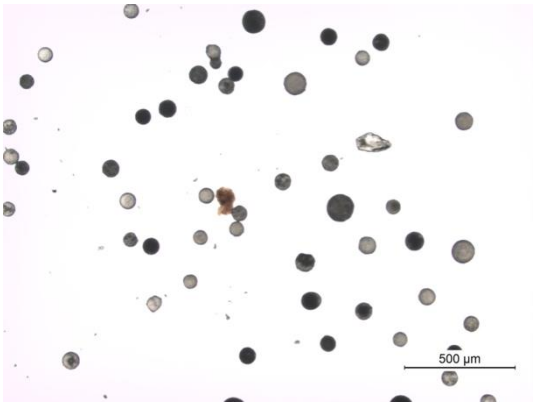

Figure 59: micrograph showing microcapsules (batch 1) recovered from fresh mortar after mixing and dispersed in water.

7.2. Cylindrical polymeric capsules

This section was adapted from the article Simulation aided design of tubular polymeric capsules for self-healing concrete (Šavija and Feiteira et al. 2017).

Polymers are generally more ductile than glass, leading to higher elongation at break and thus polymeric capsules are expected to rupture only when crossed by cracks much larger than those rupturing glass capsules. However, extruded polymeric capsules are potentially easier to manufacture than glass capsules due to their lower processing temperatures and the possibility for integrated extru-

sion, filling and sealing steps. Despite this, the development of tubular, polymeric capsules for self-healing concrete has been seldom studied.

Hilloulin et al. (2015) developed cylindrical capsules based on polymers with low glass transition temperatures and heated them above those temperatures prior to mixing into concrete, so that they would become less brittle and resist the mixing process. The capsules would then cool down below the glass transition temperature and become brittle again, so that they would rupture when crossed by a crack. Gruyaert et al. (2016) relied on a different mechanism. A plasticizer was added to the polymer, which would make the capsules less brittle and more likely to resist the mixing process. The plasticizer was expected to leach progressively into the moist environment of the young cementitious matrix, making the capsules brittle again. These studies were only partially successful, with capsules becoming insufficiently brittle or slipping in the cementitious matrix. Additionally, the mechanisms investigated are difficult to fine tune or to implement by the industry and no accurate determination of the crack size that would rupture the capsules was performed.

In this section of the book, a simpler approach is developed to solve the challenge of guaranteeing the two apparently conflicting requirements for polymeric capsules: to withstand mixing into concrete and to rupture when crossed by small cracks in concrete, narrower than 0.1 mm. Brittle polymers with low elongation at rupture were selected, which improves their likeliness of rupturing when crossed by small cracks. Capsules were then extruded from these polymers with different wall thicknesses, which in turn improves their robustness and likeliness of surviving the mixing process. Although the increased wall thickness could also reduce the chance of capsules rupturing for small cracks, a specific combination of a brittle polymer with a certain wall thickness was expected to fulfil the two requirements. A numerical model was used for prediction of the ideal combination of polymer properties and capsule dimensions, which is a critical tool to reduce the number of experiments performed to optimize polymeric capsules, while the experiments in turn were helpful in validating the model.

This research was only made possible by collaborations with other partners. The Laboratory of Polymeric and Composite Materials from the University of Mons selected and sourced the polymers and extruded the capsules, within the

scope of the CapDesign project. The numerical model was developed and adapted to this application by researchers from MicroLab at the Delft University of Technology, a partner in the healCON project.

Ultimately, even though polymeric capsules that could be used for self-healing concrete were found, none of the polymeric materials tested had a permeability to moisture low enough to allow using a moisture-curing polyurethane and thus they were not used for the upscaling tests described in chapter 8. They can however be used for encapsulation of polymers with other curing mechanisms, such as those developed by Araújo et al. (2016).

7.2.1. Crack size at rupture

Extruded polymeric tubes. In this study, five polymers have been selected as encapsulation materials. Polystyrene (PS) was supplied by BASF AG (Ludwigshafen, Germany; polystyrol VPT granule, M_n = 195,000 g/mol), polylactic acid (PLA) was obtained from NatureWorks (Blair, Nebraska, U.S.A.; PLA 4032D, 1.4% D-isomer). Two types of poly(methyl methacrylate) were used. PMMA_1 was kindly supplied by Evonik Performance Materials (Darmstadt, Germany; Plexiglas 8909, M_n = 38,000 g/mol) and PMMA_2 was also obtained from Evonik Performance Materials (Plexiglas 8N, M_n = 50,000 g/mol). PMMA_1-PEG was obtained by melt-blending PMMA_1 with 20 wt% of polyethyleneglycol monomethylether (PEG), which was purchased from Fluka (Buchs, Germany; mPEG2000, M_n = 2000 g/mol).

For the melt-blending, PMMA_1 was dried overnight under vacuum in an oven at 60 °C before compounding in a Brabender (Duisburg, Germany) mixer at 210 °C and a speed of 30 rpm for 3 min. PEG was added after PMMA was completely molten and the compounding process proceeded at 70 rpm for 7 min. PEG was added as a plasticizer for PMMA_1 to assess the feasibility of this option as a way to improve the chances of the capsules surviving the mixing process of concrete. The addition of PEG would increase the ductility of the capsules, making them less prone to be damaged by the stresses seen during concrete mixing. The PEG would then be partially and progressively leached out into the moist concrete, further lowering the ductility of the capsules so that they would rupture when crossed by small cracks in concrete. The strategy of using plasticizer migration to achieve evolving brittleness had already been tried by Gruyaert et al. [8] on capsules made out of ethyl cellulose, but leaching

was limited and the plasticizing agent leached preferentially towards the healing agent.

The mechanical properties of the polymers were then determined by tensile tests performed on dog bone-shaped samples (70 mm overall length and a straight section 40 mm long with a cross section of 1.5 mm × 5.0 mm) on a Zwick (Leominster, United Kingdom) universal tensile testing machine with a load cell of 1000 N. A preload of 0.5 N was used, the extension monitored was given by the separation between the grips and the stress-strain curves were obtained at a speed of 1 mm/min at room temperature. The results of the tensile tests are listed in Table 12.

Table 12: mechanical properties of polymers determined on dog bone specimens; average of 3 samples is shown with standard deviation.

Polymer	Tensile Strength (MPa)	Elongation at Break (%)	Young's Modulus (MPa)
PLA	67.7 ± 0.5	4.3 ± 1.3	2947 ± 22
PMMA_1	29.1 ± 3.7	1.1 ± 0.1	2234 ± 16
PMMA_1-PEG	29.9 ± 0.3	2.8 ± 0.2	1300 ± 8
PMMA_2	61.5 ± 14.3	3.0 ± 1.0	2223 ± 31
PS	38.5 ± 1.8	1.5 ± 0.5	2254 ± 20

This study also considered glass as an encapsulation material for comparison purposes. The mechanical properties of glass are listed in Table 13 and were taken from literature that investigated the use of glass capsules for self-healing concrete (Van Tittelboom 2012) and from their respective technical sheet (Hilgenberg borosilicate glass 3.3).

Table 13: mechanical properties of glass according to literature (Van Tittelboom 2012).

Material	Tensile Strength (MPa)	Elongation at Break (%)	Young's Modulus (MPa)
Glass	66	0.1	70000

To extrude the hollow tubes from which capsules were cut, pellets of polymer were dried in a hot air oven at 60 °C for one day before extrusion. The extrusion was performed on a Brabender (Duisburg, Germany) extruder equipped with a single screw and a tubular die with outer and inner diameters of 10 mm and 8 mm, respectively. The processing temperature was 225–235 °C with a screw speed of 10 min^{-1}, while the conveyor speed was adjusted to get approximately the desired external diameter and wall-thickness, which were 6 mm and 0.30 mm respectively. For PMMA_1, tubes with thicker walls were also tested. The average dimensions of the tubular sections from which the capsules were cut are listed in Table 14.

Table 14: average dimensions of the capsules used for the experimental tests.

Polymer	External Diameter (mm)	Wall Thickness (mm)
PLA	7.42 ± 0.12	0.44 ± 0.11
PMMA_1	6.37 ± 0.25	0.31 ± 0.09
	6.69 ± 0.04	0.72 ± 0.02
	8.40 ± 0.08	1.19 ± 0.01
PMMA_1-PEG	6.34 ± 0.13	0.26 ± 0.07
PMMA_2	6.14 ± 0.09	0.26 ± 0.07
PS	6.44 ± 0.16	0.42 ± 0.13

Modelling principle. Numerical models had already been developed in the context of self-healing concrete to simulate autogenous self-healing, the release of healing agent from capsules or their probability of rupturing. An overview can be found in Schlangen and Joseph (2013). The model described below and used for these experiments improves on the major drawback of the models developed to date, as it considers the mechanical properties of the capsule material and its interaction with the cementitious matrix.

The Delft lattice model was used to simulate rupture of tubular capsules subjected to mechanical loading. In lattice models, material is discretized as a set of small truss or beam elements that can transfer forces (Figure 60). In the particular case of the Delft lattice model as used herein, all individual elements exhibit linear elastic behaviour. The fracture simulation is achieved by performing a linear elastic analysis of the lattice under loading, and removing an element

which exceeds a prescribed fracture criterion (e.g. strength, strain, or energy) from the mesh. This analysis is then repeated in a step-wise manner, removing a single element in each-step. Thus, a non-linear analysis is performed by actually performing a number of linear analyses. Using this method, realistic crack patterns are found. Furthermore, even though individual elements have a brittle behaviour, a ductile global response is achieved. Details about the underlying elastic equations as well as the full computational procedure of the model are available in Schlangen (1993) and Schlangen and Qian (2009).

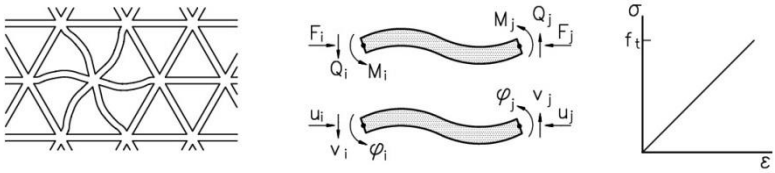

Figure 60: lattice of beam elements (a), definition of forces and degrees of freedom (b), stress-strain relation of beam element (c).

In the present work, a fracture criterion based on the tensile stress in beams is adopted. Normal force (N) and bending moments (M_x, M_y) are both taken into account by the following general relation:

$$\sigma = \alpha_N \frac{N}{A} + \alpha_M \frac{\max(M_X, M_Y)}{W}$$

where A is the beam cross-sectional area, W the cross-sectional moment of resistance, α_N and α_M are the normal force influence factor and the bending influence factor. Their values are adopted herein as 1.0 and 0.05, respectively. To simulate tubular carriers, a capsule is placed within the material domain. The capsule is connected to the matrix lattice elements through bond beam elements (Figure 61).

For matrix elements, a brittle fracture law is adopted, as presented in Figure 60. For the capsule elements, experimental data for each of the considered materials is input as a multi-linear stress/strain relation (Figure 62). Bond beams are not allowed to break in the present simulations, because a perfect bond is seen as a prerequisite for breakage of the tubular carriers.

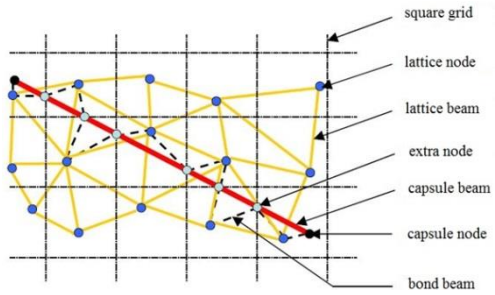

Figure 61: schematic 2D representation of capsule-lattice.

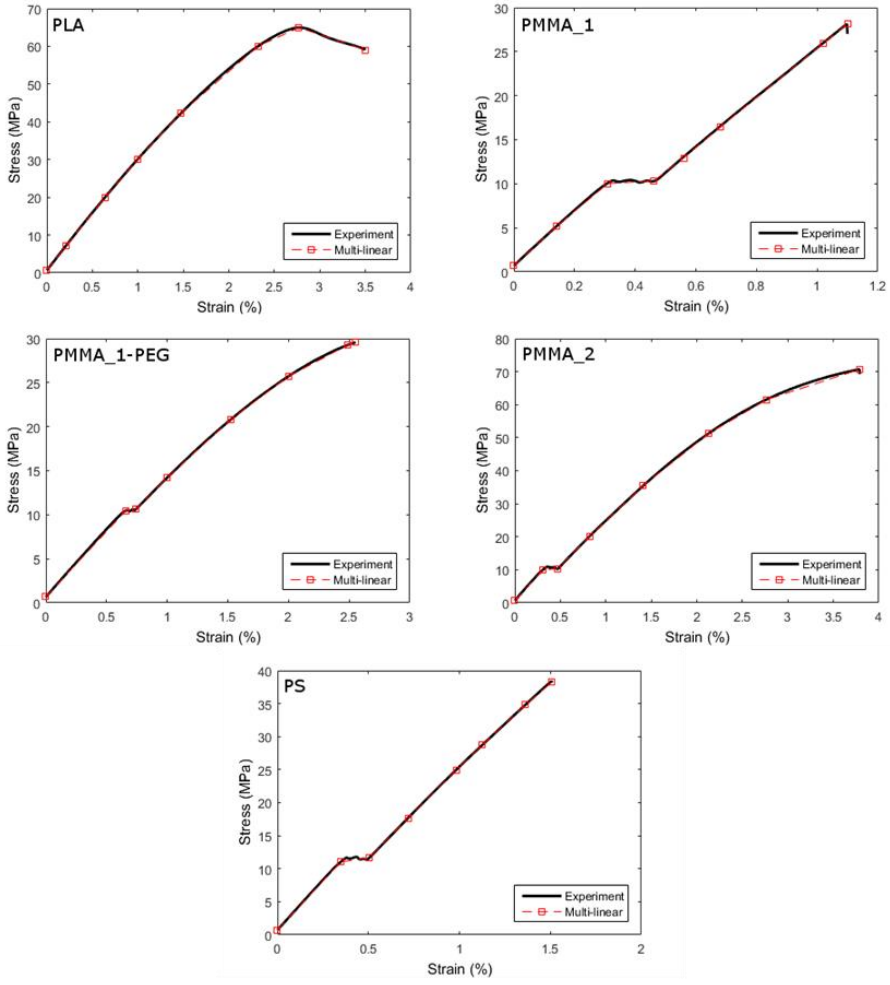

Figure 62: experimental and schematized stress/strain relationships of encapsulation materials.

In the simulations so far, a 30×30×30 mm³ mortar block with a single tubular capsule is simulated, as schematically shown in Figure 63. It is subjected to uni-axial tension along the axis of the capsule, and the breakage of the capsule is monitored. The mortar is simulated as having a Young's modulus of 20 GPa and a tensile strength of 3.5 MPa, which is within the range of values used in previous work (Šavija et al. 2013 and Luković et al. 2016).

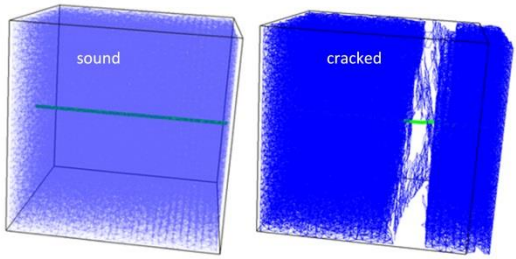

Figure 63: lattice with an embedded tubular capsule.

Experiment. To create the capsules to be tested, sections 5 cm long were cut from the polymeric tubes. The ends of the capsules were heated and shaped to create hooks for improved mechanical locking once embedded in a mortar matrix. To additionally improve adhesion to the cementitious matrix, the capsules were sanded in a direction perpendicular to their length, as highlighted in Figure 64.

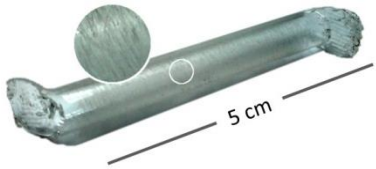

Figure 64: capsule with moulded hooked ends and sanded surface.

The capsules were then embedded in reinforced mortar prisms with dimensions 40×40×160 mm³ by placing one capsule inside each mould, 1.3 cm from the bottom and centred relative to the sides, before pouring the mortar. The mortar mix consisted of CEM I 52.5 N, and had a sand-to-cement ratio of 3:1 and a water-to-cement ratio of 0.5. Mixing and moulding were performed according to the EN 196-1 standard. The specimens contained also two reinforcing Ø2 mm smooth metal bars, placed 10 mm away from the sides and the bottom of

the specimen, to avoid complete splitting during the cracking process. Figure 65 shows the relative positions of the capsule and the reinforcement bars on a specimen split in half.

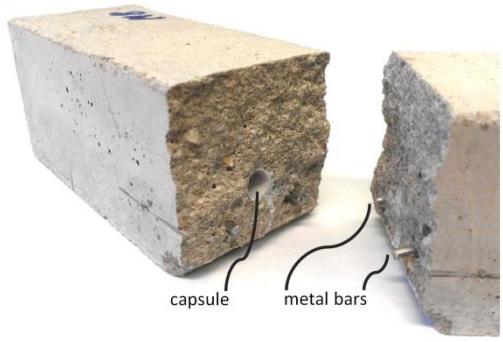

Figure 65: split 40x40x160 mm^3 specimen showing an embedded capsule ruptured during bending.

To create and progressively widen cracks that crossed the embedded capsules, the mortar prisms were loaded in a three-point bending test controlled by an external linear variable differential transformer (LVDT) (Solartron, Leicester, United Kingdom) with a 1 mm range. The LVDT was attached at one of the sides of the specimen, parallel to the embedded capsule and at the same height as its bottom fibre (Figure 66), so that it effectively measured the size of the crack crossing the capsule. To standardize the orientation of the crack, a triangular notch was molded into the bottom of the specimens, at half of their length.

Figure 66: LVDT positioned at the side face of a specimen to measure the crack size at the height of the embedded capsule.

Results. The numerical model was used to simulate the mechanical response of capsules embedded in a cementitious matrix. This was performed for the different polymers listed in Table 12, considering capsules with a 5 mm external diameter and a wall thickness in the range 0.1–1.0 mm, to have a first assessment of their fitness. The dimensions used as input for the model at this stage are representative of the typical size of capsules that can be manufactured with the extrusion equipment used. As shown in Figure 67, only capsules made of polystyrene (PS) and a polymethyl methacrylate (PMMA_1) seem fit for the intended application, as they rupture for a crack size below the targeted limit of 100 μm (see introduction), however only if the wall thickness is kept under ~0.5 mm. Of the two materials, the crack size at rupture for capsules of PMMA_1 is the least affected by the wall thickness. It is also shown that capsules of both of these materials still rupture for a crack size several times higher than the size required to rupture glass capsules of similar dimensions. The glass curve was based on the properties listed in Table 13 and assumes a perfectly-elastic brittle behaviour.

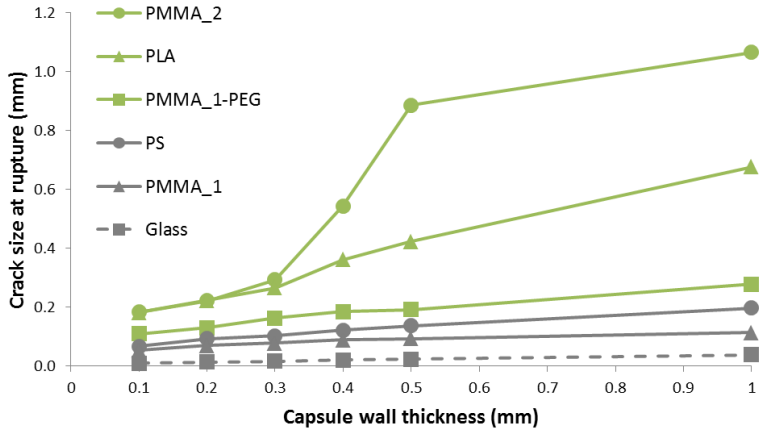

Figure 67: model output for tubular capsules with an external diameter of 5 mm embedded in a mortar matrix under tensile stress.

As a general rule, the mechanical properties of polymers, such as tensile strength, stiffness and ductility, rise with increasing molecular weight, although exceptions exist. This can be clearly observed in Figure 62, where PMMA_2 (M_n = 50,000) shows higher tensile strength and ductility than PMMA_1 (M_n = 38,000). As both types of PMMA have a similar Young's modulus, the higher

tensile strength (twice as high) and ductility of PMMA_2 result in larger elongation at break, which explains its much larger crack size at rupture. It can also be said that the inadequate performance of PLA capsules, which break only for crack sizes of ~0.2 mm or higher, is not necessarily intrinsic to the material type, but depending also on the molecular weight of the PLA used.

Overall, different combinations of tensile strength, stiffness, and ductility of the different polymer types and molecular weights result in different values of elongation at break, which is the commanding factor for guaranteeing rupturing of capsules when crossed by small cracks in concrete. Given the good predicted performance of PMMA_1 and PS capsules shown in Figure 67, and according to their elongation at break listed in Table 12, an elongation of 1.5% or less is recommended for polymers considered as encapsulating materials in self-healing concrete. Polyethylene terephthalate (PET) and polyvinyl alcohol (PVA) could potentially also fulfil this requirement for low elongation at break. However, being water-soluble, PVA would not be the best solution for application in concrete. Other factors should also be considered, such as compatibility with the encapsulated healing agent and with the extrusion process. All polymers used in this study were equally easy to melt and flowed easily during extrusion, while their cost was not as relevant, as all selected polymers were inexpensive (<1 EUR/kg).

The mechanical response of the capsules was then experimentally determined by embedding them in mortar specimens cracked under bending, where the capsules rupture under tensile stress once the crack crossing them reaches a critical size. Rupturing of the capsules induces a sharp load drop in the stress-displacement curves and a small reduction in the load capacity after that. These features were then used to experimentally determine the crack size at rupture of the capsules. Representative curves are shown in Figure 68 for the capsule types for which an average was possible to determine, i.e. for which all capsules ruptured before a 0.4 mm crack size was achieved.

The experimental data regarding the crack width at rupture for the different capsule types is plotted in Figure 69 and it confirms that the capsules extruded from PMMA_1 (wall thickness of 0.31 mm) rupture for a crack size below 100 μm, which makes them fit for the intended application.

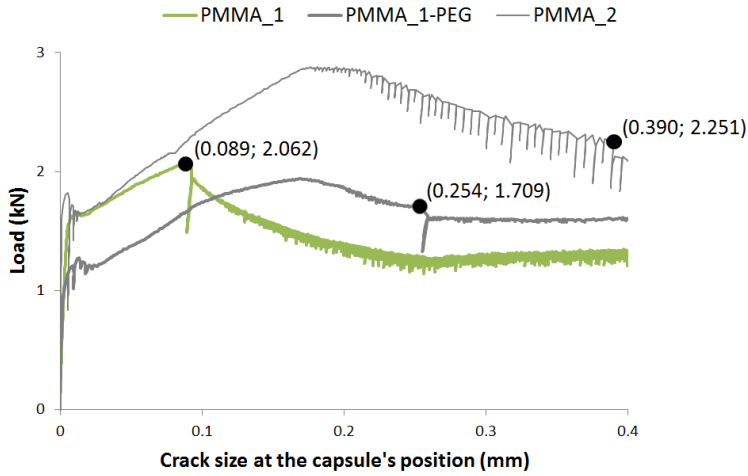

Figure 68: characteristic load drops at the moment of rupturing of capsules (black dots) embedded in mortar prims during three-point bending experimental tests. PMMA_1 curve is from the series with thinner walls of 0.31 mm.

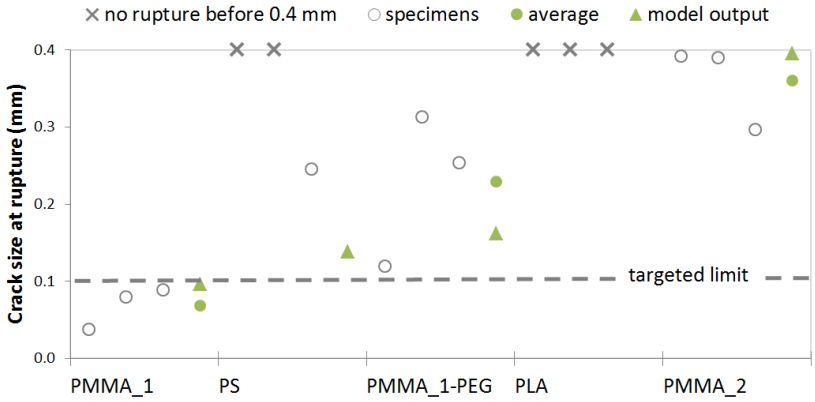

Figure 69: crack size at the moment of rupturing of the capsules, in relation to the targeted maximum crack size of 100 μm.

The results also show that PEG did not leach out of the PMMA_1-PEG material, or it did not leach out enough for capsules of this material to behave as capsules made out of PMMA_1. Rupturing of PMMA_1-PEG capsules took place for crack sizes more than twice as large as for PMMA_1. The experimental data for PMMA_1-PEG also shows more scattering and the average crack size at rupture ended up being larger than the model output, when the

opposite would be expected if there had been leaching of the PEG plasticizer. Accordingly, it was for these capsules that the model output showed its maximum deviation from the experimental results, at ~29%. The scattering of experimental data for this polymer can be due to insufficient blending of PMMA and PEG, resulting in a polymer matrix that is not homogeneous.

Given the good modelled performance for extruded PS, it was unexpected that two out of three capsules of this polymer did not rupture during the test, which achieved a maximum crack size of 400 μm. A possible explanation for this could be a somewhat worse adhesion of the PS material to the cementitious matrix, which would cause the capsules to slip instead of deforming. An additional reason could be that the mechanical properties of PS in particular were affected by the extrusion process, which would then result in a mismatch between the experimental results and the model, which used as input the mechanical properties prior to extrusion. Mechanical properties can also be affected by exposure to the alkaline environment of concrete, but that is unlikely to be the case, given the relatively short exposure of 14 days.

For the remaining polymers, the crack width at rupture was much higher than the targeted limit of 100 μm, as expected from the model output and confirming that these polymers are not good candidates for the intended application. For PMMA_2, the model output was very similar to the average crack size at rupture determined experimentally, with a deviation of ~10%. Regarding PLA capsules, it was not possible to assess how accurate the model was, given that their crack size at rupture is larger than the range of the experimental test and estimated by the numerical model to be 0.547 mm.

For the best performing PMMA_1 polymer, capsules with thicker walls were then extruded and experimentally tested and the results were compared to the model output based on the exact same dimensions. The results are plotted in Figure 70. The average crack size at rupture determined experimentally followed the same trend of the model output, i.e., an increase in crack size at rupture with increasing wall thickness (for similar external diameters), with a maximum deviation from the model of ~16% for the capsules with a 1.19 mm wall. The absolute values of crack width at rupture determined experimentally were 69 ± 22 μm, 128 ± 36 μm, and 251 ± 4 μm, respectively for capsules with an average wall thickness of 0.31, 0.72 and 1.19 mm.

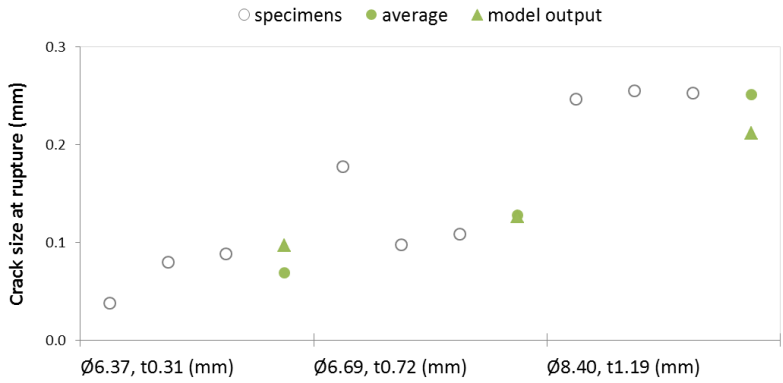

Figure 70: crack size at the moment of rupturing of PMMA_1 capsules with different external diameter (Ø) and wall thickness (t), according to both the numerical model and the experimental results.

Finally, to assess how the results were affected by the treatment of the capsules, which included sanding of the outer surface and moulding hooks at the ends (Figure 64), tests were also performed on smooth capsules without the treatment. The capsules used were from the same batch as those identified in Figure 70 as having a wall thickness of 0.72 mm. Without the treatment, the capsules did not rupture within the testing range, which achieves a crack size of 400 μm. Reintroduction of only the sanding step, without the moulded hooks at the ends, re-established rupturing for a similar range of crack sizes (111 ± 18 μm).

This proves also that it is unlikely that the poor performance of the PS capsules was related to a lack of adhesion, since the good adhesion between the best performing PMMA_1 capsules and the cement paste matrix was essentially mechanical in nature and achieved due to the roughness of the capsule's surface introduced by sanding it, i.e. not due to a particularly good compatibility between PMMA and the cement paste.

Even though PMMA_1 capsules are not compatible with the moisture-sensitive precursors used in this book, as premature hardening would occur, they have been combined with other agents by Araújo et al. (2017), who confirmed that capsules with a wall thickness of 0.7 mm do survive the mixing process when self-compacting concrete is used. The same study confirmed that these capsules can rupture and release their contents when realistic cracks are created in real-scale concrete beams.

7.3. Cylindrical glass capsules

Glass capsules have been used before as proof-of-concept capsules, typically with very thin walls that do not allow them to resist being mixed into concrete. However, due to the exceptional barrier properties of glass, they have to be considered as part of a potential upscaling solution. Given that the polymer precursors used are moisture-curing, which allows using them as a single component healing agent, water molecules should not be able to diffuse through the capsule walls. Otherwise, premature hardening of the healing agent occurs within the capsule. Good barrier properties are achieved by using glass or metal, as attested by their extensive use by the food industry. Additionally, other industries already deal with filling and sealing of glass ampoules at a large scale, so that would not be a bottleneck in upscaling of self-healing concrete using this type of capsule.

One obvious final concern with embedding glass capsules in concrete could be the potential for the deleterious alkali-silica reaction to occur, which would dissolve the reactive silica in the glass, hindering its barrier properties in the long term and cracking the surrounding cementitious matrix. However, it has been reported that boro-silicate glass can produce little, benign expansion when used as fine aggregates in concrete (Saccani 2010). It is thus expected that the capsules used in this study, also produced from boro-silicate, would result in even less expansion, as larger particles of glass have a reduced expanding potential.

7.3.1. Stability over time

Even though glass has very good barrier properties, the method and material used for sealing the glass tubes will affect the stability of moisture-curing precursors. Ideally, after filling the glass tubes, the ends would be fused by melting them with a torch, which is the method used during industrial sealing of ampoules. At a laboratory scale however, this is not practical for sealing a large number of capsules, as all the work is done manually. Additionally, once capsules with a reasonably thick wall (>0.5 mm) are used, it gets increasingly difficult to fuse them quickly with a conventional torch. Thus, at a laboratory scale, adhesives are typically used for sealing the ends of the capsules. These adhesives, being polymers, have high moisture diffusion rates compared to glass, making them preferential paths for ingress of water molecules into the capsules.

As a result, the moisture-curing polyurethanes used in this study progressively cure near the ends of the capsules, initially becoming more viscous and eventually turning into a solid polymer.

To document and quantify this effect, glass capsules with 5 mm external diameter, 0.8 mm thick walls and 50 mm long were filled with the SLV precursor and sealed with a 2-component PMMA glue. The PMMA glue at the ends was applied in such a way that it formed a plug approximately 2 mm thick. The capsules were then stored at 90% RH and ambient temperature and observed up to 24 days after encapsulation. Each time the capsules were observed, pictures were taken against a dark background, which increased the contrast between the partially reacted precursor near the ends of the capsule and the remaining section still filled with unreacted polymer.

The images of individual capsules were then turned into a binary black and white image with the GIMP image editor (Figure 71a) and the amount of black pixels, corresponding to partially reacted polymer, was counted. By dividing the amount of black pixels over the total amount of pixels contained in the capsule image, a quantification of the percentage of precursor partially reacted was achieved.

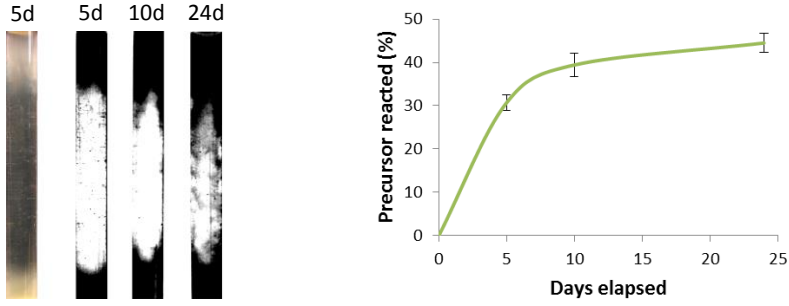

(a) (b)

Figure 71: progressive reaction of a moisture-curing precursor inside glass tubes sealed with PMMA glue (a) and data plot of 3 specimens (b); for 5d both original and binary images are shown.

The quantification results are shown in Figure 71b, where it can be seen that during the first days after sealing the precursor quickly starts reacting due to moisture ingress through the PMMA plugs. At this point, the partially reacted

precursor is not fully hardened, but its viscosity increases considerably. After 5 days, the rate of progression is reduced considerably, but it is expected that after several months most of the polymer would be either solid or too viscous.

This effect was observed for other adhesives too, such as hot glue or a 2-component epoxy, although the latter seemed to result in a slower rate of reaction. The effect also depends on the thickness of the plugs, with an increasing thickness resulting in a slower progression.

7.3.2. Crack size at rupture

Given the mechanical properties of glass, particularly its low elongation at break of 0.1%, tubular glass capsules rupture when crossed by very small crack widths. The several experiments performed proved that glass capsules are fit for self-healing and that they rupture for typical crack sizes in concrete. An accurate determination of the crack size needed to rupture glass capsules was however needed to prove that capsules with thicker walls would rupture for acceptable crack sizes. Thicker walls would increase their strength and their chance of surviving the mixing process of concrete, allowing using them as a solution for upscaling self-healing concrete based on encapsulated polymer precursors. Several tube sizes with a diameter in the same order of magnitude but different wall thickness were selected for testing. The tubes were cut in 5 cm sections, sealed with hot glue and tested in the same way as described in section 7.2. The results and the dimensions of the tubes tested are shown in Figure 72.

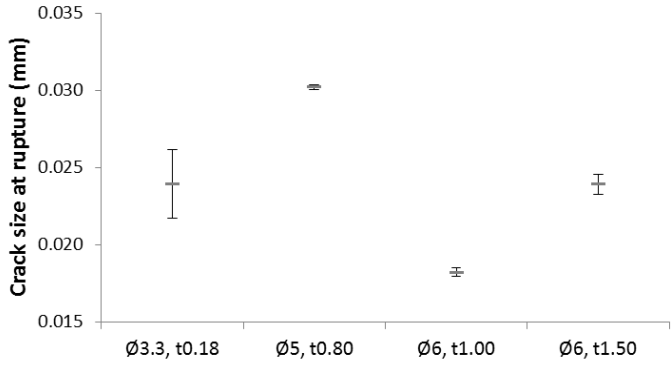

Figure 72: Crack size at rupture for glass capsules with different outer diameter (Ø, mm) and wall thickness (t, mm).

Regardless of the wall thickness, the capsules ruptured when crossed by very small cracks in the size range 15-30 μm. The capsules with thicker walls are then potentially fit for the intended application, i.e. being mixed into fresh concrete, if they survive the aggressive mixing process, which is assessed in section 7.3.4.

7.3.3. Release of healing agent

Ample evidence has already been shown in this book that a polymer precursor can be effectively released from a tubular glass capsule. However, as presented in section 7.3.1, the use of a thin plug of PMMA led to partial reaction of the precursor near the ends of the capsule. From this reaction results the release of CO_2, which creates pressure inside the capsule. It was found that this pressure improved the release of precursor into the crack, as it counteracts the capillary forces retaining the liquid precursor in the capsule. It was observed that when an improved, thick epoxy plug of approximately 3 mm was used to seal the capsules, the amount of polymer released decreased considerably, especially if specimens were tested at an early age of 14 days, which also minimizes the amount of polymer partially reacted inside the capsules and the pressure developed.

It was decided that a realistic implementation of self-healing based on encapsulated polymer precursors would have to include well sealed capsules and an alternative mechanism to pressurize the capsules. Such a mechanism was tested by Goethals (2009) and it was based on the increased pressure achieved by the phase change of a compound. Perfluoro-N-pentane in liquid state, with a boiling temperature of 21.9 °C, was encapsulated together with the healing agent and the sealed capsules were exposed to a temperature higher than 21.9 °C. At the increased temperature the compound turned into a gas, thus increasing the pressure inside the capsules. However, in this case the pressure increase remains only if the temperature stays above the boiling temperature of the compound.

A better mechanism for pressurizing capsules would be based on the decomposition of a compound, instead of a reversible phase change. That was the mechanism chosen for investigation in this book. Pressure inside the capsules was intentionally created by dissolving a small amount of benzoyl peroxide (BPO) in the SLV precursor. When capsules are exposed to temperatures above 60 °C,

BPO decomposes in a two-step reaction (Figure 73) and releases CO_2, which incidentally is the same gas generated by the reaction of the precursor, thus creating pressure.

An experiment was then performed to assess the effectiveness of this method and to quantify the effect of different amounts of BPO on the release of precursor. BPO in powder form (PEROXAN BP-Pulver 50 W+) and a small amount of fluorescent pigment were dissolved in the healing agent on a magnetic stirrer for approximately 15 minutes until all powder was dissolved. This mix was then encapsulated in 30 mm long glass capsules with a 5 mm external diameter and 0.8 mm thick walls, which were sealed with a 3 mm thick epoxy plug. It is of extreme importance that the BPO used has only residual amounts of water, otherwise premature hardening of the moisture-curing precursor will occur inside the capsules. As BPO is an unstable compound, it is usually mixed and packed with high amounts of another compound for stabilization. This stabilizing compound is often water, but the BPO product used in this experiment contained dicyclohexyl phthalate.

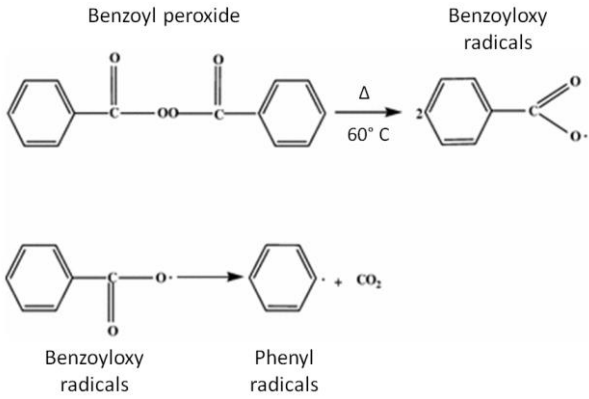

Figure 73: two-step decomposition of benzoyl peroxide and release of CO_2 to pressurize capsules.

Decomposition of BPO was stimulated by exposing the sealed capsules in an oven at 80 °C for approximately 3 hours, after which the precursor changes from a light yellow into a brown colour. The capsules were then embedded in 40x40x160 mm^3 mortar specimens reinforced with an FRP strip, which were then loaded in a 3-point bending setup to create cracks of approximately 0.25

mm (see section 4.1 for additional details on specimens and method). One capsule was used per specimen, so that after curing of the polymer and complete splitting of the mortar specimens, the area healed per capsule could be assessed.

It should be noted that the type of mortar specimens used and its effect on the speed of formation of cracks can also affect the release of precursor. With the specimens used, with FRP strips placed at the compression zone (Figure 19), a crack is formed instantly when the flexural strength of mortar is surpassed. If reinforcing metal bars had been used (Figure 7), reinforcement would still carry load after failure of the mortar matrix and the crack would develop slowly, depending on the speed of loading. A slow opening rate of a crack increases the chance of the precursor making contact with the mortar matrix before a concave meniscus is formed inside the capsule, as shown in Figure 74. Without contact with the mortar matrix, the capillary forces from the narrow crack cannot act on the precursor to pull it out of the capsules. This situation is more likely to occur if a large crack is formed instantly, such as when FRP strips are used in the compression zone. This was the method chosen for this experiment, as it would be more representative of the worst case scenario in a field structure, thus leading to conservative results.

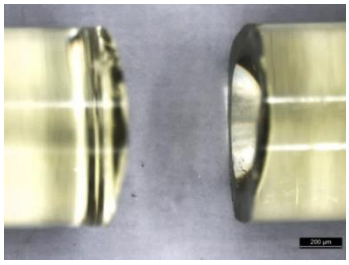

Figure 74: concave meniscus formed in the precursor once unpressurized tubular glass capsules (3.4 mm inner diameter) are ruptured.

The addition of the fluorescent pigment to the precursor made it easier to detect the healed area under near-UV light, although the fluorescent effect was not as intense for the precursor mixed with BPO, as after decomposition of BPO the mix turned dark brown. Representative images of the split crack faces after healing are shown in Figure 75 for the cases without BPO and with 5 wt% of BPO. The experiment was repeated for three specimens and for a 1 wt% dosage of BPO. As after splitting of the mortar specimens the cured polymer

stays attached to either one of the crack faces, the area healed per capsule was quantified by manually defining its limits on each crack face and counting the pixels relative to the area of the whole crack face using the GIMP image editor. The average results in terms of area healed per capsule are shown in Figure 76. An addition of just 1 wt% of BPO increased the area healed by approximately 4 times, while a higher dosage of 5 wt% did not result in further increase. It was also verified that for the specimens with BPO almost no precursor remained inside the capsules.

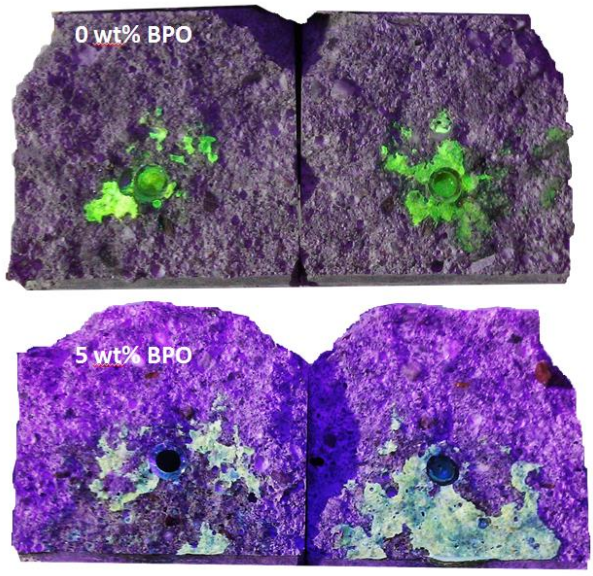

Figure 75: effect of pressurization of capsules by decomposition of BPO on the area of a crack healed with a single capsule (in green).

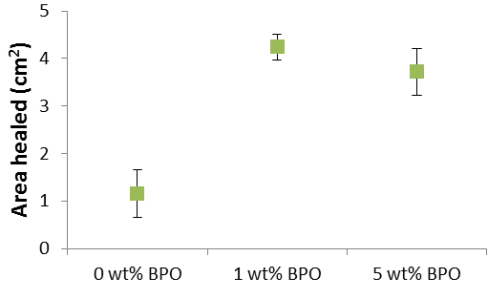

Figure 76: increase of area healed per capsule with the addition of BPO.

The release of precursor is also greatly affected by the dimensions of the inner diameter of tubular capsules, as this will also affect the magnitude of the capillary forces keeping the healing agent inside the tube. Formia et al. (2015) reported that even a very low viscosity solution of sodium silicate could not be satisfactorily released from cement paste capsules with an inner diameter of 2 mm and while the solution was effectively released from an inner diameter of 7.5 mm, a high variability of the results was still observed. Thao (2009) observed that very little moisture-curing epoxy was released from glass tubes with a 3 mm inner diameter, but an increase to 4 mm resulted in proper release and good healing efficiency. The maximum practical inner diameter is also not much larger than 4 mm, as larger diameters make it increasingly difficult to seal the capsules with liquid adhesives. Larger inner diameters up to 8 mm have also been tried in this study, but it was found that if well sealed and without pressurization of the capsules, the volume of the SLV precursor released was still very low.

7.3.4. Resistance to mixing

After confirming that glass capsules with thicker walls up to 1.5 mm were still able to rupture when crossed by very small cracks in concrete with sizes below 30 μm, it was assessed if the thicker walls would allow them to survive mixing into concrete, which was a major bottleneck at the start of the research program.

The tubes were cut, filled with SLV precursor mixed with a fluorescent pigment (for easier localization in the fresh concrete) and sealed with hot glue. The capsule dimensions tested corresponded to the ones for which the crack width at rupture was assessed in section 7.3.2. A batch of 27 litres of ordinary concrete with a slump of 45 mm was mixed for 3 minutes in a 50 litre vertical shaft mixer. The mix consisted of 0/5 mm sand (640 kg/m^3), gravel 2/8 mm (462 kg/m^3), gravel 8/16 mm (762 kg/m^3), CEM I 52.5 N (360 kg/m^3) and water (165 kg/m^3).

Capsules with two different lengths, 30 mm and 50 mm, and different diameters and wall thickness were then added together to the fresh concrete during mixing (10 capsules per combinations) at a dosage of approximately 3 capsules per litre of concrete and mixed in for an additional 5 minutes. Finally, the fresh concrete was passed through a sieve with a 4 mm aperture under flowing water,

to remove the fresh cement paste, and any capsules found were retrieved, cleaned and counted.

The results are shown in Figure 77. Out of 10 capsules added for each series, none survived in the case of capsules with a very thin, 0.18 mm wall, regardless of their length. For 3 cm long capsules, similar results were achieved for all the other series with wall thickness in the range of 0.80 mm to 1.50 mm, with a minimum of 8 and a maximum of 10 capsules surviving, corresponding to almost the total of the capsules added. In the case of 5 cm long capsules, the survivability decreased, with 6 to 7 capsules found intact and 2 capsules per series found mostly intact but damaged at the ends, which resulted in a compromised seal and potential hardening of the healing agent inside the capsules in the long term.

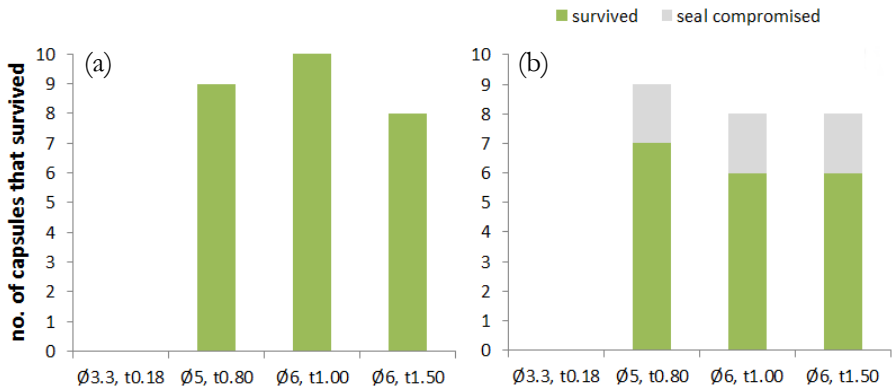

Figure 77: survivability of glass capsules 3 cm (a) and 5 cm (b) long when added to concrete during mixing; 10 capsules were added per series; glass capsules with different outer diameter (Ø, mm) and wall thickness (t, mm).

7.4. Chapter overview

Several configurations of capsules in terms of materials, shape and dimensions were tested in order to assess their potential as carriers for polymer precursors used as self-healing agents in self-healing concrete. The performance of the capsules was assessed in terms of their barrier properties, their resistance to mixing in concrete and their capability of rupturing when crossed by small cracks in concrete. Additionally, experimental results for cylindrical polymeric capsules were compared to the output of a numerical model predicting the crack size needed to rupture them.

While spherical polymeric microcapsules did not rupture when crossed by a crack, cylindrical polymeric capsules were not able to keep a moisture-curing polyurethane stable. Cylindrical glass capsules were then determined to be the best encapsulating technique when moisture-sensitive healing agents are used, as they fulfilled all major requirements for this application. A mechanism of pressurizing the capsules was also developed, leading to a considerable increase of healed area. More detailed conclusions are listed below.

Regarding spherical polymeric microcapsules:

- ► 6 different batches of capsules with a diameter of 50-100 μm were tested;
- ► a 40% core content stable over the period of several weeks was achieved;
- ► the capsules detached from the cementitious matrix and did not rupture when crossed by a crack;
- ► capsules were found to consist of multiple small cores, which would make it difficult to release their content;
- ► multi-core capsules were robust enough to resist mixing into mortar.

Regarding cylindrical polymeric capsules:

- ► 5 different polymers were tested as encapsulation materials in the form of cylindrical capsules with external diameters of ~7 mm;
- ► a PMMA type of capsule was found to rupture when crossed by small cracks in concrete of ~100 μm even for fairly thick capsule walls of 0.7 mm, which would increase their likeliness of also surviving mixing into concrete;
- ► a numerical model satisfactorily predicted the crack size at rupture, proving to be a valuable tool in the design of capsules for this application, reducing the number of experiments needed;
- ► ultimately, cylindrical polymeric capsules were found to be incompatible with the moisture-curing polyurethanes used in this study as healing agent, as their permeability to moisture resulted in premature hardening of the polyurethane precursor.

Regarding cylindrical glass capsules:

► it was found that the adhesives used to seal the capsules slowly allow ingress of moisture, resulting in partial reaction of the moisture-curing polyurethane at the ends;

► partial reaction of polyurethane precursor releases CO_2 and pressurizes the capsules, which has a beneficial effect on its release into the crack;

► capsules with thicker plugs were more stable, avoiding considerable reaction of the polyurethane precursor and a mechanism based on the decomposition of benzoyl peroxide was implemented as an alternative to pressurize them;

► addition of 1 wt% of benzoyl peroxide relative to the polyurethane precursor increased the healed area by 4 times;

► even glass capsules with thick walls of 1.5 mm ruptured when crossed by very small cracks of ~25 μm;

► glass capsules with a wall thicker than 0.8 mm had high resistance to mixing in concrete (8-10 out of 10) for a capsule length of 30 mm, decreasing slightly (6-7 out of 10) for 50 mm long capsules.

8. UPSCALING OF SELF-HEALING CONCRETE

8.1. Concrete specimens with randomly distributed glass capsules

Glass capsules with wall thickness larger than 0.8 mm and a length of 30 mm were shown to resist the mixing process of concrete in section 7.3. This allows testing self-healing at a larger concrete scale, with capsules added during mixing, which is a solution that could be easily implemented by the industry.

Specimen preparation. This upscaling solution was tested by using the capsules with an external diameter of 5 mm and a wall thickness of 0.8 mm. These capsules were chosen above the capsules with a wall thickness of 1 mm or 1.5 mm, as the thinner walls make them easier to cut and process manually. Two different dosages were tested by adding either 13 or 36 capsules per litre of concrete. The capsules were prepared by cutting the respective glass tubes to a length of 30 mm and sealing them with a 2-component epoxy plug of approximately 2 mm. This was a critical part of the process, as for the series with a dosage of 36 capsules per litre of concrete the capsules were pressurized with the process described in section 7.2.3. The series with 13 capsules per litre did not use pressurized capsules, as it was prepared before a pressurizing method was accomplished.

The efficiency of healing was evaluated by performing water flow tests across the cracked sections with a newly developed setup based on the setup used to assess water flow through cracks in small mortar specimens, described in section 5.1. For each dosage of capsules, three concrete specimens with dimensions 55x15x15 cm^3 were moulded. The moulds were crossed by two Ø6 mm reinforcement bars placed at the tensile zone of the specimen and three glass tubes with an external diameter of 10 mm and a wall thickness of 1 mm placed at the compression zone. The glass tubes were meant to rupture at the specimen's cracked section during loading and used later to inject water into the cracks to assess the healing efficiency.

The specimens were moulded using ordinary vibrated concrete with a slump of 45 mm. For the mixes including capsules, a volume equivalent to the total volume of capsules was removed from the larger gravel size, so that a similar amount of cement paste relative to particles (aggregates and capsules) was achieved. The composition of the mixes is listed in Table 15. Concrete batches of approximately 40 litres were mixed for 3 minutes (1 minute dry plus 2 minutes wet) in a 50 litre vertical shaft mixer. The capsules were then added to the fresh concrete while mixing, which was continued for an additional 2 minutes. Each batch was used to mould the three large concrete specimens for each series and the remaining concrete was used to mould 2-4 small concrete cubes of 10 cm sides to assess compressive strength. For the reference (REF) series, a total of two batches were mixed. All specimens were demoulded after one day cured for 21 days at 90% RH. An example of a large concrete specimen with indication of the relevant dimensions is shown in Figure 78.

In total, more than 2100 usable capsules had to be manually prepared. The total number of capsules prepared was even larger, considering that 5-10% of the capsules were not perfectly sealed, which meant that for the pressurized capsules the precursor partially leaked out and they had to be discarded. It is clear that for real-scale tests an industrial partner would have to perform the encapsulation with an automated process.

Table 15: concrete mix compositions.

Material	Dosage (kg/m^3)		
	REF	13 capsules/litre	36 capsules/litre
Sand 0/5 mm	640	640	640
Gravel 2/8 mm	462	462	462
Gravel 8/16 mm	762	742	705
CEM I 52.5 N	360	360	360
Water	165	165	165

To create the cracks to be tested for water flow, the specimens were loaded under 4-point bending, with a span between load points of 25 cm and a span between supports at the underside of 45 cm. Loading was performed at a constant 0.005 mm/s displacement rate of the loading plates. This resulted in 2-3

cracks per specimen. Once all the cracks were large enough to fit several small metallic spacers 0.5 mm thick, loading was held and the spacers were introduced. For some specimens the healing agent could already be seen leaking out of the cracked plane at this point, as shown in Figure 79. As the cracks did not open at the same rate and for the larger cracks some particles inside the cracked plane can be displaced, or because the spacers were inserted at weak spots, the final crack sizes after unloading covered a wide range of 0.2-1.1 mm.

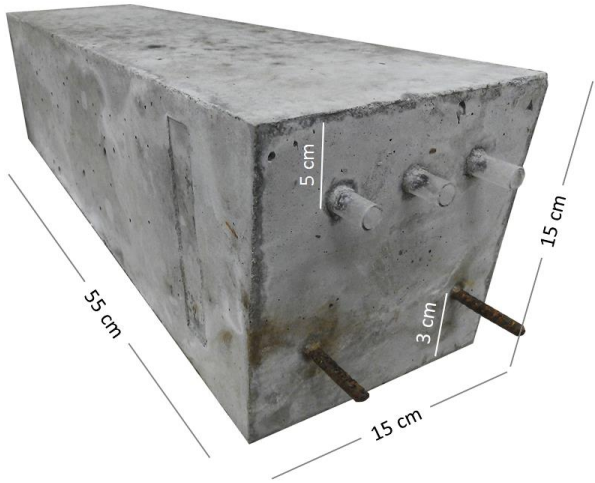

Figure 78: concrete specimen with randomly dispersed capsules and glass tubing for testing of water flow across cracked sections.

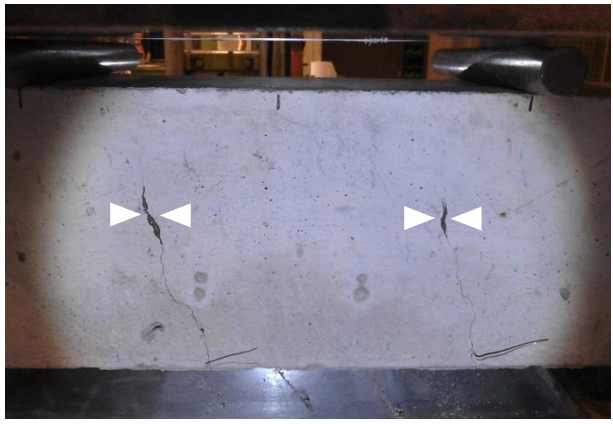

Figure 79: leaking of healing agent (between arrows) during cracking of a concrete specimen under 4-point bending.

Water flow test. To assess the healing efficiency, the cracked specimens were subjected to a water flow test. The glass tubes crossing the specimen were sealed at one side and the opposite side was connected via a flexible tubing to a reservoir containing water under a pressure of 1 bar. The pressure was applied to the reservoir by connecting it to a source of pressurized air controlled with a valve. Before performing the test, the sides of the specimens were sealed with adhesive aluminium foil, so that the water would flow only from the glass tubes at the top of the cracked plane to the bottom of the specimen. After leaking out of the crack mouth, the water was collected individually for each crack in plastic containers. A scale with automatic logging of weight change was used to determine the water flowing into the containers and was alternated between them. Water flow was measured for a period of at least 5 minutes and in all cases the weight change was perfectly linear, which allowed accurate calculation of a flow rate. The details of the setup described are shown in Figure 80.

Figure 80: test setup for determination of water flow through cracked planes.

Results. The results of the water flow test are shown in Figure 81. This figure clearly shows the large range of crack sizes achieved with the same cracking procedure, which is due to the 4-point bending setup used, as explained. In total, 26 cracks were tested for water flow. The results for the REF series, which contained no capsules, show two important aspects. On one hand no flow is expected if the crack mouth size is under 0.4 mm, as for such range the crack size at the intersection with the glass tubes supplying the water is too small. On the other hand, some scatter can also be observed, especially for large

crack mouth sizes above 0.8 mm. This is unavoidable, as the cracks planes in large specimens can have very different geometries and levels of tortuosity and frequently develop crack branching.

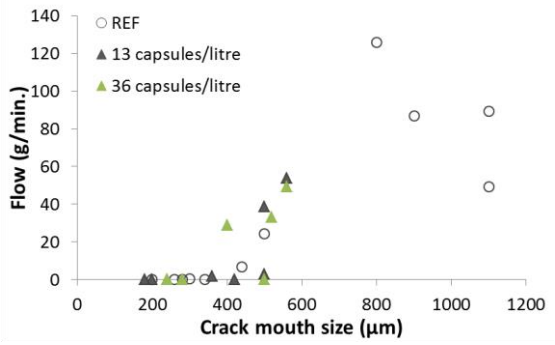

Figure 81: water flow through cracked planes in concrete specimens.

The usable results in Figure 81 are thus located in the crack mouth range of 0.4-0.6 mm for which water flow is expected and several data points for the series with added capsules are available. This is more clearly shown in Figure 82. Despite evidence of healing during the cracking procedure for many of these specimens, complete blocking of the water flow was only observed for 2 out of the 6 cracks shown in Figure 82 for crack sizes of 0.5 mm or larger, i.e. for which a considerable flow was expected. For the remaining cracks, healing was not widespread enough to result in perfect sealing of the cracked plane and their water flow was at the same level of a specimen from the REF series containing no capsules.

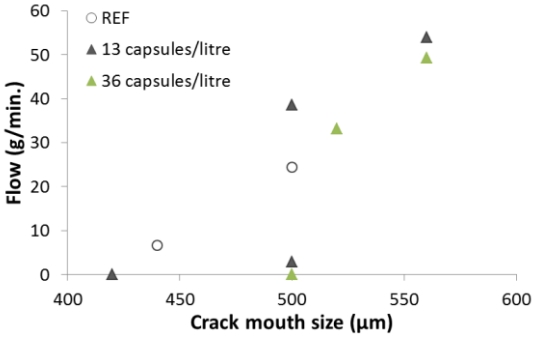

Figure 82: water flow through cracked planes with a crack mouth size within the 0.4-0.6 mm range.

For the series with 13 capsules per litre, several cross sections were cut from the specimens to count the amount of capsules intersected by the cut plane. An average of 4 capsules were intersected and a representative example is shown in Figure 83. With a total of 4 capsules available for healing, they have to be very precisely located for the polymer precursor to flow out and form a barrier against water flow. In any case, the aim of using randomly dispersed capsules is not achieving complete healing of a cracked plane, but to have enough polymer dispersed inside the crack in such a way that the healed areas are interlinked, forming a barrier.

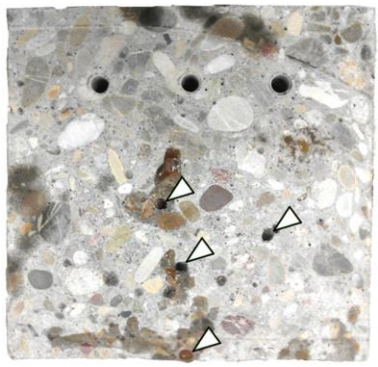

Figure 83: cross section cut from a concrete specimen containing 13 capsules per litre, where intersected capsules are highlighted with arrows.

For the series with 36 capsules per litre, the cracked section were split by loading the specimens in a 3-point bending setup with a loading point over the crack tip. This allowed assessing the amount of capsules intersected but also the area healed, which was found covered with polymer on both crack faces. With this higher dosage of capsules, an average of 8 capsules were intersected by the cracked plane and ruptured. It was also clearly observed that capsules parallel to the cracked plane do not rupture and these were not counted even if intersected.

The split plane corresponding to the crack with a mouth size of 0.5 mm is shown in Figure 84, where the boundaries of the areas covered by polymer were marked in green. For this crack, the intersected capsules were position in a way that allowed the polymer to disperse and form a perfect barrier against water flow. When splitting the cracked plane, the hardened polymer stays at-

tached to either one of the crack faces, so areas marked in green in the left and right faces in Figure 84 do not correspond exactly, which can give the impression that there is a gap in the barrier line. Additionally, at the bottom left corner of Figure 84 it can be seen that the specimen did not split at the cracked plane, leaving the same impression of a gap in the barrier line. An example of a crack for which considerable flow was observed despite a large area of the cracked plane being covered by polymer is shown in Figure 85. In this case, the capsules were not favourably positioned, leaving gaps at the sides of the specimen. This was clearly observed during testing, as the central part of the crack mouth was completely dry but a considerable water flow was noticed closer to the sides of the concrete specimen. It can thus be concluded that a large area of a cracked plane can be healed with a dosage of 36 capsules per litre, but consistent sealing of the plane would require a higher dosage, estimated to be about 50 capsules per litre, corresponding to a 30% increase.

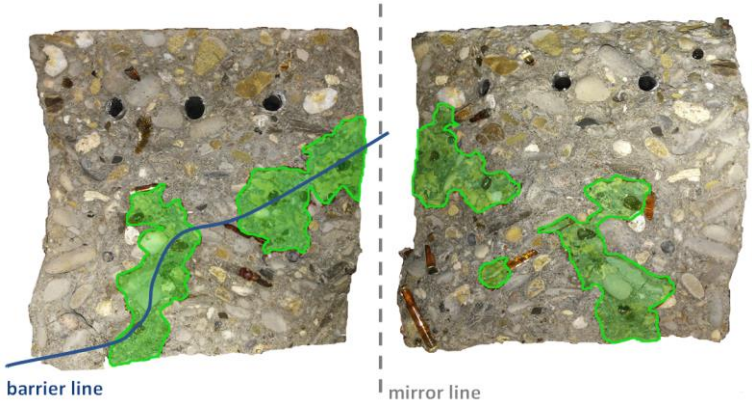

Figure 84: split cracked plane of a concrete specimen containing 36 pressurized capsules per litre, where healed areas (in green) formed a barrier against water flow.

Regarding the effect of the embedded capsules on the mechanical properties of concrete, the compressive strength was reduced by 5% and 8%, respectively for a dosage of 13 and 36 capsules per litre, compared to the strength of concrete containing no capsules. With the 4-point bending setup used it was not possible to achieve clear conclusions regarding the effect of capsules on the stiffness and tensile strength, but Tsangouri et al. (2013) reported that even thin walled cap-

sules positioned in parallel relative to the reinforcement bars can also act as local reinforcement and increase the bearing load of a concrete specimen.

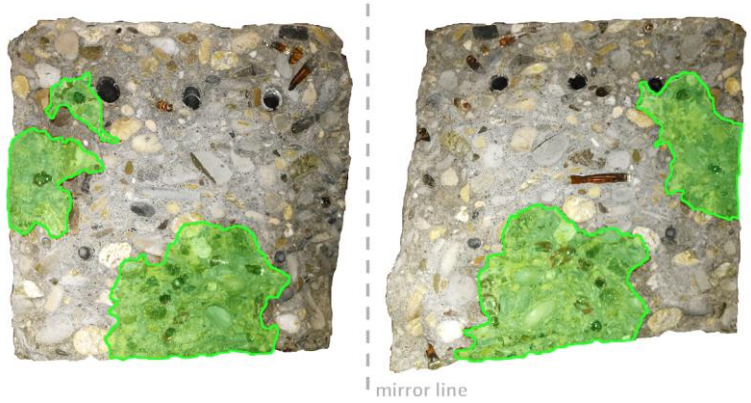

Figure 85: split cracked plane of a concrete specimen containing 36 pressurized capsules per litre, where water could flow between healed areas (in green).

8.2. Cost assessment

Once a self-healing mechanism based on encapsulated polymer precursors is optimized, proved to be compatible with conventional field practices and an estimation of effective dosage is achieved, cost assessment is a critical step to prove the feasibility of its practical implementation.

Implementation of engineered self-healing mechanisms adds an extra cost to conventional concrete at the same time that it potentially improves its durability or water tightness in the long term. Ideally, this extra cost would compare favourably to the cost of existing alternatives that can achieve the same effect of improved durability and water tightness. However, this assessment has been seldom performed for any of the mechanisms in the literature.

Van den Heede et al. (2016) compared the cost of self-healing concrete based on encapsulated polymer precursors to the cost of the multiple repair actions required to replace the cover concrete of an element exposed to chlorides within a time span of 100 years. The additional cost of implementing self-healing was prohibitive, as it was assumed that thin and expensive glass capsules would be used, by pre-placing them attached to a mesh inside the formwork and using self-compacting concrete to minimize potential damage to the capsules.

In this section of the book, a cost assessment of the solution implemented in section 8.1 is presented. It consists thus of 30 mm long glass capsules with a diameter of 5 mm and a wall thickness of 0.8 mm. The capsules are added to concrete during mixing, so they are randomly distributed in the hardened concrete. The solution studied here assumes however a dosage of 50 capsules per litre, which is higher than the dosages used in section 8.1. This was the estimation of the amount of capsules needed to consistently achieve water tightness of a cracked concrete section, based on the partial sealing results achieved with the lower dosages used.

The additional cost of this solution will be compared to the cost of potential alternatives: (a) conventional repair of cracks, (b) additional reinforcement to reduce maximum crack size to 0.05 mm, (c) self-healing concrete only at the outer layer of the element, with a thickness of 50 mm. Solution (b) assumes that if crack sizes are kept below 0.05 mm, complete autogenous healing eventually occurs. Solution (c) aims at minimizing the cost by reducing the amount of capsules needed (the same dosage per litre is used), but also results in more effective placement of the released healing agent. As the capsules are concentrated in the cover concrete, both water tightness and durability related to reinforcement corrosion are improved. If self-healing concrete is used across the whole concrete element, although water tightness of the cracked section is achieved, it is expected that parts of the reinforcement can still be exposed to the environment, as shown in section 8.1.

The calculations are done on a section of slab with the same dimensions used by Van den Heede (2014, 2016), i.e. a section 1 m wide, a span of 5 m and a thickness of 0.17 m. Solution (b) will also be based on the calculations of Van den Heede (2014), which determined that to reduce the maximum crack size from approximately 0.2 mm to 0.05 mm under a variable load of 5 kN/m^2, 14 Ø16 ribbed reinforcement steel bars would be needed instead of 6.

The cost of the components of the slab are shown in Table 16. Regarding solution (a), the cost of a repair action varies considerably depending on the local cost of labour. Considering that proper sealing of cracks requires routing, which enlarges the crack so that it can be filled with a sealing material, labour has a large weight on the cost of repair actions. In the following calculations it is assumed that repairing the whole 1 m wide slab would cost 200 €, which

would include the cost of a full work day in a developed country and the required materials. The cost of the capsules listed in Table 16 corresponds to the market cost of 30 mm of glass tubing and it is assumed that the additional cost of filling and sealing the capsules would be balanced by the potential cost reductions of buying the required materials in bulk, directly from the manufacturers. Based on these individual costs, the total cost of the four different solutions was calculated and is shown in Figure 86.

Table 16: cost of individual components.

Component	Unit cost
Concrete	65 €/m^3
Reinforcement	1 €/m
Polyurethane precursor	0.003 €/capsule
Glass capsules	0.01 €/capsule

Figure 86 shows that the cheapest solution (40 €) by a considerable margin is the use of additional reinforcement bars, so that the maximum crack size is kept below 0.05 mm and autogenous healing can quickly occur. However, the appeal of this solution will depend on how acceptable the increase in density of the reinforcement is for a contractor. With such density, the space between bars is only 5 cm, which can negatively affect the quality of concrete by making it difficult to use a conventional needle vibrator to compact it. Additionally, the labour necessary to install the extra reinforcement was not considered in the calculations and could have a substantial weight in the final cost of this solution in countries with expensive labour.

Another obvious conclusion is that addition of self-healing concrete in the whole element can become prohibitively expensive even for a thin slab element due to the large amount of capsules needed, even if the cost of individual capsules is very low. This solution was more than twice as expensive as conventional repair and thus it would be difficult to justify. It can however compare favourably to conventional repair in case other factors are considered, such as poor accessibility to the element, which would make it difficult to perform a repair action. Conventional repair itself can easily cost more than the cost of the reinforced concrete element (200 € vs. 85 €). If self-healing concrete is ap-

plied only at the outer 50 mm layer of the concrete element, the cost of a self-healing solution is reduced considerably to 163 € and becomes 19% cheaper than conventional repair. However, partial application of self-healing only at the outer surface with a capsule dosage of 50 capsules per litre has yet to be tested to determine that indeed it leads to consistent healing across the whole cracked element.

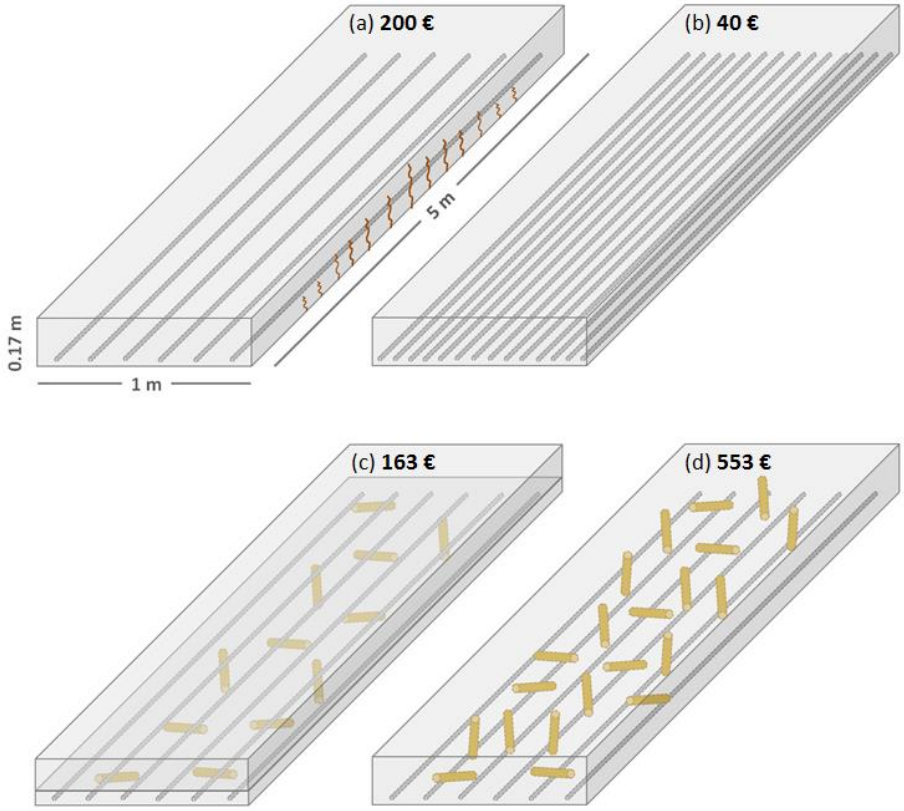

Figure 86: additional cost of different solutions: (a) conventional repair of cracks, (b) additional reinforcement, (c) self-healing concrete only at the outer 50 mm layer of the element and (d) self-healing concrete.

8.3. Chapter overview

This chapter showed the test results of an upscaling solution for self-healing concrete based on encapsulated polymer precursors. Cylindrical glass capsules 30 mm long that were proven to withstand the mixing process of concrete in

the previous chapter were embedded into concrete specimens at a dosage of 13 and 36 capsules per litre. Several cracks were created in the specimens and were tested individually for water flow, as a way to assess the potential of this technique to effectively and automatically seal cracks. Additionally, a cost assessment of this solution was performed and compared to alternative options.

More detailed conclusions are listed below:

- crack size was difficult to control and some degree of scattering should be expected for the water flow results, but enough results were available in the usable crack mouth size range of 0.4-0.6 mm;
- the amount of capsules intersected by a cracked plane was 4 and 8 respectively for dosages of 13 and 36 capsules per litre;
- 2 out of 6 cracked planes with a crack mouth size of 0.5 mm or higher were well sealed by the polymer dispersed inside the crack, with no observed water flow;
- a higher dosage of capsules, estimated to be about 50 capsules per litre would be required to achieve a consistent sealing effect;
- addition of capsules to a whole concrete slab would be too expensive compared to a typical repair action;
- if self-healing concrete is applied only to the outer 5 cm layer of the concrete element, the cost of this solution becomes 19% cheaper than conventional repair;
- the cheapest solution to achieve waterproof cracks is using additional reinforcement to keep the crack size below 0.05 mm, so that naturally occurring autogenous healing can take place; this solution leads however to very dense reinforcement which may be unacceptable in most situations.

9. CONCLUSIONS

A selection of moisture-curing precursors of polyurethane were screened based on their low viscosity and high elongation and good adhesion to concrete, resulting in 8 series, which covered a wide range of properties in terms of viscosity, foaming potential and mechanical properties after hardening. Series SLV (for super low viscosity) stood out as the best performing due to its better dispersion upon release from the capsules and a reduction of water uptake through the healed cracks to the level of sound specimens, resulting in a healing efficiency of 109%. This polymer was able to withstand a strain level of at least 50%, after which it detached from the crack faces. Such strain limit may be below the crack movement magnitude occasionally found in field structures, which was shown to exceed 100% in some cases. In the case of foaming polymers, failure occurred essentially due to rupturing of the foam cells. Of all the series tested, stiffness regain due to healing was at best 35% (SLV series), even when cracks were fully healed. Stiffness regain was however not seen as an advantage, as it would increase the likeliness of failure in the case of an active crack due to increased stress at the interface between polymer and cementitious matrix.

Continuous monitoring techniques were used to detect failure of polymers to follow crack movement, as an alternative to stepwise methods. Detection of failure through acoustic emission analysis coupled with DIC was possible only in case of failure due to brittle fracture of a rigid foam (elastic modulus of 22 MPa), which generated acoustic events with an energy level of at least one order of magnitude higher than the background noise. DIC tests performed in parallel detected a high rate of increase in the crack opening during failure, which allowed very accurate detection of failure at a strain of 9%. None of these features could be observed however during loading of specimens healed with a flexible polymer foam (elastic modulus of 5 MPa), whose failure would be best assessed through tests that determine the barrier properties of healed cracks under strain. Direct observation of interfaces with SEM in-situ loading allowed

determination of failure of a rigid foam due to cracking of the polymer matrix and detachment at the interface with the cementitious matrix, with an onset at 5% strain and complete detachment at 16% strain. For a flexible, continuous film of polymer based on a non-foaming precursor, detachment occurred before 50% strain. The lower elastic modulus also reduced the stress transferred across the crack faces during bending and avoided the opening of new cracks next to the original one, which occurred for specimens healed with the rigid polymer. Assuming adequate adhesion to a cementitious matrix (>2 N/mm^2), polymers with high elongation (>100%) and modulus of elasticity much lower than 10 MPa are suggested if cracks subjected to a realistic amplitude of movement are targeted.

The best performing SLV precursor was also tested under more realistic conditions. Resistance against high hydrostatic pressure and fatigue due to cyclic crack movement were determined, with the latter involving parallel monitoring with transmitted ultrasound pulses. The specimen configurations used for these tests required improving the release of precursor from the ruptured capsules to guarantee consistent and complete healing of the cracked sections. This was achieved by mixing the precursor with benzoyl peroxide, which can be decomposed to release CO_2 and pressurize the capsules. With the improved release an average self-healing efficiency of 82% under hydrostatic pressure was achieved. The healed cracks remained sealed under all pressures tested, up to 2 bar (or 20 m of water column). The resistance to high hydrostatic pressure remained even if a crack was widened by 40% of its initial size, but a progressive increase of water flow was observed for higher strain levels. Strain limits were further reduced to below 20% of the original crack size due to fatigue under hundreds of bending cycles. Monitoring of the upper envelope of maximum amplitude of ultrasound pulses during the multiple loading cycles allowed detecting failure. More specifically, considerable decreases or increases of the envelope were related respectively to a detachment of the polymer or a release of remaining precursor from the capsules after failure of the hardened polymer bridging the crack. Ultrasound transmission also allowed monitoring of healing and consistently revealed a considerable increase of maximum amplitude of the ultrasound pulses during the first 10 hours after the cracking, which was due to the dispersion and hardening of the precursor inside the crack. After approximately 48

hours the amplitude stabilized, which should then be the minimum time needed for curing of the precursor under in-situ conditions, inside a crack.

Performance assessment proceeded at a larger scale with concrete specimens healed with the best performing SLV precursor, but still using thin, pre-placed glass capsules which would not be compatible with a field application. The larger specimen size allowed using multiple non-destructive techniques. With ultrasound transmission analysis it was again possible to detect and monitor healing, with similar results to those obtained on mortar specimens on which all previously mentioned tests had been performed. For the concrete specimens, a considerable 47% or 74% regain of strength, depending on the dimensions of the specimens, was achieved due to healing of a large part of the cracked plane, while stiffness increased by either 19% or 75%. Trials were performed with additional non-destructive techniques. Vibration analysis was easy to implement and able to detect both a decrease and an increase of elastic modulus of the concrete specimens respectively after cracking and after healing. Localization of acoustic events made acoustic emission analysis particularly useful, as it allowed guaranteeing that specific emissions were due to damage occurring at the healed section.

Several configurations of capsules were tested in order to assess their potential for upscaling of self-healing concrete. Spherical polymeric microcapsules with a diameter of 50-100 μm and 40% core content (SLV precursor) did not rupture when crossed by a crack, as they detached from the cementitious matrix. The microcapsules were also found to consist of multiple small cores which would make it difficult to release their liquid core. On the other hand, none of the larger cylindrical polymeric capsules with an external diameter of ~7 mm were able to keep a moisture-curing polyurethane stable, so they could not be used with the polyurethane precursors used in this study. They could however be compatible with other healing agents that are not moisture-sensitive. Out of five different polymers tested as encapsulation material, PMMA capsules were found to rupture when crossed by small cracks in concrete of ~100 μm even for fairly thick capsule walls of 0.7 mm, which would increase their likeliness of also surviving mixing into concrete. A numerical model satisfactorily predicted the crack size at rupture for different polymers, proving to be a valuable tool in the design of capsules for this application by reducing the number of experiments needed. Cylindrical glass capsules were then determined to be the best

encapsulating technique when moisture-sensitive healing agents are used. They also ruptured when crossed by very small cracks in concrete of ~25 μm and survived concrete mixing if their wall was at least 0.5 mm thick. It was found that the adhesives used to seal the capsules slowly allowed ingress of moisture, resulting in partial reaction of the moisture-curing polyurethane. Unexpectedly, this had a beneficial effect on the release of precursor into the crack, as partial reaction released CO_2 and pressurized the capsules. Thicker plugs of adhesive sealing the capsules avoided considerable reaction of the precursor and an alternative mechanism for pressurizing the capsules was developed. Decomposition of benzoyl peroxide at high temperatures also results in the release of CO_2 and the addition of 1 wt% relative to the polyurethane precursor increased the healed area by 4 times.

To test a final upscaling solution, glass capsules 30 mm long and with a wall thickness of 0.5 mm were mixed into concrete at a dosage of 13 and 36 capsules per litre and moulded into specimens, on which multiple cracks were created to more realistically mimic field conditions. Partial success was obtained, as 2 out of 6 cracked planes, with a crack width for which a considerable flow was expected, were well sealed when tested for water flow under high pressure. A higher dosage of capsules, estimated to be about 50 capsules per litre, would be required to achieve a consistent sealing effect. Finally, a cost assessment of this solution was performed and compared to alternative options to achieve waterproof cracks. Addition of capsules to a whole concrete slab would be too expensive compared to a typical repair action. However, if capsules are applied only to the outer 5 cm layer of the concrete element, the cost of this solution becomes 19% cheaper than a typical repair action. The cheapest solution is however using additional reinforcement to keep the crack size below 0.05 mm, for which autogenous healing would easily occur, although this leads to a problematic, high density of reinforcement.

SUGGESTIONS FOR FUTURE STUDIES

Further improvement of self-healing based on encapsulated polymer precursors targeting active cracks should be focused on the development of healing agents that cure into a product with a very low modulus of elasticity. A very low modulus of elasticity, ideally similar to that of a gel-like substance would reduce the likeliness of detachment from the crack faces at very high strains and thus would be compatible with a broader range of field conditions.

The mechanical performance testing of elements healed with materials of such low modulus may be particularly challenging, as the load bearing capacity of the healing materials would be very limited and thus typical mechanical tests may not be fit. In this regard, non-destructive tests, particularly those based on ultrasound transmission can be further improved, with the possible benefit of being adaptable to field conditions.

Additional efforts should be put into finding an industrial partner to properly seal glass capsules at a large scale. An industrial partner for encapsulation would improve the consistency of sealing, which is crucial in case moisture-sensitive healing agents are used.

Polymeric PMMA capsules to encapsulate healing agents that are not moisture sensitive can be improved to guarantee rupture at even smaller crack sizes or alternative polymeric materials can be investigated, as they can potentially be easier to process at a large scale, when compared to glass capsules.

The production of large batches of capsules would also allow testing of real-scale concrete elements, which is critical to increase awareness and acceptance of self-healing technologies by the concrete and construction industries.

ACKNOWLEDGEMENTS

More than anything else, I would like to acknowledge the opportunity given by my supervisor Nele De Belie to be part of a European research project focusing on such an exciting topic. I am also very grateful for all the effort put into assuring the near perfect research conditions I benefited from.

To my other supervisor and super-woman Elke Gruyaert, I should thank all the load that was frequently taken off me.

A considerable part of the research work presented in this book would not be possible without the cooperation of other researchers in PhD and post-doc positions such as Adelaide Araújo, Branko Šavija, Eleni Tsangouri, Fabian Malm and Sutima Chatrabhuti. Thanks also to MSc student Valerie Couvreur for her contribution.

Similarly, I am grateful for the effort of people working in different companies: Alexandre Beirão, Ivo Pais, Maxime Durka, Piet Kempenaers and Roberto Teixeira.

The help from all the technicians of the Magnel Laboratory was essential and special thanks go to Dieter Hillewaere for the time shared imagining and putting together various test setups.

Secretaries Christel Malfait and Marijke Reunes took another considerable load off me and did that with a smile.

I'm also very grateful for the excellent office mates I had throughout the years, too many to mention, that kept it light and saw the funny side of science.

Writing this section, it's impossible not to become aware of the amount of people and the complexity involved in the journey undertook in the last four years, which makes it extra clear that I should be thankful also for that lucky star that keeps looking out for me.

ABOUT THE AUTHOR

The author obtained an MSc degree on Civil Engineering with a focus on construction materials at IST (Instituto Superior Técnico, Lisbon). His MSc thesis topic was the performance of liquid-applied waterproofing systems.

Previous experience include working at LNEC (National Laboratory for Civil Engineering, Lisbon) on a research project related to polymer-modified cementitious materials and at IST on a research project related to cementitious materials containing aerogels.

The combined research to date resulted in 9 peer reviewed scientific articles in A1 journals as main author or with a major contribution, which are listed below.

Morgado F, Grandão Lopes J, de Brito J, Feiteira J (2012). Portuguese Irrigation Canals: Lining Solutions, Anomalies, and Rehabilitation. Journal of Performance of Constructed Facilities 26:507-515.

Feiteira J, Custódio J, Ribeiro MSS (2013). Review and discussion of polymer action on alkali-silica reaction. Materials and Structures 46:1415-1427.

Feiteira J, Grandão Lopes J, de Brito J (2013). Mechanical Performance of Liquid-Applied Roof Waterproofing Systems. Journal of Performance of Constructed Facilities 27:244-251.

Feiteira J, Ribeiro MSS (2013). Polymer action on alkali–silica reaction in cement mortar. Cement and Concrete Research 44:97-105.

Mendes P, Grandão Lopes J, de Brito J, Feiteira J (2014). Waterproofing of Concrete Foundations. Journal of Performance of Constructed Facilities 28:242-249.

Tuna J, Feiteira J, Flores-Colen I, Pereira M, de Brito J (2015). In Situ Characterization of Damaging Soluble Salts in Wall Construction Materials. Journal of Performance of Constructed Facilities 29.

Feiteira J, Gruyaert E, De Belie N (2016). Self-healing of moving cracks in concrete by means of encapsulated polymer precursors. Construction and Building Materials 102:671-78.

Feiteira J, Tsangouri E, Gruyaert E, Lors C, Louis G, De Belie N (2017). Monitoring crack movement in polymer-based self-healing concrete through digital image correlation, acoustic emission analysis and SEM in-situ loading. Materials & Design 115:238-246.

Šavija B and Feiteira J, Araújo M, Chatrabhuti S, Raquez J-M, Van Tittelboom K, Gruyaert E, De Belie N, Schlangen E (2017). Simulation aided design of tubular polymeric capsules for self-healing concrete. Materials 10 (open access).

REFERENCES

ACI - American Concrete Institute (2001). 224R-01: Control of cracking in concrete structures. ACI, Farmington Hills.

ACI - American Concrete Institute (2007). 224.1R-07: Causes, evaluation, and repair of cracks in concrete structures. ACI, Farmington Hills.

Ahn T-H, Kishi T (2010). Crack self-healing behaviour of cementitious composites incorporating various mineral admixtures. Journal of Advanced Concrete Technology 8:171-186.

Akhavan A, Shafaatian S-M-H, Rajabipour F (2012). Quantifying the effects of crack width, tortuosity, and roughness on water permeability of cracked mortars. Cement and Concrete Research 42:313-320.

Araújo A, Van Vlierberghe S, Feiteira J, Graulus G-J, Van Tittelboom K, Martins JC, Dubruel P, De Belie N (2016). Cross-linkable polyethers as healing/sealing agents for self-healing of cementitious materials. Materials & Design 98:215-222.

Araújo A, Gruyaert E, Alderete N, Van Tittelboom K, Chatrabhuti A, Raquez J-M, De Belie N (2017). Application of polymeric capsules in concrete beams: survival during mixing and sealing ability of cracks. ICSHM 2017 - Sixth international conference on self-healing materials, Friedrichshafen, Germany (submitted).

CEN - European Committee for Standardization (2004a). Eurocode 2, EN 1992, Design of concrete structures - Part 1-1: General rules and rules for buildings. CEN, Brussels.

CEN - European Committee for Standardization (2004b). EN 1504, Products and systems for the protection and repair of concrete structures - Definitions, requirements, quality control and evaluation of conformity - Part 5: Concrete injection. CEN, Brussels.

CEN - European Committee for Standardization (2006). Eurocode 2, EN 1992, Design of concrete structures - Part 3: Liquid retaining and containment structures. CEN, Brussels.

Criel P, Caspeele R, Matthys S, Taerwe L (2014). Creep experiments and analysis of T-shaped beams subjected to loading and unloading at young age. IALCCE 2014 - Fourth international symposium on life-cycle of structural systems: design, assessment, maintenance and management, Tokyo, Japan.

Cruz CM, Raupach M (2016). Durable surface repair of waterway engineering structures with sprayed textile reinforced concrete. Concrete Solutions - Sixth international conference on concrete repair, Thessaloniki, Greece.

De Rooij M, Van Titttelboom K, De Belie N, Schlangen E (2013). Self-healing phenomena in cement-based materials – State-of-the-art report of RILEM Technical Committee 221-SHC. Springer.

Dong B, Wang Y, Fang G, Han N, Xing F, Lu Y (2015). Smart releasing behavior of a chemical self-healing microcapsule in the stimulated concrete pore solution. Cement & Concrete Composites 56:46-50.

Dry C (2000). Three designs for the internal release of sealants, adhesives, and waterproofing chemicals into concrete to reduce permeability. Cement and Concrete Research 30:1969-1977.

Dry C, Corsaw M, Bayer E (2003). A comparison of internal self-repair with resin injection in repair of concrete. Journal of Adhesion Science and Technology 17:79-89.

Edvardsen C (1999). Water permeability and autogenous healing of cracks in concrete. ACI Materials Journal 96:448-454.

Feiteira J, Gruyaert E, De Belie N (2016). Self-healing of moving cracks in concrete by means of encapsulated polymer precursors. Construction and Building Materials 102:671-78.

Feiteira J, Tsangouri E, Gruyaert E, Lors C, Louis G, De Belie N (2017). Monitoring crack movement in polymer-based self-healing concrete through digital image correlation, acoustic emission analysis and SEM in-situ loading. Materials & Design 115:238-246.

Flohr K, Malm F, Grosse CU (2015). Schallemissionsanalyse zur untersuchung der effizienz von selbstheilungsmechanismen in beton (in German). 20. Kolloquium Schallemission, Garmisch-Partenkirchen, Germany.

Formia A, Terranova S, Antonaci P, Pugno NM, Tulliani JM (2015). Setup of extruded cementitious hollow tubes as containing/releasing devices in self-Healing systems. Materials 8:1897-1923.

Gardner D, Jefferson A, Hoffman A, Lark R (2014). Simulation of the capillary flow of an autonomic healing agent in discrete cracks in cementitious materials. Cement and Concrete Research 58:35-44.

Goethals J (2009). Autogene en autonome zelfheling van beton. MSc thesis (in Dutch), Department of Structural Engineering, Ghent University.

Granger S, Loukili A, Pijaudier-Cabota G, Chanvillard G (2007). Experimental characterization of the self-healing of cracks in an ultra high performance cementitious material: Mechanical tests and acoustic emission analysis. Cement and Concrete Research. 37:519-527.

Große CU, Ohtsu M (2008). Acoustic emission testing. Basics for research – applications in civil engineering. Springer.

Gruyaert E, Feiteira J, De Belie N, Malm F, Nahm M, Grosse CU, Tziviloglou E, Schlangen E, Tsangouri E (2015). Non-destructive testing techniques to evaluate the healing efficiency of self-healing concrete at lab-scale. Proceedings of the 6th International Conference on Emerging Technologies in Non-Destructive Testing, Brussels, Belgium.

Gruyaert E, Van Tittelbooma K, Sucaet J, Anrijs J, Van Vlierberghe S, Dubruel P, De Geest BG, Remon JP, De Belie N (2016). Capsules with evolving brittleness to resist the preparation of self-healing concrete. Materiales de Construcción 323:e092.

Hilloulin B, Van Tittelboom K, Gruyaert E, De Belie N, Loukili A (2015). Design of polymeric capsules for self-healing concrete. Cement & Concrete Composites. 55:298-307.

Huang H, Ye G, Qian C, Schlangen E (2016). Self-healing in cementitious materials: Materials, methods and service conditions. Materials & Design 92:499-511.

In C-W, Holland RB, Kim J-Y, Kurtis KE, Kahn LF, Jacobs LJ (2013). Monitoring and evaluation of self-healing in concrete using diffuse ultrasound. NDT&E International 57:36-44.

Karaiskos G, Deraemaeker A, Aggelis DG, Van Hemelrijck D (2015). Monitoring of concrete structures using the ultrasonic pulse velocity method. Smart Materials and Structures 24(11).

Li V, Lim Y, Chan Y (1998). Feasibility study of a passive smart self-healing cementitious composite. Composites Part B 29B:819-827.

Litina C (2015). Development and performance of self-healing blended cement grouts with microencapsulated mineral agents. Ph.D. thesis, University of Cambridge, United Kingdom.

Luković M, Šavija B, Schlangen E, Ye G, van Breugel K (2016). A 3D lattice modelling study of drying shrinkage damage in concrete repair systems. Materials 9:575.

Malm F, Große CU (2014). Examination of reinforced concrete beams with self-healing properties by acoustic emission analysis. 31st Conference of the European Working Group on Acoustic Emission (EWGAE), Dresden, Germany.

Mignon A, Snoeck D, Schaubroeck D, Luickx N, Dubruel P, Van Vlierberghe S, De Belie N (2015). pH-responsive superabsorbent polymers: A pathway to self-healing of mortar. Reactive and Functional Polymers 93:68-76.

Minnebo P, Lefever G, Van Tittelboom K, De Belie N, Hemelrijck (2016). Tube shape alterations for improved concrete pouring survivability in vascular self-healing concrete. HealCON conference, Delft, The Netherlands.

Neild S, Williams M, McFadden P (2003). Nonlinear vibration characteristics of damaged concrete beams. Journal of Structural Engineering 129:260-268.

Ohtsu M (2010). Recommendations of RILEM Technical Committee 212-ACD: acoustic emission and related NDE techniques for crack detection and damage evaluation in concrete. Test method for classification of active cracks in concrete structures by acoustic emission, Materials and Structures 43:1187-9.

Pelto J, Sinilehto HM, Beirão A, Leivo M (2016). Encapsulation of superabsorbent polymer hydrogel particles for self-healing concrete. healCON conference, Delft, The Netherlands.

Pilegis M, Davies R, Lark R, Gardner D, Jefferson A (2016). Challenges of self-healing concrete scale-up and site trials. 9th International Conference on Fracture Mechanics of Concrete and Concrete Structures, Berkeley, U.S.A.

Pollock AA (2011). Material Brittleness and the Energetics of Acoustic Emission, Experimental Mechanics on Emerging Energy Systems and Materials, Volume 5, 73-79, Springer.

Raupach M (1996). Chloride-induced macrocell corrosion of steel in concrete - theoretical background and practical consequences. Construction and Building Materials 10:329-338.

Reinhardt HW, Große CU (2004). Continuous monitoring of setting and hardening of mortar and concrete. Construction and Building Materials 18:145-154.

Reinhardt H-W, Jooss M (2003). Permeability and self-healing of cracked concrete as a function of temperature and crack width. Cement and Concrete Research 33:981-985.

Saccani A, Bignozzi MC (2010). ASR expansion behavior of recycled glass fine aggregates in concrete. Cement and Concrete Research 40:531-536

Šavija B, Luković M, Pacheco J, Schlangen E (2013). Cracking of the concrete cover due to reinforcement corrosion: A two-dimensional lattice model study. Construction and Building Materials 44:626-638.

Šavija B and Feiteira J, Araújo M, Chatrabhuti S, Raquez J-M, Van Tittelboom K, Gruyaert E, De Belie N, Schlangen E (2017). Simulation aided design of tubular polymeric capsules for self-healing concrete. Materials 10 (open access).

Schlangen E (1993). Experimental and numerical analysis of fracture processes in concrete. Ph.D. thesis, Delft University of Technology, The Netherlands.

Schlangen E, Qian Z (2009). 3D modeling of fracture in cement-based materials. Journal of Multiscale Modelling 1:245-261.

Schlangen E, Joseph C (2013). Modelling of Self-Healing Cementitious Materials. Self-Healing Phenomena in Cement-Based Materials – State-of-the-art report of RILEM Technical Committee 221-SHC, Springer, pp. 217-240.

Sierra-Beltran M, Jonkers H, Mera-Hortiz W (2015). Field application of self-healing concrete with natural fibres as linings for irrigation canals in Ecuador. ICSHM 2015 - Fifth international conference on self-healing materials, Durham, U.S.A.

Simon C (2016). Novel solutions for multi-functional nano-additives in the manufacturing of concrete structures. Self-healing concrete ie-net workshop, Ghent, Belgium.

Sutton M, Orteu J, Schreier H (2009). Image Correlation for Shape, Motion and Deformation Measurements: Basic Concepts, Theory and Applications. Springer.

Thao TDP, Johnson TJS, Tong QA, Dai PS (2009). Implementation of self-healing in concrete - Proof of concept. The IES Journal Part A: Civil & Structural Engineering 2:116-125.

Tsangouri E, Aggelis DG, Van Tittelboom K, De Belie N, Van Hemelrijck D (2013). Detecting the activation of a self-healing mechanism in concrete by acoustic emission and digital image correlation, The Scientific World Journal (open access).

Tsangouri E, Karaiskos G, Deraemaeker A, Van Hemelrijck D, Aggelis D (2016). Assessment of acoustic emission localization accuracy on damaged and healed concrete. Construction and Building Materials 129:163-171.

Tziviloglou E, Jonkers HM, Schlangen E (2014). Bacteria-based self-healing concrete to increase liquid tightness of cracks. First conference on ageing of materials and structures, Delft, The Netherlands.

Van den Heede P, Maes M, De Belie N (2014). Influence of active crack width control on the chloride penetration resistance and global warming potential of slabs made with fly ash + silica fume concrete. Construction and Building Materials 67:74-80.

Van den Heede P, Van Belleghem B, De Belie N (2016). The cost and environmental impact of service life extending self-healing engineered materials for

sustainable steel reinforced concrete. Sustainable Built Environment (SBE) Regional Conference, Zurich.

Van Tittelboom K, De Belie N, Van Loo D, Jacobs P (2011). Self-healing efficiency of cementitious materials containing tubular capsules filled with healing agent. Cement & Concrete Composites 33:497-505.

Van Tittelboom K (2012). Self-Healing Concrete through Incorporation of Encapsulated Bacteria- or Polymer-Based Healing Agents. Ph.D. thesis, Ghent University, Belgium.

Van Tittelboom K, De Belie N, Lehmann F, Grosse CU (2012). Acoustic emission analysis for the quantification of autonomous crack healing in concrete, Construction and Building Materials 28:333-41.

Van Tittelboom K, De Belie N (2013). Self-healing in cementitious materials - a review. Materials 6:2182-2217.

Van Tittelboom K, Tsangouri E, Van Hemelrijck D, De Belie N (2015). The efficiency of self-healing concrete using alternative manufacturing procedures and more realistic crack patterns. Cement & Concrete Composites 57:142-152.

Wang K, Jansen DC, Shah SP (1997). Permeability study of cracked concrete. Cement and Concrete Research 27:381-393.

White SR, Sottos NR, Geubelle PH, Moore JS, Kessler MR, Sriram SR, et al. (2001). Autonomic healing of polymer composites. Nature 409:794-797.

Xiong W, Tang J, Zhu G, Han N, Schlangen E, Dong B, Wang X, Xing F (2015). A novel capsule-based self-recovery system with a chloride ion trigger. Scientific Reports 5:10866.

Xu J, Du Y, Jiang Z, She A (2015). Effects of calcium source on biochemical properties of microbial $CaCO_3$ precipitation. Frontiers of Microbiology (open access) 2 December 2015.

Yang Z, Hollar J, He X, Shi X (2011). A self-healing cementitious composite using oil core/silica gel shell microcapsules. Cement & Concrete Composites 33:506-512.

List of abbreviations and chemical formulas

AE – acoustic emission

BPO – benzoyl peroxide

DIC – digital image correlation

EDF – extended depth of field

FRP – fibre reinforced polymer

LVDT – linear variable displacement transducer

PEG – polyethyleneglycol monomethylether

PET – polyethylene terephthalate

PLA – polylactic acid

PMMA – poly(methyl methacrylate)

PS – polystyrene

PVA – polyvinyl acetate

RH – relative humidity

SAP – superabsorbent polymer

SEM – scanning electron microscope

TUM – Technical University of Munich

UGent – Ghent University

UV – ultraviolet

$CaCO_3$ – calcium carbonate

$Ca(OH)_2$ – calcium hydroxide

CO_2 – carbon dioxide